TUM

Technische Universität München
Fakultät für Medizin

The Impact of High- and Low-LET Irradiation on the Invasion of Glioblastoma Multiforme Cells

Michaela Anna Wank

Vollständiger Abdruck der von der Fakultät für Medizin
der Technischen Universität München
zur Erlangung des akademischen Grades
eines Doktors der Naturwissenschaften (Dr. rer. nat.)
genehmigten Dissertation.

Vorsitzender: Prof. Dr. Claus Zimmer

Prüfende der Dissertation:

1. Prof. Dr. Stephanie E. Combs
2. Prof. Dr. Gabriele Multhoff

Die Dissertation wurde am 18.09.2018 bei der Technischen Universität München
eingereicht und durch die Fakultät für Medizin am 20.02.2019 angenommen.

Contents

1 Abstract

The Glioblastoma multiforme (GBM) is one of the most common primary brain tumors. In spite of extensive molecular characterization, still today the standard treatment concept consists of a multimodal treatment regimen, combining surgery with chemo- and radiotherapy. Nevertheless, the prognosis for patients with GBM is poor with a 5-year survival of less than 10 %. This is caused by natural highly-infiltrative capacities, as well as high levels of radio- and chemo-resistance. Gliomas are known to follow a dose-response relationship, however, toxicity limits dose-escalation.

Ionizing radiation is one of the gold-standards in cancer treatment and it has been proven in many studies that it offers a clear survival benefit for most cancer types. Likewise, it plays an important role in the multimodal treatment concept of gliomas. However, it was noted that the photon irradiation, currently used most often in the clinics (low-LET), might even cause a radiation-enhanced invasion and promoted proliferation, thereby lowering the overall survival. This finding was concluded from studies applying established cell lines and is discussed controversially. Established and commercially available cell lines are the most commonly used cell systems but are not as close to the human biology as necessary. Therefore, in this thesis a new system ("the RadGlio study")was established, which allows the isolation of primary cells from patient-derived tumor tissue and the analysis of their basal invasive capacities and radiation-triggered invasion, as well as the correlation with clinical data.

It is of great interest to investigate the mechanisms leading to glioma invasion and radiation-enhanced invasion to counteract the poor prognosis of glioma patients. Therefore, this Ph.D. thesis analysed the invasion of several established and patient-derived primary glioma cell lines after high- and low-LET irradition. In a first step, glioma cell lines were characterized by colony formation assays, cell doubling time, cell cycle distribution and DNA damage analysis. Secondly, the basal invasive capacity was measured and compared to the invasion after high- and low-LET irradiation. For explanation of the observed, low-LET radiation-enhanced invasion, which was not visible after high-LET irradiation, RNA- and protein-levels were analysed and potential pathways were examined. In a last step, the results from *in vitro* experiments were correlated to clinical data.

In summary, this study provided novel evidence for low-LET radiation-enhanced invasion of GBM cells and proposes high-LET irradiation as an alternative treatment option to pre-

vent radiation-induced invasion. Furthermore, the need for a more personalized treatment concept is stated. In addition, signaling pathways like the AKT-, NOTCH1 and TGF-β have been proposed as responsible mechanisms for low-LET enhanced invasion.

2   Motivation

Today about 50% of all diagnosed cancer patients are treated with radiotherapy [14]. In 90% of the cases, the applied radiation is photon irradiation [6].

The maximal dose of conventional low-LET photon irradiation is limited as there is always some energy deposition to the neighbouring healthy tissue. To protect healthy tissue the tumor irradiation has to be split into several fractions. Therefore, patients generally receive fractionated radiotherapy, five times a week, over several weeks, using single doses of 1.8 - $2\,\mathrm{Gy}$.

Glioblastoma multiforme (GBM), a very aggressive primary brain cancer with a very poor survival rate (5-year survival $< 10\%$), is treated with a combination of surgery, chemo- and radiotherapy (with photons) [6, 79]. Still, in 90% of cases, tumor cells recur in close (1-2 cm) proximity to the primary tumor [56]. One of the main possible reasons for tumor recurrence is the high natural invasive potential of GBM cells. Recently, there was first evidence that low-LET radiation enhances the invasive capacity of GBM cells but this is still controversially discussed [43, 101]. Due to the improved physical and radiobiological properties of high-LET radiation, it is assumed to be superior to photon radiotherapy for several tumor entities [91]. High-LET radiation allows a more precise dose deposition to the tumor while sparing healthy tissue. Another radiobiological advantage of high-LET irradiation is the generation of a more complex and clustered DNA damage, which cannot be repaired quickly and therefore causes higher cancer cell killing [72]. There is also first evidence that high-LET in contrast to low-LET irradiation does not affect the migratory and invasive potential of GBM cells *in vitro* [102].

The Institute of Innovative Radiotherapy (iRT) of the Helmholtz Zentrum München is tightly connected to the Department of Radiation Oncology of the Klinikum rechts der Isar (TUM) and enables to close the gap between basic research and translational clinic research. This unique combination is a necessary prerequisite for this study by providing easy access to GBM patient samples from the clinics and enabling the application of different radiation qualities for the experimental research part. By investigating the impact of different radiation qualities on the invasion of GBM cells this study aimed to demonstrate new evidence for the beneficial role of high-LET irradiation as an alternative treatment option for GBM. Using patient-derived primary glioma cells, new insights into radiation-induced patient-specific invasion is provided.

3   Introduction

3.1   Glioblastoma multiforme

According to the World Health Organization (WHO), 8.8 million people worldwide die every year because of cancer, which corresponds to almost one of six global death cases. According to Metha et al. 23,130 tumors of the central nervous system (CNS) are diagnosed in the US every year, of which 87 % arise in the brain [86]. As already written in the hallmarks of cancer by Hanahan and Weinberg, a healthy cell gains certain attitudes that turns it into a cancer cell [54]. The six well-known hallmarks are sustainment of proliferation, evasion of growth suppressors, activation of invasion and metastasis, immortalisation of replication, induction of angiogenesis and resistance to cell death. In 2011 Hanahan and Weinberg introduced two more emerging hallmarks of tumor cells – deregulation of cellular energetics and avoidance of immune destruction – both not yet fully validated [54].

The question why healthy cells are prone to genomic instability, is up to now not fully understood. Some physical, as well as environmental influences like radiation, smoke of tobacco or consumption of toxic material, are suggested [84]. After suffering from various symptoms like headache, seizure and trouble with walking or speaking, diagnosis is usually performed via computed tomography or magnetic resonance imaging and confirmed by tissue sampling. The CNS comprises three types of glial cells: astrocytes (most frequent in the CNS, star-shaped, establish metabolic balance), oligodendrocytes (responsible for myelination) and microglial cells (phagocytosis of microbes) [96]. Primary brain tumors arising from glial cells are referred to as gliomas [46]. Gliomas can be separated in low- and high-grade gliomas [97]. Only 10 % are low-grade gliomas, which are considered to be a diverse group of tumors located throughout the CNS [86]. The patient outcome depends on treatment, as well as pathological and biological factors but overall treatment success is still better than of high-grade gliomas. Low-grade gliomas can be subdivided into several WHO classifications, which were updated in 2016. Grade I tumors (giant cell astrocytomas, pilocytic astrocytomas) are considered to be benign and grade II tumors are considered to be the most common type (Astrocytoma, Oligodendroglioma and mixed Oligoastrocytoma). Grade II tumors already show diffuse infiltration and anaplastic transformation [79]. Approximately 50-60 % of astrocytomas show p53 mutations whereas oligodendroglioma show loss of 1p/19q [40, 66]. As both mutations are mutually exclusive mixed oligoastrocytoma can carry only one of those mutations, suggesting their lineage. IDH1 mutations, in con-

trast, occur in 70-80 % of low-grade gliomas independent of the p53 or 1p/19q status. As the IDH1 mutation is an early event in tumorigenesis it can be used to differentiate between primary and secondary gliomas [40, 62]. Approx. 80 % of all secondary GBM show a mutated IDH whereas only 5 % of the primary tumors express mutated IDH [3].

Approximately 80 % of the diagnosed brain tumors are highly malignant and considered as high-grade gliomas. The correlation of grading and treatment outcome is generally known: the higher the grading the worse the prognosis [70]. High-grade gliomas can be differentiated between WHO III (anaplastic astrocytoma, anaplastic oligodendroglioma, anaplastic ependymoma, anaplastic ganglioglioma and anaplastic meningioma) and WHO IV (glioblastoma and embryonal tumors) [80]. Glioblastoma multiforme (GBM), which is categorized as grade IV, is the most common and malignant primary brain tumor with an incidence rate of 3-4/100,000 persons in the USA, affecting more males than females [85]. The peak incidence is at approximately 60 years of age. The location of the primary tumor is most likely in the frontal part of the cerebrum. GBM is likewise displaying the hallmarks proposed by Hanahan and Weinberg: uncontrolled cellular proliferation, diffuse infiltration, robust angiogenesis, resistance to apoptosis and genomic instability. Additionally, intratumoral heterogeneity as well as resistance to chemo- and radiotherapy result in a very poor prognosis for GBM patients [79]. Even though the incidence rate, 2 % of all primary tumors, is low, the mortality is very high. The 5-year survival is below 10 % [79]. Additionally, GBM is known for its high relapse propensity. Recurrence was repeatedly demonstrated as inevitable after 32 to 36 weeks after surgery [4, 23]. Some incidences indicate that GBM is caused by inheritance (Turcot's syndrome or Li-Fraumeni syndrome) but for most cases no genetic predisposition is to be attributed [71]. Likewise, there are no specific risk factors known. Despite the poor prognosis, survival is influenced by age, gender, tumor size and tumor location, as well as the Karnofsky performance score [32, 88].

3.2 Radiation

Living organisms are exposed to natural or even man-made radiation consistently. Radiation can be subdivided into several groups like electromagnetic-, particle-, acoustic- and gravitational radiation. Electromagnetic (EM) radiation is a diverse group, compromising radio- and microwaves, UV-light, γ-rays and X-rays [2]. Therefore, EM radiation is

subdivided into two subgroups, ionizing and non-ionizing radiation. According to the International Atomic Energy Agency (IAEA), $90\,\%$ of ionizing radiation exposure is due to natural sources like cosmic rays and terrestrial sources [2]. Ionizing means, that the irradiation has the ability to strip electrons from atoms or molecules creating a positively charged ion. Ionizing radiation is characterized by short wavelengths ($10^{-12}\,\text{m} - 10^{-10}\,\text{m}$) and high frequencies ($3 \cdot 10^{20}\,\text{s}^{-1} - 3 \cdot 10^{18}\,\text{s}^{-1}$) [136] (see figure 1).
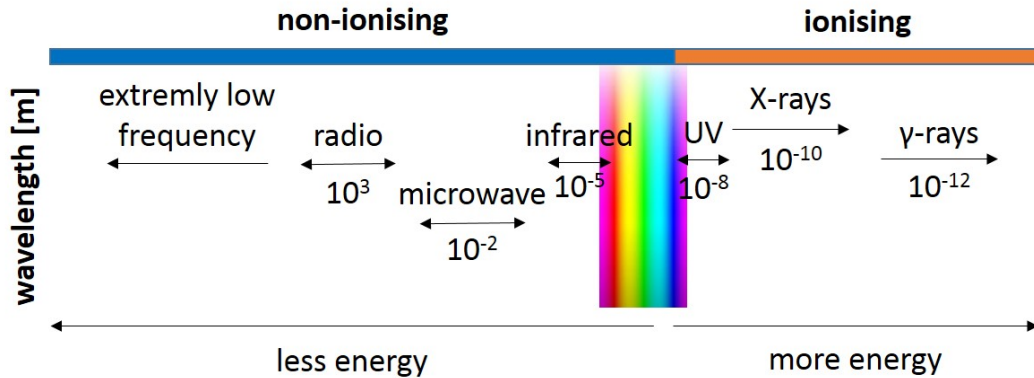
Figure 1: **Radiation spectrum**
X-rays and γ-rays are part of the continuous spectrum of electromagnectic radiation that also includes infrared, heat, visible and ultraviolet light. It is to be noted that high frequencies are related to low wavelengths.

Radiation is generally known to cause cancer but it can also be used to treat cancer. Since Wilhelm Conrad Röntgen discovered X-rays in 1895, which were later named after him, cancer therapy improved decisively [44]. Emil Grubbe was probably the first physician using X-rays for cancer treatment in the late 19$^{\text{th}}$ century [50]. Since then, photon irradiation has become a standard modality of cancer care. However, cancer incidences are still increasing and keep challenging researchers over decades. As approximately $50\,\%$ of all cancer patients receive radiation therapy, it is, besides surgery and chemotherapy, one important treatment modality [14]. In current medical applications, using photons or ions, both forms of ionizing radiation, energy is deposited into the targeted cells by ionization in the biological material.

3.3 Radiation damage and repair

According to Hall et al. the most critical cellular molecule that can be affected by ionizing radiation is deoxyribonucleic acid (DNA) [52]. The DNA is the carrier of the genome, encoded and stored in the nucleus of a cell. Usually, the DNA is constructed as a double

helix, built from nucleotides consisting of four bases (purines: Adenine and Guanine; pyrimidines: Thymine and Cytosine), the sugar molecule deoxyribose and a phosphate residue.
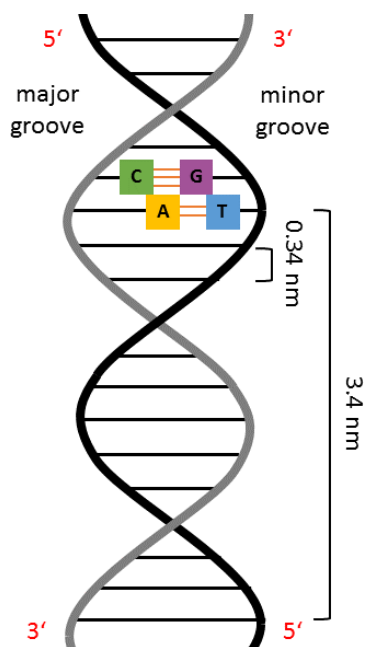
Figure 2: **Composition of the DNA**
The picture is a schematic drawing showing the composition of the DNA.

The genes in the DNA encode for the transcription of the ribonucleic acid (RNA), which is in turn the basic element for the construction of proteins. Three bases in the DNA encode for one amino acid. In order to format the well-known DNA double helix one purine and one pyrimidine (A-T; G-C) base connect via hydrogen bridge linkages, see figure 2. As the bondage always occurs between the same bases, the opposite base sequence can be predicted (complimentary base pairing) and the distance between the two strengths is regular. The helix has a diameter of $2\,\mathrm{nm}$ and after 10 bases one total turn ($360\,^{\circ}\mathrm{C}$) is completed ($3.4\,\mathrm{nm}$). Chromatin fibres organize the DNA in the nucleus, as one single chromosome holds one DNA double strand coiled around Histones [129].

Ionizing radiation can interact with the DNA in two different ways (see figure 3). Firstly, the interaction can be direct, with enough kinetic energy, disrupting the molecular structure and harming the DNA. Secondly, indirect by interacting with water or other organic molecules in the cell [52]. As a result, reactive intermediates can be formed (HO• or RO2•). Free radicals are very reactive and therefore may react with the DNA molecules, causing molecular damage. In the presence of oxygen hydrogen peroxide (H_2O_2) is formed. H_2O_2 is likewise toxic for the DNA. As $80\,\%$ of the cellular mass consist of water this type of radical interaction is of huge impact for the living cell [73].

DNA molecules can be damaged by ionizing radiation as DNA bases get modified or strands even break. Those DNA mutations cause changes in the genome, which lead to wrong base pairing or even lethal effects. There are varying levels of DNA damage (base damages, single- and double strand breaks, etc), leading to different severities in a cells' fate and repair capacity. Breakage in one DNA strand (single strand break (SSB)) has only little consequences for the cell, as the second strand can serve as a template for the repair. More dangerous for the cell are two single strand breaks which are located on both opposite DNA strands and lead to DNA double strand breaks (DSBs). Since those lesions often cause

misrepair or even remain unrepaired they are considered to be the reason for the biological consequences (e.g. cell death due to apoptosis or senescence) that can be observed after ionizing radiation. The formation of DSBs increases linearly with the radiation dose [77].
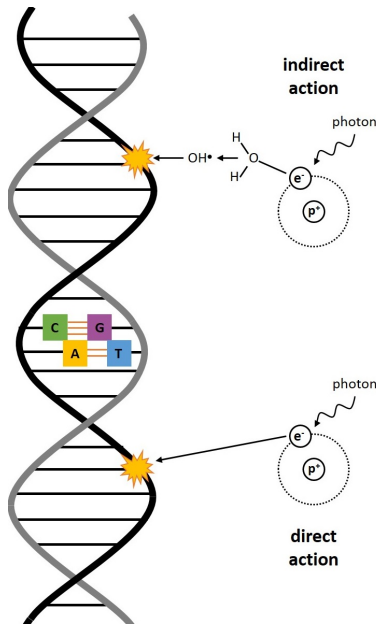
Figure 3: **Direct and indirect DNA damage**
The picture illustrates the two ways of interaction of ionizing irradiation with DNA causing DNA damage.

Because of the deleterious effects like genomic instability, carcinogenesis, etc., the damage to the DNA has to be recognized and repaired by the cell before the next mitosis.

Therefore, the cell has several DNA repair mechanisms. To provide enough time for repairing and preventing accumulation of damaged DNA, the cell cycle can be arrested in different phases by activating checkpoints [106]. Depending on the type of damage different repair pathways get activated. The two most important pathways are the non-homologous end-joining (NHEJ), responsible for most DSB repairs and the homologous recombination (HR) [18], see figure 4. NHEJ is a very fast but error-prone repair pathway and is mainly applied when the cell is in the G1-phase. Unlike HR, NHEJ does not require a homologous template as it ligates any free ends of DNA together. First, the ends of the DNA DSB have to be recognized by the NHEJ complex (Ku70/Ku80), which forms a ring around the DSB and attaches to its sugar backbone [127]. Once bound, the Ku heterodimer recruits other factors of the NHEJ complex like DNA-PKcs, X-ray cross complementing protein 4 (XRCC4), DNA Ligase IV, CRCC4-like factor and Aprataxin- and PNK-likefactor (APLF) [35]. The complex maintains the stability of the DSB ends by the protection of non-specific processing. In order to create compatible ends, DNA processing enzymes (like Artemis, PNKP, Polymerases μ and Λ, etc.) are required to resect the ends, fill gaps and remove endgroups. Eventually, the damaged strands are ligated via the DNA ligase IV and the NHEJ complex is released [35]. As NHEJ ligates any DNA ends together it is prone for chromosome aberrations and loss of information. On the other hand, HR is dependent on a homologous template (G2-phase). However, being slower than NHEJ HR is considered to be error-free. As the template is a sister chromatid, HR can only be active during S and G2 phase. NBS1 recognizes the DSB, recruits the MRN complex,

which again recruits ATM that, in turn, activates the histone H2AX by phosphorylation.
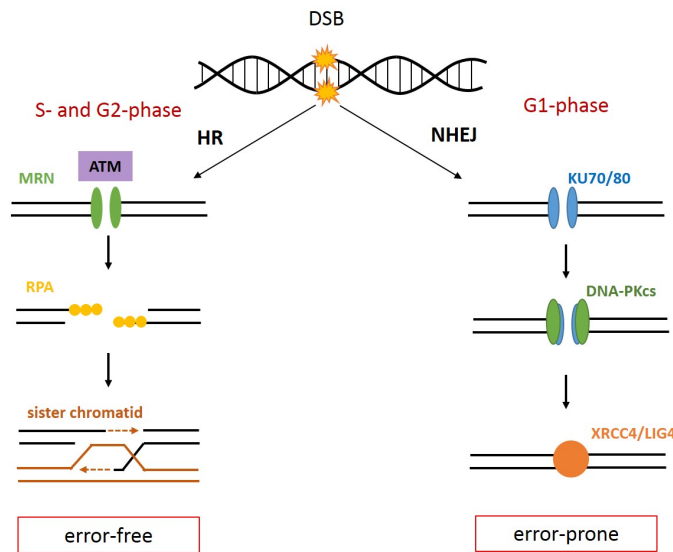
Figure 4: **Schemas of the major repair pathways**
The picture illustrates schematically the process of NHEJ and HR.

The phosphorylated γH2AX is a well-known marker for DSBs as it is detectable approximately 20 seconds after the DSB has occurred [105]. Once the Histone H2AX is phosphorylated, the MRE11-Rad50-NBS1 (MRN) complex is assembled, which resects the 5'-end and enables the formation of a short 3'-single-stranded DNA overhang. Another protein complex consisting of Rad51/Rad54 and the replication protein A (RPA) then binds to the 3' overhang to find a complementary sequence on the sister chromatid. Finally, the DNA polymerase synthesizes a new homologous strand.

Another important protein for the cellular response to DSBs is the p53 binding protein 1 (53BP1). 53BP1 recognises a specific histone code and is recruited to damaged chromatin within minutes after exposure to IR. The complete function of 53BP1 is not yet fully understood, however it is supposed, that after relocation to the site of the DNA strand break, 53BP1 becomes hyperphosphorylated and might function as a substrate for the ataxia telangiectasia-mutated (ATM) kinase [107]. The 53BP1 protein promotes the NHEJ pathway while preventing the HR [93].

3.4 High- and low-LET irradiation

The energy deposited per unit track length (KeV/μm) is defined as linear energy transfer (LET). High ionization densities mainly cause direct interaction, referred to as high-LET, while indirect interaction occurs already at low ionization densities [52]. Photons like γ- and X-rays exhibit low masses and low charges, hence they do not cause a lot of ionizations, during penetrating material, referred to as low-LET. The measure for ionizing radiation is the absorbed energy per mass with the SI derived unit Gray (Gy) named after Louis

Harold Gray, a British physicist and radiobiologist. 1 Gy is the quotient of the absorbed energy and the mass of matter (J/kg). As a rule of thumb 1 Gy of γ-rays causes 10^5 ionizations per cell, leading to 1000-2000 SSBs and 30-40 DSBs per nucleus [10]. Heavy ions like carbon ions and alpha particles are referred to as densely ionizing, have a high LET ($> 10\,\mathrm{keV}/\mu$m), cause more severe DNA damage and breaks in close proximity [72]. Additionally, high-LET irradiation demonstrated higher induction rates of mutations and chromosome aberrations. Hence, high-LET irradiation results in more unrepaired damages than low-LET irradiation as it has been proven [5, 57]. It can be concluded, that with increasing LET the DNA damage complexity is increasing and the DNA repair efficiency is decreasing [72].

The relative biological efficiency (RBE) compares the responses of two different radiation types, using the same biological outcome as it calculates the ratio of a certain dose of a reference radiation, causing a certain effect towards the dose of another radiation, which is necessary to cause the same biological effect. The RBE of charged particles is increasing up to a maximum of $100\,\mathrm{keV}/\mu$m by increasing the ionization density, thus the RBE is dependent of the applied dose and the LET [52]. The LET is dependent on the charge and velocity of the ions. Fast ions show a low LET and the RBE is comparable to X-rays. In contrast, slow and heavy ions show a high-LET and an enhanced RBE.
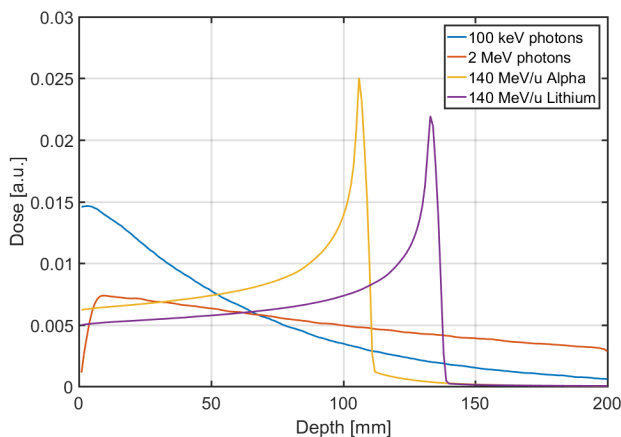
Figure 5: **Dose-depth profile**
Low-LET irradiation like X-rays and γ-rays deposit only small quantities of energy while positively charged particles like alpha rays and other heavy ions (e.g. Lithium) deposit more energy on targeted areas, referred to as Bragg Peak. Credits to Dr. Stefan Bartzsch, who simulated the curves in the image.

The enhanced RBE of heavy ions enables cell killing independent of the genetic background. For example approximately 50 % of tumor cells exhibit p53 mutations, thus decreasing apoptosis and increasing resistance to low-LET irradiation as it is dependent on this programmed cell death. Heavy ions, on the other hand, induce cell killing independent of apoptosis but via direct induction of clustered DNA damages [42]. The higher LET of heavy particles, compared to photons has been

credited to the different way of energy deposition during the penetration through matter. While most of the energy of X-rays is absorbed at the entrance followed by an exponential decrease of radiation dose with increasing depth, charged particles lose only a little energy at the surface and deposit most energy where they are supposed to stop in the tissue. Heavy ions and protons therefore show an inverse dose-depth profile, which exploits a maximal dose deposition at a certain depth, which is referred to as Bragg-peak [75], see figure 5.

In order to irradiate the whole tumor the Bragg Peak needs to spread out, thus beams of different energies are superimposed [42].

A typical radiation therapy for solid cancer takes 30-35 fractions of photon irradiation to deliver 60-70 Gy. In theory, every tumor could be controlled, if the dose could be maximized but side effects in the surrounding, healthy, normal tissue limit the applicable dose, hence the therapy success [42]. Therefore, sparing healthy tissue is indispensable to improve radiotherapy. Because of physical and radiobiological benefits high-LET irradiation is an emerging technique since 1950 when the first metastatic breast carcinoma was treated with charged particles [42]. Carbon ion centers have been build, e.g. in Germany (Heidelberg and Marburg), Italy (Pavia) and China (Shanghai and Lanzhou) and are currently under construction. Due to the size of the required linear acceleration the construction of treatment facilities are very expensive and require large areas. This limits an increase of further facilities being built and also causes ongoing debates about the cost/benefit ratio of high-LET irradiation. In 2010 already 5,000 patients were determined that would benefit from high-LET irradiation, by receiving a carbon ion treatment [42].

3.5   Glioblastoma multiforme therapy

A variety of different therapeutic strategies were applied in the past and resulted in a multimodal treatment concept combining surgery, chemo- and photon radiotherapy, referred to as Stupp scheme [115]. This concept suggests a first treatment phase, consisting of surgery plus daily low-dose Temozolomide (TMZ) plus daily photon irradiation (2 Gy per day for 5 consecutive days a week and 6 weeks up to 60 Gy in total). After 4 weeks of recovery the second phase of adjuvant chemotherapy, for six months, with TMZ is added. But still, despite this extensive treatment, the therapy of GBM remains poor as every therapy modality shows its own limitations [47].

The first step, surgical removal of the primary tumor, is often challenging for the neurosurgeon as the location of the primary tumor might also be inaccessible and surgery sets the patient at a high risk to suffer from neurological impairment. As the GBM is prone to infiltrate into the surrounding tissue tumor cells might infiltrate in the tumor microenvironment, making a complete tumor resection almost impossible (figure 6). Likewise, the effect of chemotherapy is limited, as due to the blood-brain-barrier only a few chemotherapeutics are accessible [122]. Temozolomide has certainly shown the largest benefit in terms of progression-free and overall survival [121]. The infiltrative feature of the GBM is a burden for radiotherapy. The currently applied radiation is low-LET photon (X-ray) irradiation. Tumor cells, which are infiltrating into the surrounding tissue, do not get the full necessary dose, therefore, they keep surviving and proliferating. Gliomas are known to follow a dose-response relationship however, toxicity limits dose-escalation. Next, to these limitations, GBM is

Figure 6: **MRI scans of a GBM**
The picture shows exemplary MRI scans of a patient with a right temporal GBM. A) shows the presurgical scan (arrow points to the GBM). B) is a scan after surgery and radiation therapy (clear cavity). C) is a MRI image six month later, with a recurrent- and a second tumor. D) is a scan after resection of the recurred primary and the second tumor. E)is a scan performed three month after resection of the two first tumors, showing the tumor recurring.
Image was taken from E. Holland, Glioblastoma multiforme: The terminator, published in PNAS, 2000; With kind permission from copyright (2000) National Academy of Sciences, U.S.A

considered to be highly radioresistant. This finding can be attributed to two properties of glioma cells. First, due to their infiltrative nature tumor cells might only receive sub-lethal doses and second, the cells utilize their repair mechanisms very efficiently [69].

Another possible reason for radio-resistance are cancer stem cells (CSCs), which are supposed to play a major role in tumor development and progression [24]. Tumors that exhibited lower amounts of CSCs have shown higher local control rates [13]. As CSCs have the potential for unlimited proliferation, they are able to repopulate the whole tumor [24]. Hence, it is essential to fully eradicate them to achieve success with anti-cancer therapies. Several studies have already proven, that incomplete CSC elimination can be attributed to the failure of radiotherapy [12, 39]. Surface markers like CD133, Nestin or Sox2 allow to identify and sort glioma cells for CSCs [8, 65].

As the GBM consists of a very heterogeneous cell population (e.g. cancer stem cells, genetic aberrant cells and oxygen deprived hypoxic cancer cells), each exhibiting distinct radiosensitivities, the effective radiation dose is quite variable but limited due to the surrounding healthy tissue [113]. Thus, the heterogeneous biology of GBM likewise limits therapy efficiency [47].

3.6   Molecular mechanisms of GBM

Despite huge effort that was put into the elucidation of underlying pathways and molecular changes that may explain the progress of the malignancy of gliomas after treatment, clinically, molecular markers are missing for the most part. By analyzing those molecular changes, the aim is to develop targeted therapies, thereby improving patient outcome. To date, few molecular markers in glioma have reached real clinical relevance. There is only one known correlation: the methylation of the promoter region of the O6-methylguanine methyltransferase (MGMT), which enables a prognosis concerning the response to TMZ. The MGMT is a protein which usually takes part in the repair of alkylated DNA. During DNA replication MGMT removes the methyl or alkyl adducts from the O6 position (O6-MG) of the guanine of the DNA, transferring it to a cysteine residue of its active side. Repair of O6-MG is therefore limited to the MGMT level of a cell. As DNA methylation mainly occurs at CpG-rich sites, MGMT serves as a perfect target [33]. MGMT promoter methylation causes reduced MGMT expression and therefore decreased activity. On the other hand, the alkylating agent TMZ adds alkyl or methyl groups to the O6 position of

guanine [103]. Approximately 50 % of GBM patients have an MGMT promoter hypermethylation, which was observed to result in good response to TMZ, therefore, show prolonged survival [55].

Furthermore, molecular classifiers of outcome include LOH of 1p19q, TERT, ATRX or IDH-1 or -2 mutations [111]. However, despite of their correlation with outcome non of them has resulted in a breakthrough in molecularly targeted treatments. Therefore, identifying molecular markers that can be correlated with specific phenotypes, such as invasion could be a promising approach.

3.7   Invasion

The primary cause of cancer mortalities is in 90 % tumor metastasis [110]. Since the discovery of extensive natural invasion as a hallmark of GBM, this is believed to be one reason for limited therapy success [96]. The infiltration of GBM is a highly complex, multi-step process that has not yet been fully understood. Several molecular pathways, microRNAs and genetic modifications have been reported to facilitate GBM invasion. Despite huge improvements in technology, GBM still recurs within 1-2 cm of the primary tumor cavity [56]. While other aggressive tumors have shown to metastasize into other organs, GBM has rarely been observed to spread outside the brain. As the invasive process of GBM seems to play such a fundamental role in tumor progression it is indispensable to analyse the reasons for GBM motility.

Invasion can be observed as a single, mesenchymal or amoeboid cell or as clustered cell collective. GBM has majorly been observed to infiltrate via the amoeboid way, expressing several proteases [123]. But typically, GBM cells underlie several biological changes that cause mobility and degradation of Extracellular matrix (ECM) in order to be capable to migrate through the extracellular space [96]. Alterations of the cell shape, like morphological polarization and development of membrane protrusions, are the first steps of invasion [31] followed by the interaction with components of the ECM. Physical interactions like anchoring to ligands of the ECM, using them as a direction sign, pulling themselves forward but also chemical interactions are a common phenomenon of GBM cells [22]. In order to degrade the ECM several proteolytic enzymes have been suggested, headed by Matrix-Metalloproteinases (MMPs) [117].

Another important mechanism to enable invasion is the epithelial to mesenchymal tran-

sition (EMT). The EMT is characterized by cells, losing their epithelial characteristics
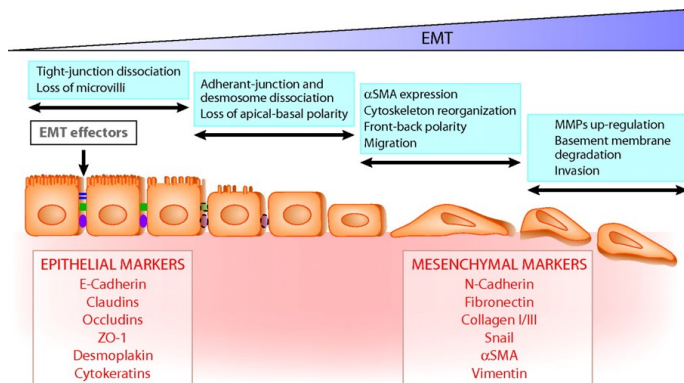

Figure 7: **Key-events of epithelial-to-mesenchymal transition(EMT)**
The picture illustrates the four key-events of epithelial-to-mesenchymal transition and the most common epithelial as well as mesenchymal markers. Image was taken from the journal of the american society of nephrology, with kind copyright permission by ASN.

while gaining more mesenchymal properties, see figure 7. EMT is transient and reversible and can be differentiated into 3 subtypes. The first subtype is EMT during development, second, during wound healing and third, EMT during cancer metastasis [68]. During the EMT cells lose their cell-cell contacts by disassembly of tight- and adherens junctions while underlying several cytoskeletal changes which promote cell migration. Epithelial genes get suppressed and mesenchymal genes are favoured. MMPs, as well as N-Cadherin or integrin's, are increased as they facilitate cell motility [68].

In connection with the EMT the protein kinase B (AKT), as a central feature of EMT became a more relevant research object, studying invasion [22]. AKT activation revealed to play a major role in cancer cell invasion as it down-regulates epithelial markers like E-Cadherin [82]. AKT plays an important role in the PI3K/AKT/mTOR pathway, which is an intracellular signaling pathway and a major regulator of the cell cycle. Phosphorylated PI3K activates AKT which is then localized in the plasma membrane, where it can have several downstream effects [96]. Seoane et al. [109] could show that if the PI3K-AKT pathway is hyperactive in GBM, another relevant pathway in glioma invasion, the TGF-β pathway, looses its response. Usually, the TGF-β, a cytokine, binds and activates the membrane receptor serine/threonine kinase complex, thereby phosphorylating SMAD2/3. SMAD2/3 in turn accumulates in the nucleus and regulates the transcription [17]. TGF-β was shown to play a dual role, it can act as a tumor suppressor or an oncogene. It was shown to influence tumor cell proliferation and invasion of several cancer types e.g. glioblastoma multiforme [38, 53]. But also pathways like the canonical Wingless/Int1 (Wnt) signaling (also referred to as β-Catenin dependent pathway) have been proposed to play an important role in the invasion of GBM, as this pathway primarily regulates cell motility and polarity [96]. The Wnt protein binds to its receptor Frizzled, as well as to the co-receptor

low-density-lipoprotein-related protein 5/6 (LRP5/6), thereby activating the protein disheveled which in turn inhibits the protein complex glycogen synthase kinase-3β (GSK3β), adenomatous polyposis coli (APC) and Axin-1. This complex usually degrades β-Catenin but as the complex is inhibited, β-Catenin degradation is enriching in the cytoplasm, as well as in the nucleus. The accumulated β-Catenin then forms a complex with T-cell factor (TCF)/ lymphoid enhancer factor (LEF) and activates specific target genes like MMPs [96]. In general, several players of the β-Catenin-dependent pathway have been shown to play a major role in GBM invasion [96].

3.8 Radiation-enhanced invasion

In 1991, the first evidence showed that the currently applied photon irradiation might favour the invasive capacity of GBM [124]. Since then the low-LET irradiation-enhanced invasion of GBM has been shown several times [36, 43, 90, 101]. However those findings are controversially discussed [45, 49, 135]. Although low-LET irradiation is the standard of radiation treatment of GBM, high-LET irradiation can also be applied [57]. That high-LET irradiation has beneficial physical, biological and potential clinical advantages has been proven long time ago [99, 108]. Furthermore, there are several clinical studies showing the advantage of high-LET irradiation on progression-free as well as the overall survival of GBM patients [26, 87].

Up to date, GBM grading, the Karnofsky Index, as well as several molecular alterations were used to predict patient outcome. However, as already discussed, not all patients benefit equally from all therapy concepts, some patients even show adverse effects from the GBM treatments [92]. The radiation-enhanced migratory and invasive capacity of glioma cells is an important but barely understood component causing the poor prognosis of glioma patients. Since basically all glioma patients are treated with low-LET irradiation, radiation-enhanced invasion might play a critical role in patient survival.

Several *in vitro* studies showed that the influence of irradiation on the invasion is divergent [7, 36, 45, 49]. The controversial data might be attributed to the natural heterogeneity of glioma cells. Furthermore, the different radiation-response demonstrates that there is a need for a personalized radiation treatment concept. Thus, considering future glioma therapy a more personalized-treatment concept may be essential. In this thesis "the RadGlio trial" was established to gain patient-derived primary cells from tumor tissue. With this

translational concept basic research can be performed on patient-derived primary cells that may help finding an improved and personalized glioma therapy. Finally, being able to differentiate between patients benefiting from photon irradiation and those showing adverse effects, limiting their therapy success, might help to improve patient outcome.

Additionally, a deeper knowledge of the GBM biology is necessary to understand the molecular events that lead to (radiation-enhanced) GBM invasion. To avoid radiation-promoted invasion it might be promising to identify molecular markers correlating with specific phenotypes, such as invasion. Being able to differentiate between patients benefiting from photon irradiation and those showing adverse effects, which limits their therapy success, might help to improve patient outcome. In summary, these findings demonstrate, that further molecular and cellular investigations are of clinical importance to improve GBM treatment.

4   Hypothesis and research questions

The goal of this thesis was to improve glioma treatment by optimization of the radiation treatment which does not increase the invasion of GBM cells. Therefore, this study compared the effects of low- and high-LET irradiation on the invasion of three established human GBM cell lines, as well as on primary patient-derived tumor cell lines.

In this thesis four research questions were examined on glioma cell lines:

1.) Does patient-specific invasion exist?

2.) Does radiation-induced invasion exist?

3.) Can the invasive capacity be correlated with patient outcome?

4.) Does high-LET irradiation offer advantages for glioma therapy?

5   Material and Methods

5.1   Study protocol

The RadGlio trial ("Strahlenbiologische Untersuchungen an Glioblastomen für Forschungs-zwecke"), referred to as RadGlio trial, was founded to analyse primary patient-derived glioma cell lines for their invasive capacity with the objective of optimizing glioma therapy. The study was performed in cooperation with the neurosurgery of the Klinikum rechts der Isar and in accordance with the ethical standards of the institutional research committee. The RadGlio study is a non-randomized, unicentric, prospective trial that recruited glioma patients over a period of 36 months. A glioma primary tumor or a relapse were decided as a prerequisite for participation. Furthermore, patients had to be at least ≥ 18 years of age and had to agree to a patient information. Pregnant or breast-feeding women were excluded, as well as patients with non-resectable tumors. After isolating primary cells from patient-derived tumor tissue, primary glioma cell lines were established and could be used for further analyses and correlations with clinical data. In total 67 patient-derived tumor samples from the RadGlio trial were dissected to obtain primary glioma cells (see Fig. 8).

| GBM patient | tumor cell isolation | primary cell cultivation | validate glial origin | irradiation | perform invasion analysis |
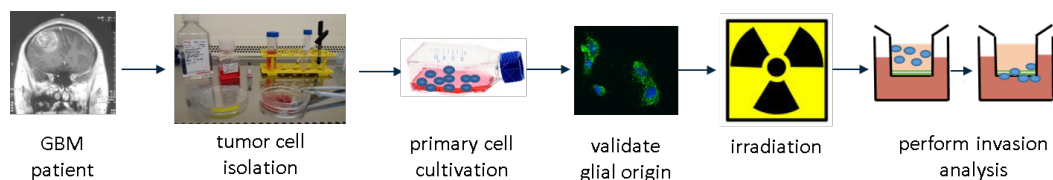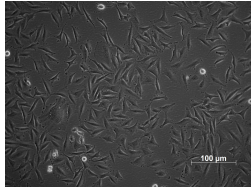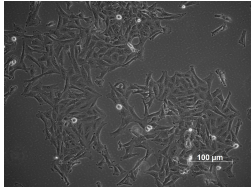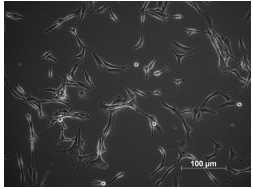
Figure 8: **The RadGlio trial**
Picture shows the schematic process of the RadGlio trial.

5.2   Cell culture and cell characterisation assays

Established human glioblastoma cell lines were obtained from the University Hospital of Heidelberg. Cell line authentication was performed by Eurofins Genomics, Germany. LN229 and LN18 were cultivated in RPMI-1640 (#R8758, Sigma) supplemented with 10 % FCS (#F7524, Sigma) and 1 % penicillin/streptomycin (#P0781, Sigma) (P/S). U87 was maintained in DMEM supplemented with 10 % FCS and 1 % P/S. Human fibroblasts deriving from a neuroblastoma, MC-IXC, were purchased from ATCC. The fibroblasts were cultured in a 1:1 mixture of EMEM (#30-2003, ATCC) and F12 Medium (#30-2006, ATCC) supplemented with 10 % FCS and 1 % P/S. Colorectal adenocarcinoma cells,

CaCo2, were cultured in EMEM (#30-2003, ATCC), supplemented with 20 % FCS and 1 % P/S. CHO-K1 cells were cultivated in RPMI-1640 supplemented with 10 % FCS, 1 % P/S, 1 % L-Glutamine and 1 % sodium pyruvate. All cells were kept at 37 °C in a controlled atmosphere with 5 % CO_2 and 95 % humidity.

Table 1: Characteristics of the established cell lines

	LN229	LN18	U87
Organism	homo sapiens, human	homo sapiens, human	homo sapiens, human
Tissue	brain, frontal right	brain, cerebrum	brain
Disease	GBM IV	GBM IV	likely glioblastoma
p53	mut	mut	wt
PTEN	wt	wt	mut
p16	del	del	del
Morphology	epithelial, adherent	epithelial, adherent	epithelial, adherent
Image			

5.2.1   Primary cell isolation from patient-derived tumor tissue

Primary GBM cells were obtained from the RadGlio trial, a study found by myself in cooperation with the neurosurgery of the Klinikum rechts der Isar.

Patient-derived tumor tissue was mechanically cut into small pieces and enzymatically digested in a mixture consisting of DNase (2000 u/ml, #LK003170, Worthington) and Papain (20 u/ml, #LK003176, Worthington) both dissolved in Earle's Balanced Salt Solution (EBSS, #LK003188, Worthington) and incubated at 37 °C for 30 minutes. Papain is known for brain dissociation in order to keep neurons at maximum vitality. Enzymatic activity was stopped with an Ovomucoid inhibitor (10 mg/ml, #LK003182, Worthington) followed by an erythrocyte lysis (VersaLyse, #A09777, Beckman Coulter) for further 20 minutes. Afterwards cells were transferred through a 70 μm and 40 μm filter into a GelTrex or Matrigel coated plastic flask. The coating material was dependent on the tissue composition, e.g. if tissue was rich in necrotic areas cells attached more successfully to matrigel coated flasks compared to GelTrex coated flasks. Exemplary morphologies are shown in figure 9.
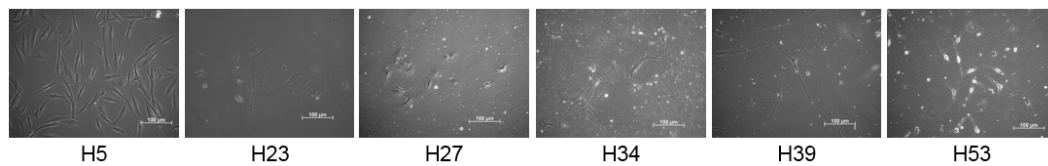
Figure 9: **Exemplary primary glioma morphologies**
Shown are exemplary pictures of the different morphologies of the freshly-isolated patient-derived primary glioma cells

Primary cells generated from patient-derived tumor tissue were cultivated in RPMI-1640 (#R8758, Sigma) supplemented with 10 % FCS (#F7524, Sigma) and 1 % P/S (#P0781, Sigma). All cells were kept at 37 °C in a controlled atmosphere with 5 % CO_2 and 95 % humidity. Patient-derived tumor tissue was analysed by the pathology of the Klinikum rechts der Isar for histopathological features. Results are listed in table 2. Not determined values are signed with n.d..

Table 2: Characteristics of the primary cell lines. Glioblastoma mulitforme is abbreviated by GBM, Astrocytoma by Astro. and Oliogdendroglioma by Oligo.. Subtypes are abbreviated as diff. for diffuse, pilocyt. for pilocytic and anaplast. for anaplastic. Isocitrate dehydrogenase (IDH) expression was marked with wild-type (wt) or mutated (mut). If the expression was not determined, the column is marked with n.d. R stands for relapse.

#	WHO class.	IDH	MGMT [%]	1p19q codeleted	relapse
T75	GBM IV	wt	0	n.d.	
T76	GBM IV	wt	0	n.d.	
T84	GBM IV	wt	16.9	n.d.	R
H5	GBM IV	wt	0	n.d.	
H19	GBM IV	wt	1	n.d.	
H33	GBM IV	wt	0	n.d.	
H34	GBM IV	wt	0	n.d.	
H41	GBM IV	wt	45	n.d.	
H46	GBM IV	wt	100	n.d.	
H1	Astro. II	wt	0.3	not	
H23	diff. Astro. II	mut	25	not	
H24	pilocyt. Astro.	wt	n.d.	n.d.	
H27	diff. Astro. II	mut	4	n.d.	
H37	Astro. II	mut	20	yes	R
H45	Astro. II	mut	27	not	
H9	anaplast. Oligo. III	mut	59	n.d.	R

5.2.2   Coating of primary cell culture flasks

Freshly isolated primary glioma cells grew mainly as free-floating spheroids, therefore commercially available cell culture flasks needed additional coating in order to attach primary cells to the flask bottom. Only attached cells can be irradiated homogeneously, as this is a prerequisite to ensure equal dose distribution. Therefore, matrigel (20.7 mg/ml, #354248, Corning) or GelTrex (15 mg/ml, #A14132-02, Gibco) were thawed on ice, diluted in pure, cold RPMI (Matrigel 1:62.5; GelTrex 1:100) using cold tips and plated as a thin (0.5 mm) layer on the cell culture flasks. After a 30 min incubation period at 37 °C, 5 % CO_2 and 95 % humidity the remaining coating liquid was removed and the flasks were washed with PBS supplemented with Ca^{2+} and Mg^{2+} (#14040-133, Gibco). Prepared flasks containing PBS were sealed with parafilm and stored for up to two weeks at 4 °C.

5.2.3   GFAP staining

$2 \cdot 10^4$ cells were seeded on a sterilized cover slip. The next day cells were fixed with 4 % paraformaldehyde (PFA) for one hour. After two PBS washing steps, blocking buffer consisting of 1 % BSA and 0.1 % Triton X-100 in PBS, was applied for 60 minutes. The primary antibody (GFAP rabbit-anti-human, #Z0334, DAKO) diluted 1:500 in blocking buffer with the addition of 2.5 % normal goat serum was incubated on the primary cells overnight at 4 °C. The following day the secondary antibody (Alexa-488 anti-rabbit, #A11008, life technologies), diluted 1:500 in PBS, was allowed to bind for one hour at room temperature. After another PBS washing step, mounting medium with 4',6-Diamidin-2-phenylindol (DAPI) (#H-1200, Vectashield)was used to mount the microscope slide. Images were taken using the Axioskop 2 plus (Zeiss) at 20x magnification.
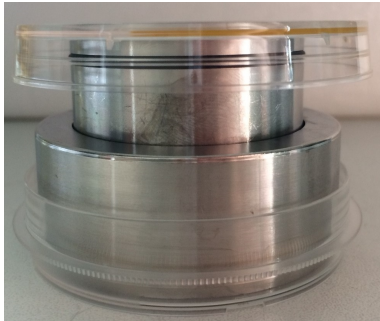
5.2.4   The ring system

Figure 10: **The ring system**
The upper and lower ring clamp
the PP foil. The ring system
is stored in 6 cm petri-dishes to
keep cells sterile.

Cells were cultured in regular cell culture flasks. Before experiments were performed, cells were seeded and irradiated in the ring system (see figure 10) to enable irradiation in the alpha irradiation source as well. Therefore, two metal rings were assembled with a polypropylene (PP) foil ($4.7\,\mu$m) in between, measuring an attachment area of $10\,\text{cm}^2$. For better cell attachment the foil was coated with CellTak ($1\,\mu$g/cm^2, #FALC354241, Corning). Cells were seeded 24 hours prior to irradiation at a density of $4 \cdot 10^5$ cells and allowed to attach for 24 hours at $37\,^\circ$C before experiments were performed.

5.2.5   Colony formation assay (CFA)

Rings were prepared and cells were seeded as described before. Five rings were irradiated per dose and immediately after irradiation plated into three 12-well plates. For higher doses, higher cell seeds were applied. 12 days after plating colonies were fixed with ice-cold methanol and stained with 0.1 % crystal violet. Finally, 180 wells were evaluated per dose. Colonies consisting of at least 50 single cells were counted as one colony. Counting was performed manually and survival curves were fitted according to the linear quadratic model with the equation $\ln SF = -\alpha \cdot D - \beta \cdot D^2$. Each CFA was performed twice (n = 2).

5.2.6   CFA with drop-seeded cells
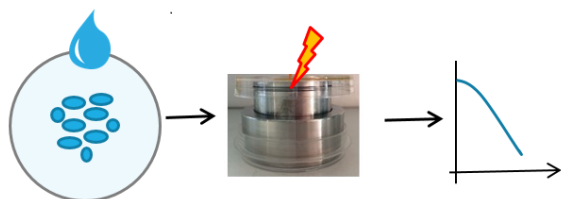

Figure 11: **Drop seeding procedure**
Illustration of the CFA with cells that were only
seeded in the ring centre.

To exclude inhomogeneous irradiation caused by cells attaching to the outer boarder of the ring system, therefore not being irradiated but trypsinized and seeded for the CFA, another CFA with cells only seeded in the ring centre was performed and analysed (see figure 11).

5.2.7   CFA with non-cancerogeneous cells

The CFA with CHO-K1 cells was performed likewise but only $2 \cdot 10^5$ cells were seeded per ring and incubation time till fixation was shortened to 5 days after irradiation.

5.2.8   CFA to compare plastic and ring system

For comparing cell culture flasks and the ring system $4 \cdot 10^5$ cells were seeded 24 hours before irradiation into $3 \cdot 6$ T25 flasks or $3 \cdot 6$ rings. A CFA was performed as described before. The survival fractions of colonies from plastic culture flasks were compared to the surviving populations from the ring system.

5.2.9   Cell size measurement

Cells were seeded as described before in the ring system. 24 hours after seeding supernatant was removed, cells were washed with PBS and Höchst (10 mg/ml,#H-33342, Sigma) was applied. 10 minutes after incubation with Höchst, diluted 1:2000 in PBS, cells were measured with the Zeiss Axio Observer Z1 with 20x magnification. Two ring systems of each cell line were stained and 500 cells of each ring were measured. Size measurements were performed with a script in ImageJ, written by Dr. Judith Reindl.

5.2.10   Doubling time calculation

24 hours before irradiation $4 \cdot 10^5$ cells were seeded in the ring system and allowed to attach at 37 °C. Immediately after irradiation cells were harvested from the ring system and $2 \cdot 10^4$ cells were seeded in 12-well plates. Every 24 hours after seeding, for up to 4 days, cells were detached from three wells with trypsin and counted with a Neubauer counting chamber. Doubling times (t2) were calculated with the formula t2 = duration $\cdot$ log(2)/(log(final) $-$ log(initial)).

5.2.11   CD133 FACS analysis

$2 \cdot 10^5$ cells of each cell line, cultured in cell culture flasks, were collected in two FACS tubes (one for the antibody and one for the IgG control) and washed with 500 μl FACS buffer, consisting of PBS supplemented with 10 % FCS. Cells were stained with CD133/1-VioBright

FITC, human (#130105226, Miltenyi Biotec) diluted 1:5 in FACS buffer or pure IgG1-PE (X40) (#345816, BD) for 30 minutes at 4 °C. In order to analyse the samples another washing step was performed and cells were resuspended in FACS buffer supplemented with propidium iodide (1 mg/ml, #537059, Calbiochem). Cells were detected with the BD FACSCalibur™ (Becton Dickinson, USA). Analysis was performed using the CellQuest Pro™ 6.0 Software. Only viable (propidium iodide negative) cells were analysed for CD133 expression.
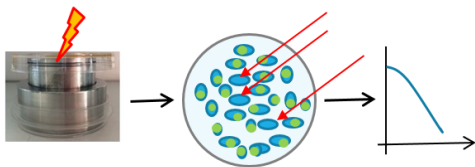
5.2.12 γH2AX foci assay

Figure 12: γ**H2AX staining in the ring system**
Illustrated is the procedure of the γH2AX staining in the ring system to exclude inhomogeneous irradiation.

In order to exclude inhomogeneous irradiation of the α-particle device LN229 cells were seeded in the ring system as described above (see figure 12). 30 minutes after irradiation with 3.2 Gy α-particles, cells were washed with PBS and fixed with 2 % paraformaldehyde (PFA) for 15 minutes in the ring system. After another PBS wash cells were permeabilized with 0.15 % Triton X-100. Unspecific binding was blocked using a blocking buffer, consisting of PBS, 0.15 % Glycine and 1 % Bovine Serum Albumin (BSA). Samples were incubated with the primary antibody H2AX clone JBW301 (#05-636, Millipore), diluted 1:300 in blocking buffer, overnight at 4 °C. The next day cells were washed with PBS, treated with 0.15 % Triton X-100, as well as blocking buffer prior to addition of the secondary antibody, Alexa Fluor 488 goat-anti-mouse (#A11017, Invitrogen), diluted 1:500 in PBS, for one hour at room temperature. Samples were washed with PBS and remaining liquids were removed to finally apply the mounting medium supplemented with DAPI. The total area of the ring was checked for cells that do not exhibit any γH2AX signal with the Zeiss Axio Observer Z1 at a magnification of 20x. Additionally, to keep the procedure more close to the protocol of the CFA, another γH2AX Foci assay was performed. Therefore, cells were seeded in the ring system as usually and irradiated with 3.2 Gy α-particles. Comparable to the procedure in the CFA assay, cells were trypsinized from the ring system immediately after irradiation, seeded to coverslips and allowed to attach for 4 hours. Afterwards cells were fixed and stained as described above.

5.2.13   53BP1 foci assay

24 hours prior to irradiation $4 \cdot 10^5$ cells were seeded in the ring system and allowed to attach at $37\,°C$ in a humidified incubator. 30 minutes as well as 24 hours after irradiation cells were washed with PBS and fixed with 2 % paraformaldehyde (PFA) for 15 minutes. After another PBS wash, cells were permeabilized with 0.15 % Triton X-100. After blocking unspecific bindings with a blocking buffer consisting of PBS, 0.15 % Glycine and 1 % Bovine Serum Albumin (BSA), three circles of approximately 1 cm were marked with an ImmEdge Pen (#H-4000, Vector Laboratories) on the PP-foil of the ring system and the primary antibody (53BP1 rabbit, #NB100-035, Novus), diluted 1:300 in blocking buffer was allowed to incubate over night at $4\,°C$ in a humidified chamber. The next day cells were washed with PBS, treated with 0.15 % Triton X-100 as well as blocking buffer prior to addition of the secondary antibody mixture (Alexa-555 goat anti-rabbit, #A21429, life technologies, 1:500 in PBS), for one hour at room temperature. The PP-foil was cut out of the ring system using a sharp scalpel and placed on extra-large microscopy slides (75x50 mm, #2947-75X50, Corning). The remaining liquid was removed and mounting medium with DAPI was applied. Slides were sealed with nail polish and images were taken with 10x magnification at the Axioskop 2 plus (Zeiss). Foci of 300 cells were counted and calculated relative to the foci count of sham irradiated cells.

5.2.14 γH2AX flow cytometry

Cells were seeded in the ring system as described above. 6 hours and 24 hours after irradiation cells were trypsinised from the ring system and fixed with 2 % PFA for 15 minutes at room temperature. After a PBS washing step, a 0.5 % Triton X-100 solution permeabilized the cells for 15 minutes at room temperature. After another washing step, 0.4 % BSA in PBS was applied for one hour to block unspecific binding. Cells were resuspended in primary antibody (1:500 in PBS; mouse monoclonal anti-phospho-Histone H2A.X Ser139 primary antibody clone JBW301; Millipore) and incubated for 1 hour at room temperature. After a PBS wash, cells were stained with the secondary antibody, Alexa 488 goat-anti-mouse (F(ab)2 conjugate, Invitrogen, #A11017), diluted 1:500 for 45 min at room temperature. Finally, cells were washed in FACS buffer (PBS + 10 % FCS) and analysis was performed using the FACSCalibur$^{\text{TM}}$(Becton Dickinson, USA). The CellQuest Pro 6.0 Software was used to determine the mean-fluorescence intensity of the γH2AX signaling.

5.2.15   Cell cycle distribution

24 hours after irradiation cells were collected from the ring system by trypsinization, centrifuged at 500 g for 5 min at 4 °C and the supernatant was discarded. Cell pellets were resuspended in cold PBS and transferred dropwise to ice-cold ethanol (70 %). Cells were fixed for at least 24 hours at -20 °C. Afterwards, fixed cells were pelleted at 500 g for 5 min at 4 °C. Pelleted cells were stained with a PI staining solution (0.02 mg/ml PI (#537059, Calbiochem) + 0.1 % Triton X-100 (#T8787, Sigma) in PBS + 0.2 mg/ml DNase free RNase A (#R4875, Sigma) for one hour at room temperature. After the staining procedure cells were detected by FLOW cytometry (BD FACSCalibur^{TM}Becton Dickinson, USA) and cell cycle distribution was analyzed with the ModFit LT software, Verity Software House Inc..

5.2.16   Invasion assay

The invasive potential was measured using matrigel coated invasion inserts (#354480, Corning) stored at -20 °C. After equilibrating the inserts for 15 minutes to room temperature, 0.5 % serum containing medium was loaded into the lower and upper chamber of the insert. The matrigel^{TM}coated membranes were rehydrated for two hours in the incubator. Meanwhile, cells seeded in the ring system were washed two times in serum free
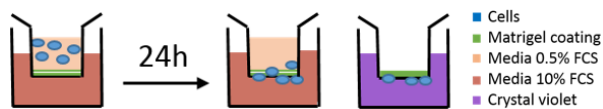

Figure 13: **The invasion assay**
Picture illustrates the typical process of the invasion assay.

medium, counted and adjusted to $2 \cdot 10^4$ cells/insert. Rehydration medium was carefully removed from the inserts and medium containing 10 % FCS (chemoattractant) was filled into the lower chamber. The upper chamber was loaded with the cell suspension supplemented with 0.5 % FCS and allowed to invade in a humidified tissue culture incubator at 37 °C. After 24 hours non-invaded cells were removed on the upper side of the chamber using a cotton tip. Invaded cells on the lower side of the membrane were fixed with ice-cold methanol and stained with 0.1 % crystal violet, see figure 13. Membranes were cut out off the insert and transferred onto a glass slide were they were fixed with Eukitt$^®$ Quick-hardening mounting medium (#03989, Sigma). Five independent microscope fields of each membrane were acquired for counting, using a Zeiss Imager Z1 microscope at 10x magnification. Relative invasion was normalized to human fibroblasts deriving from a neuroblastoma.

5.2.17 Radiation dependent invasion

Directly after irradiation the standard medium in the ring system was exchanged by medium containing 0.5 % FCS (serum starvation). 24 hours after irradiation, 8 μm pore sized control inserts control (#354578, Corning) and matrigel coated invasion inserts (#354480, Corning) were used as described above. The invasion was calculated as the mean number of cells, invading through the matrigel coated membrane divided by the mean number of cells migrating through the uncoated membrane (control insert). Relative invasion of irradiated cells was normalized to sham irradiated cells.

5.3   Cell irradiation
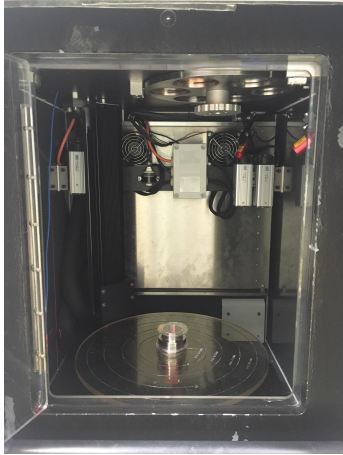
5.3.1   Low-LET irradiation

Figure 14: **Ring system in the X-ray irradiation device**
The picture illustrates the ring system as it was irradiated in the Gulmay RS22A.

Low-LET X-ray irradiation was performed either using the RS225A irradiation device (Gulmay/Xstrahl, UK) at a dose rate of $1\,\mathrm{Gy/min}$ ($15\,\mathrm{mA}$, $200\,\mathrm{kV}$) or the clinical linear accelerator (ONCOR, Siemens) at a dose rate of $3\,\mathrm{Gy/min}$ ($6\,\mathrm{MV}$ photons with $2\,\mathrm{cm}$ water-equivalent build-up). As both sources deliver low-LET photon irradiation (LET $<$ $2\,\mathrm{keV}/\mu\mathrm{m}$) the radiobiological differences are very small and could be neglected. Radiation with the RS225A could be performed with the ring system (see figure 14) as described before. For irradiation at the clinical linear accelerator conventional cell culture flasks were applied.
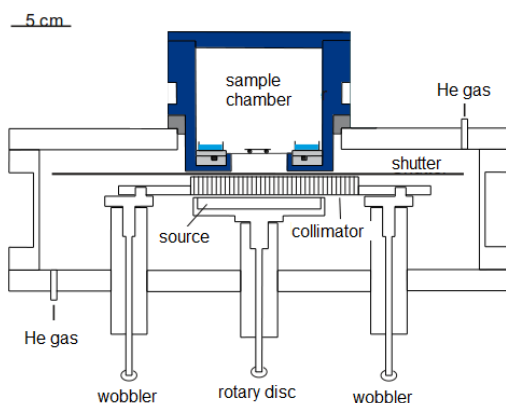
5.3.2   High-LET irradiation

Figure 15: **α-particle irradiation device**
The picture illustrates the composition of the α-particle irradiation device.

Cells were seeded $24\,\mathrm{hours}$ prior to irradiation at a density of $4 \cdot 10^5$ cells per $10\,\mathrm{cm}^2$ in a ring system to enable irradiation in the alpha irradiation source. High-LET α-particle irradiation was performed using an especially designed cell irradiation platform [17], which uses Americium-241, emitting α-particles with an energy of $5.49\,\mathrm{MeV}$ (LET $=$ $85\,\mathrm{keV}/\mu\mathrm{m}$). An activity of $0.37\,\mathrm{GBq}$ and an energy of the particles at the cell surface of $2.7\,\mathrm{MeV}$ (LET $= 146\,\mathrm{keV}/\mu\mathrm{m}$) caused a dose rate of $0.12\,\mathrm{Gy/min}$. The additional dose of secondary X-rays, applied to the cells, is 10^{-4} of the α-particle dose and can therefore be neglected. The fluence of the α-particles was

determined by irradiation and etching of CR39 plastic nuclear track detectors and resulted in (4.68 ± 0.03) $10^{-3}\mathrm{min}^{-1}\mu\mathrm{m}^{-2}$. Applying a dose of $1.3\,\mathrm{Gy}$ leads to (50.7 ± 0.4) $10^{-3}\mu\mathrm{m}^{-2}$. Measurements of cell size showed a mean nucleus size of $150\,\mu\mathrm{m}^2$, which causes 7.60 ± 0.06 hits per nucleus, according to Poisson statistics. Thus, $94\,\%$ percent of cell nuclei get at least a dose of $0.5\,\mathrm{Gy}$ whereas $0.5\,\%$ of the cell nuclei are not hit.

5.4   Molecular biology

5.4.1   Quantitative Polymerase Chain Reaction (qPCR)

Cells were seeded and irradiated in the ring system as described above. Immediately after irradiation cells were serum starved for 24 hours. Cells of two rings were pooled and total RNA was isolated by using the RNeasy Mini Kit (#74104, Qiagen) for established cell lines respectively the RNeasy Plus Micro Kit (#74034, Qiagen) for primary cells. $1\,\mu\mathrm{g}$ RNA of established cells respectively $0.5\,\mu\mathrm{g}$ were used for cDNA transcription with the QuantiNova Reverse Transcription Kit (#205410, Qiagen). SYBR Green qPCR amplification and detection was performed with the QuantiNova SYBR Green PCR Kit (#208152, Qiagen) in the 96-well LightCycler R480 (Roche). For a detailed description of the applied primer pairs see table 3. Relative gene expression was calculated via the $\Delta\Delta Ct$ method. Beta-Actin (Actβ), β-2Microglobulin (B2M) and Glyceraldehyde 3-phosphate dehydrogenase (GAPDH) were used as housekeeping genes, as the expression of those genes is known to remain constant after irradiation. The mean of the housekeeping genes was subtracted from the single cp-values of the samples.

Table 3: List of primers for potentially relevant genes for invasion

Gene symbol	Cat. no.	Manufacturer
ACTB	QT00095431	Qiagen
B2M	QT00088935	Qiagen
CDH1	QT00080143	Qiagen
CSTA	QT00241038	Qiagen
CTSA	QT00087381	Qiagen
CTSD	QT00020391	Qiagen
GAPDH	QT00079247	Qiagen
MMP2	QT00088396	Qiagen

Table 3: Continuation primer list

Gene symbol	Cat. no.	Manufacturer
MMP3	QT00060025	Qiagen
MMP10	QT00001470	Qiagen
PLAU	QT00013426	Qiagen
SerpineB8	QT00059822	Qiagen
Serpine1	QT00062496	Qiagen
TIMP1	QT00084168	Qiagen
TIMP2	QT00017759	Qiagen

5.4.2 EMT RT^2 Profiler

After isolating the RNA as described above $0.5\,\mu$g were used for cDNA transcription with the RT^2-first strand kit (#330401, Qiagen) according to manufacturer's instructions. The generated cDNA was pipetted together with the RT^2 SYBR Green qPCR Mastermix (#330500, Qiagen) into pre-coated EMT-RT^2 Profiler 96-well plates and measured according to manufacturers instructions. Only Act-β, GAPDH and B2M were used as housekeeping genes. The mean value of their ct-value was subtracted of the sample ct-values. As described above the relative gene expression was then calculated via the $\Delta\Delta Ct$ method.

5.5 Protein biochemistry

5.5.1 Pierce BCA Protein Assay

The Pierce BCA Protein Assay (#23225, Thermo Scientific) was used according to manufacturers instructions. Standard dilution was 2000, 1500, 1000, 750, 500, 250, 125, $25\,\mu$g/ml. A 4-parameter fit was applied to calculate sample concentration. For cell lysates RIPA buffer served as standard diluent and blank, whereas for supernatant samples serum free RPMI-1640 was used.

5.5.2 Proteome Profiler

$4\cdot 10^5$ cells were seeded in the ring system and irradiated as described above. Immediately after irradiation the serum was exchanged with serum free medium ($0.5\,\%$ FCS).

24 hours after irradiation, serum free supernatants were harvested by centrifugation and frozen at -80 °C until usage. Cell culture supernatants were analyzed by the Proteome Profiler (#ARY025, R&D systems) according to manufacturer's instructions. Membranes were photographed in the ChemiDoc Touch Imaging System (Bio-Rad) with automated detection. Intensity was quantified with ImageJ, bare membrane was used as background correction. Relative expression was normalized to sham irradiated samples.

5.5.3   Enzyme Linked Immunosorbent Assay (ELISA)

$4 \cdot 10^5$ cells were seeded and irradiated in the ring system as described above. Immediately after irradiation cells were serum-starved for 24 hours and the serum free supernatant was collected and frozen at -80 °C. To detect secreted MMP-2 and uPA, Duo-set sandwich ELISAs of R&D Systems (MMP-2: #DY902, uPA: #DY1310) were applied according to the manufacturer's instructions. Absorbance was measured at 450 nm with a wavelength correction at 540 nm with the Microplate Reader EL808 from BioTek Instruments Inc.. Basal secretion was measured in ng/10^6 (MMP-2) respectively pg/10^6 (uPA) cells. Relative secretion was normalized to sham irradiated samples.

5.5.4   MMP activity assay

The Abcam MMP Activity Assay (#ab112146) was applied to measure generic MMP activity in the GBM samples in dependency on their irradiation status. Cells were seeded and irradiated in the ring system as described before. Immediately after irradiation medium was exchanged by serum free medium. MMP activity was measured 24 and 48 hours after 0 and 4 Gy irradiation on supernatants as well as on lysates, generated 24 hours or respectively 48 hours after irradiation under serum starvation. Lysates were generated by trypsinsing the cells from the ring system in a falcon, followed by the incubation with RIPA buffer (150 mM NaCl + 50 mM Tris + 0.1 % SDS + 1 % Triton X-100 + 0.5 % sodium deoxychalat) for 20 minutes, on ice with regular vortexing. In order to keep samples comparable the protein concentration was determined with the Pierce BCA Protein Assay Kit as described before. 11 μg of protein from the lysates and 6 μg protein from the supernatant were used for the experiments. Sample activity was normalized to unirradiated controls.

5.5.5   Epithelial to mesenchymal transition (EMT) staining

Cells were seeded and irradiated in the ring system as described before. Immediately after irradiation cells were trypsinized and $2 \cdot 10^4$ cells were seeded in a drop of $100 \, \mu l$, three times on a cover slip. 24 hours after irradiation cells were fixed with 4% PFA and blocked for one hour in blocking buffer, consisting of PBS supplemented with 5% normal goat serum and 0.3% Triton X-100. The conjugated antibody Vimentin D21H3 XP® Rabbit mAb (Alexa Fluor® 594 Conjugate, #7675, Cell Signaling) was diluted 1:50 in antibody dilution buffer, consisting of PBS, 1% BSA and 0.3% Triton X-100 and applied to fixed cells overnight at $4\,°C$. One of the three cell seedings served as antibody control, were pure antibody dilution buffer was applied instead of antibody dilution in antibody dilution buffer. The next day cells were washed with PBS, remaining medium was removed and mounting medium with DAPI was applied. Pictures were taken with the Axioskop 2 plus (Zeiss), 20x magnification. In cooperation with Dr. Stefan Bartzsch a package on Matlab, allowing an automated quantification of the fluorescent signal, was developed. Vimentin intensity was normalized to the unirradiated control. Likewise, the DAPI and Vimentin correlation was normalized to the sham irradiated sample.

5.5.6   Western Blotting

The first step was to prepare the separating gel by mixing 30% acrylamide / 0.8% bisacrylamide with $1\,M$ Tris (pH 8.8), dest. H_2O, 10% SDS, 10% ammoniumpersulfat and TEMED. Table 4 shows the mixed volumina for two 10% separating gels. The separating gel was covered with isopropanaol in order to generate a flat top. Gels were allowed to polymerize for at least 45 minutes at room temperature or overnight at $4\,°C$.

Table 4: Composition of the separating gel

Substance	Volume [ml]
Acrylamide/Bis	3.3
H_2O	2.8
1 M Tris pH 8.8	3.8
10 % SDS	0.1
10 % APS	0.1
TEMED	0.01

The next step was the preparation of the collecting gel as described in table 6. Remaining isopropanol was removed from the separating gel and the collecting gel was filled on top of the separating gel in the gel chamber. 15-well combs were added and the gel was allowed to polymerize for 45 minutes at room-temperature. Once the gel was polymerized, the combs were carefully removed and the gels were transferred into the electrode chamber. The chamber was filled with 1x running buffer (25 mM Tris, 250 mM Glycin and 0.1 % SDS) and 15 μl of each sample, mixed with 1 · Laemmli buffer and heated at 95 °C for five minutes, were loaded. 5 μl protein latter, Precision Plus Protein Standard Dual Color (#161-0374, Bio-Rad), was applied. Protein separation was performed for 90 minutes at 15 mA at room temperature. After performing the protein separation, the gel chamber was opened and the gel released. In order to equilibrate the gel it was washed quickly in TOWBIN buffer, consisting of 25 mM Tris, 192 mM Glycin, H_2O and 20 % MeOH. A Wet-blot system (Criterion, Bio-Rad) was applied to transfer the proteins from the gel to a Nitrocellulose (NC) membrane (#Protran BA83, Schleicher& Schüll). Therefore, two sponges and two papers were soaked in TOWBIN buffer. The electrophoresis tank system was prepared by filling the tank with TOWBIN buffer and a thermalpack that was cooled to -20 °C. The transfer-sandwich consisting of sponge, paper, NC membrane, gel, paper, sponge was fixed in the electrophoresis chamber. With constant 100 V over 90 minutes at 4 °C the proteins were transferred to the NC membrane.

To check for a successful protein transfer Ponceau-red was applied. To get rid of the Ponceau-red membranes were washed with H_2O. Bands of the protein latter were labeled with a biro. The membrane was fixed for three hours at room temperature with 1x RotiBlock (#A151.2, Roth) before the primary antibody was applied overnight at 4 °C. For antibody dilution see table 5. The next day the membrane was washed three times with TBST (4.2 g Tris, 26 g Tris-HCl, 80 g NaCl, 900 ml H_2O, 10 ml Tween20) and the secondary antibody, diluted in 8 % milk, was applied. The secondary antibody was allowed to incubate for one hour at room temperature. After another TBST washing step ECL Select Luminol Solution (#RPN2235V1, Amersham) was mixed 1:1 with ECL Select Peroxide Solution (#RPN2235V2; Amersham) and allowed to incubate on top of the membrane for one minute at roomtemperature. Images were taken with the FluorChem HD2 from Alpha Innotech. If necessary membranes were stripped with Restore PLUS Western Blot Stripping Buffer (#46430, ThermoScientific) for 15 minutes at room temperature. After another TBST washing step and an one hour blocking with 1x RotiBlock a new primary antibody

was applied overnight. The Image J software was applied to quantify the bands. Therefore background was substracted, than values were normalized to the loading control, Actin-β and finally normalized to their sham irradiated control.

Table 5: List of antibodies applied for Western Blotting

antibody	species	article nr.	manufacturer	dilution
Actin-β	mouse mAb	014M4759	Sigma	1:20000
AKT	rabbit mAb	9272S	Cell Signaling	1:1000
β-Catenin	rabbit mAb	9582S	Cell Signaling	1:1000
GSKB	rabbit mAb	12456S	Cell Signaling	1:1000
phospho-AKT	rabbit mAb	9271S	Cell Signaling	1:1000
phospho-β-Catenin	rabbit mAb	9567S	Cell Signaling	1:1000
phospho-GSK3B	rabbit mAb	9336S	Cell Signaling	1:1000
phospho-SMAD2/3	rabbit mAb	MAB8935	R&D Biotechne	1:100
SMAD2/3	rabbit mAB	8685S	Cell Signaling	1:1000
IgG HRP conjugated	anti-rabbit	A16096	life technologies	1:10000
IgG HRP conjugated	anti-mouse	A16066	life technologies	1:10000

Table 6: Composition of the collecting gel

Substance	Volume [ml]
Acrylamide/Bis	0.6
H_2O	2.6
1 M Tris pH 6.8	0.5
10 % SDS	0.04
10 % APS	0.04
TEMED	0.004

5.5.7   Immunohistochemistry

Patient-derived tumor tissue, that was used for the RadGlio trial was also stored in the pathology of the Klinikum rechts der Isar, where the tissues were PFA fixed and stored. In the RadGlio trial, patient-derived tissue was mechanically and enzymatically digested to isolate primary GBM cells, which were then cultured and passaged before cellular assays

were performed. To extend the single cell analysis, cryo-sections of the fixed patient-derived tumor tissues were produced and in cooperation with the pathology of the Helmholtz Zentrum München, E-Cadherin and Vimentin stainings were performed. As the patient-derived tumor material is very limited only three microtom sections, of each $3\,\mu$m, were applied for each staining. A H&E counter staining, as well as E-Cadherin and Vimentin were stained on the progressive dies. Afterwards, from each section up to ten visual fields, that did not contain blood vessels, necrotic areas or even healthy tissue, were chosen and the complementary section was determined. On those chosen fields several factors from the staining were analysed with the Definiens Developer XD$^{\text{TM}}$Software from Definiens Inc., e.g. average marker intensity, mean border index but also morphological features like compactness of the cells. Finally, these features of the stained patient-tissue were compared to the basal invasive capacity of the isolated primary cells, determined with the invasion assay.

5.6   LEM Modelling

In cooperation with the GSI Darmstadt, Dr. Thomas Friedrich applied the local effect model (LEM) on the experimentally determined values of the low-LET photon irradiation. Alpha and beta values were assumed and corrected by the standard errors of the already performed measurements ($\alpha \pm \Delta\alpha, \beta \pm \Delta\beta$). 12 LEM simulations were calculated (2 cell lines $\cdot$ 2 photon experiments $\cdot$ 3 alpha and beta combinations) by means of standard cell geometries (Vn = $500\,\mu$m^3, rn = $5\,\mu$m, cdist = $0.54\,\mu$m). The Cutoff parameter of the LQ Modell (Dt) was chosen to be equal the empirically determined connection Dt = $4+1.1\alpha/\beta$.

5.7   Ingenuity pathway analysis

On the basis of the experimentally determined proteomics and genomics data sets the Ingenuity® Pathway Analysis (IPA®, Qiagen), in cooperation with the Institute of Radiation Biology (ISB) from the Helmholtz Centre Munich, was applied. The IPA is an analysis method that uses differences in the 'omics data sets to identify new target candidates in order to determine underlying pathways. For this analysis only two cell lines were chosen. One with radiation-enhanced invasion (LN229) and one with no increased invasion response (LN18). The IPA was applied to the experimentally determined mRNA expression patterns of the qPCR results from LN229 and LN18 that changed due to irradiation with $4\,$Gy X-ray or the equivalent dose of $1.3\,$Gy α-particle irradiation by at least

20 %. First, several pathways of LN229 and LN18 were compared for activation levels after X-ray irradiation. Second, the activation levels between one cell line after X-ray and α-particle treatment were compared and finally, two potentially important pathways for GBM invasion were chosen. From those two pathways several proteins were selected and their activation by phosphorylation was determined via Western Blotting.

5.8   Correlation of the relative invasion with clinical outcome

For correlation of the experimental findings of the RadGlio study with the clinical outcome, the relative invasion of primary glioma cell lines was compared to patient data concerning radio-and chemotherapie, progression-free, as well as overall survival that were listed in the PKIS system.

5.9   Statistics

Mean values were calculated and are presented as $\pm$ standard error of the mean (SEM). In order to provide significance, the Student's t-test was applied with Graph Pad Prism. A p-value of ≤ 0.05 was considered as statistically significant.

6   Abbreviations

Table 7: List of abbreviations

abbreviation	full name
AKT	Protein kinase B
APLF	Aprataxin- and PNK-like factor
APC	Adenomatous poyposis coli
APS	Ammonium persulfate
ATM	Ataxia telangiectasia-mutated kinase
BSA	Bovine serum albumin
CFA	Colony formation assay
CNS	Central nervous system
CSC	Cancer stem cell
DAPI	4',6-Diamidin-2-phenylindol
del	deleted
DNA	Deoxyribonucleic acid
DSB	Double strand break
ECL	Enhanced chemiluminescence
ECM	Extracellular matrix
EM	Electromagnetic
EMEM	Eagle's Minimum Essential Medium
EMT	Epithelial-mesenchymal transition
FACS	Fluorescence-activated cell sorting
FCS	Fetal calf serum
GBM	Glioblastoma multiforme
GFAP	Glial-fibrillary-acidic protein
GSC	Glioblastoma stem cell
GSK3β	Glycogen synthase kinase-3β
HR	Homologous repair
IAEA	International Atomic Energy Agency
IDH	Isocitrate dehydrogenase
IPA	Ingenuity pathway analysis
iRT	Institute of innovative Radiotherapy

Table 7: Continuation list of abbreviations

abbreviation	full name
ISB	Institute of Radiation Biology
LEF	Lymphoid enhancer factor
LEM	Local effect model
LET	Linear-energy-transfer
LQM	Linear-quadratic-model
LRP5/6	lipoprotein-related protein 5/6
MGMT	Methylguanine-methyltransferase
MMP	Matrix-Metalloproteinase
MRN	MRE11-Rad50-NBS1
mut	mutated
NC	Nitrocellulose
n.d.	not determined
NHEJ	Non-homologous end joining
OER	Oxygen enhancement ratio
PBS	Phosphate-buffered saline
PE	Plating-efficiency
PFA	Paraformaldehyde
PP	Polypropylene
qPCR	Quantitative polymerase-chain-reaction
R	Relapse
RBE	Relative biological effectiveness
RNA	Ribonucleic acid
RPA	Replication protein A
RPMI	Roswell-Park Memorial Institute
RT	Radiotherapy
SDS	Sodium dodecyl sulfate
SF	Survival fraction
SSB	Single strand break
TBST	Tris-buffered saline with Tween20
TCF	T-cell factor

Table 7: Continuation list of abbreviations

abbreviation	full name
TEMED	Tetramethylethylenediamine
TMZ	Temozolomide
TRIS	Tris(hydroxymethyl)aminomethane
TUM	Technical University of Munich
uPA	urokinase-type plasminogen activator
WB	Western Blot
WHO	World health organization
WNT	Wingless/Int1
wt	wild-type
XRCC4	X-ray cross complementing protein 4
53BP1	p53 binding protein 1

7 Results

7.1 Setting up the α-irradiation device

7.1.1 Cell survival fractions after high- and low-LET irradiation
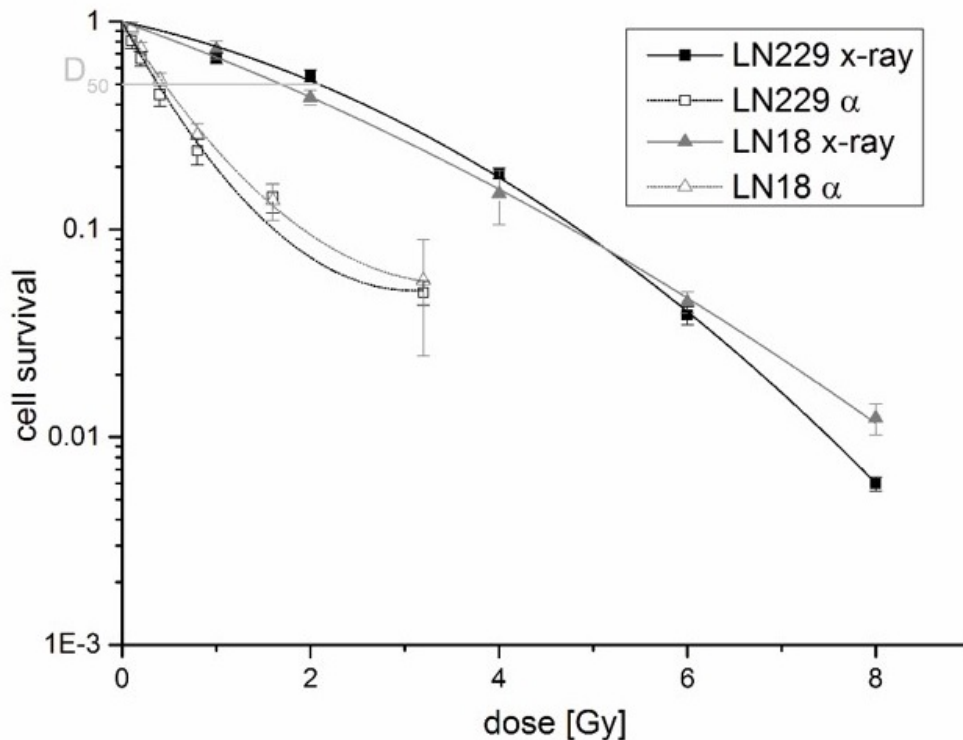
Figure 16: **Colony formation assay (CFA) of the two established cell lines LN229 and LN18 after X-ray and α-particle irradiation**
Shown are the survival curves of LN229 and LN18 fitted to the linear-quadratic model. One survival value was calculated as mean of two biological replicates with each 180 measuring values. Error bars where calculated via error propagation.

Table 8: α and β values were derived from the linear quadratic equation from the CFA of LN229 and LN18 after X-ray and α-particle irradiation.

	$\boldsymbol{\alpha}$ [**Gy**$^{-1}$]	$\boldsymbol{\beta}$ [**Gy**$^{-2}$]
LN229 X-ray	0.22	0.05
LN229 alpha	1.93	-0.31
LN18 X-ray	0.37	0.02
LN18 alpha	1.65	-0.24

In order to determine the equivalent dose of α-particle irradiation for the X-ray dose applied, CFAs were performed after X-ray and α-particle irradiation. Plating efficiency (PE) of LN229 was determined as $56\% \pm 2\%$ and $56\% \pm 3\%$ for LN18. A dose-dependent cell survival for X-ray irradiation as well as α-particle irradiation was observed, see Fig. 16. As typical for high-LET irradi-

ation, there was less cell survival after α-particle irradiation than after X-ray irradiation.

The dose where 50 % of the cells survived (D50) after X-ray irradiation was determined as 2 Gy whereas the D50 after α-particle irradiation was 0.5 Gy. Therefore, the RBE was calculated as 4. At a dose of 1 Gy X-ray irradiation the well-known shoulder formation could be detected, this was not observed after α-particle irradiation. Corresponding alpha and beta values are listed in table 8. The equivalent α-particle dose to 4 Gy X-ray irradiation was calculated as 1.3 Gy.

7.1.2   Examination of irradiation homogeneity of the α-particle irradiation device

The cell survival at 3.2 Gy α-particle irradiation showed an unexpected, high survival of approximately 6 %, indicated by the survival curve bending upwards. Further experiments were performed to ensure that all cells in the ring system are homogeneously irradiated in the α-particle irradiation device.
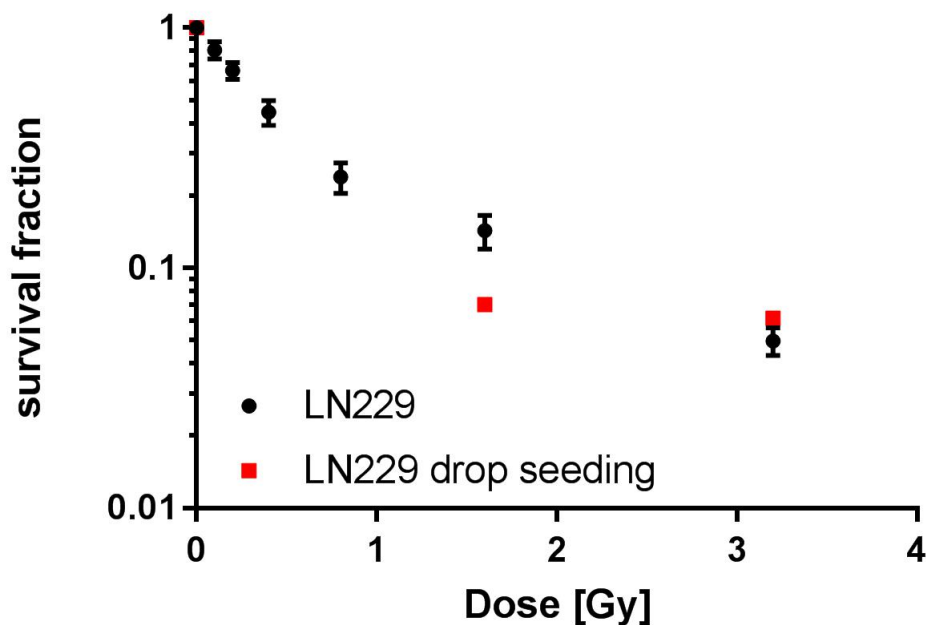
Figure 17: **CFA after α-particle irradiation of drop seeded cells**
Shown are the survival fractions of LN229 after usual seeding, as well as the surviving values after 0, 1.6 and 3.2 Gy, when cells were only seeded as a drop in the ring centre. Values are mean values of 180 measuring points. The drop seeding experiment was only one time performed. Error bars show the SEM.

Drop seeding to exclude cell attachment at the outer boarder of the ring system
LN229 cells were seeded only in the ring centre (see Fig. 11 in the methods chapter), irradiated with 0, 1.6 and 3.2 Gy of α-particles and a CFA was performed. The same survival was observed compared to the usual seeding procedure (Fig. 17). A dose of 1.6 Gy α-particles caused a survival fraction of 7 % ± 0.1 % and a dose of 3.2 Gy α-particles 6 % ± 0.1 %.

High dose irradiation to validate survival after α-particle irradiation
Another CFA with LN229 was performed, but additionally to 0, 0.1, 0.2, 3.2 Gy a dose
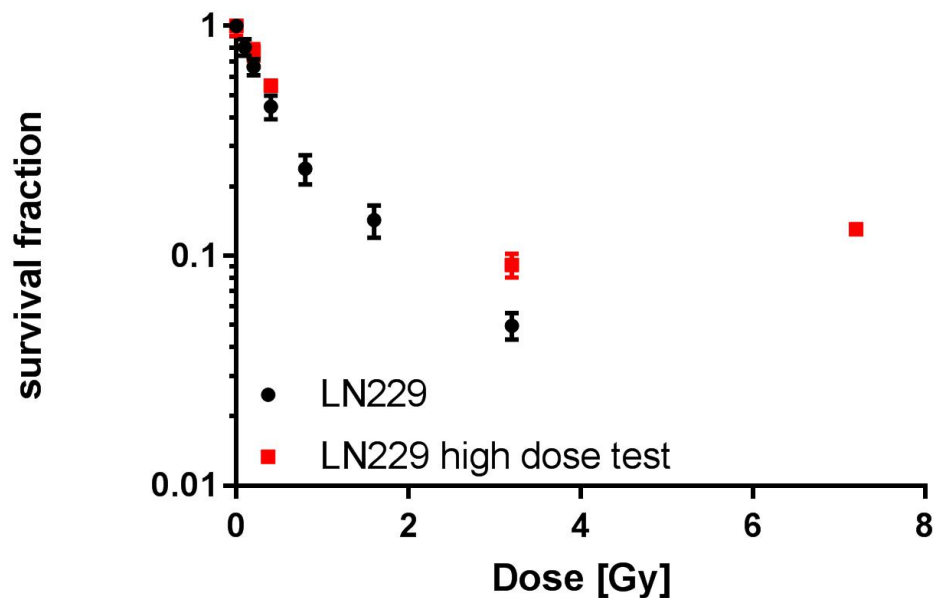
Figure 18: **CFA after α-particle irradiation with high doses**
Shown are the survival fractions of LN229 after usual seeding and irradiation with 0, 0.1, 0.2, 0.4, 0.8, 1.6 and 3.2 Gy α-particles (black dots). Additionally, the graph shows the surviving values after 0, 0.1, 0.2, 3.2 and 7.2 Gy (red dots). Values are mean values of 180 measuring points. The high dose experiment was only performed once. Error bars show the SEM of the technical replicates.

of 7.2 Gy α-particles was applied. As figure 18 shows, a dose of 0.2 Gy α-particles caused a survival fraction of 77 % ± 6.3 %, 0.4 Gy 55 % ± 3.3 %, 3.2 Gy 9 % ± 1.1 % and 7.2 Gy caused a survival fraction of 13 % ± 0.5 %.

7.1.3 γH2AX assay to validate irradiation homogeneity in the ring system
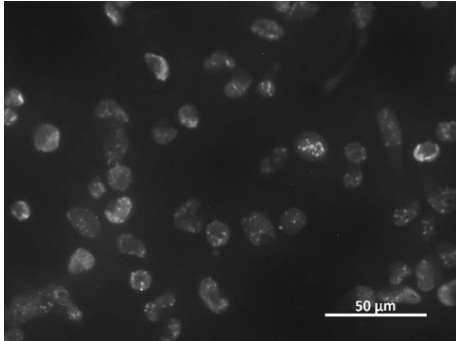
Figure 19:   **Exemplary image of γH2AX foci of LN229 after 3.2 Gy α-particle irradiation**
Cells were fixed 30 min after irradiation and stained for γH2AX in the total ring system. The small grey dots represent the γH2AX foci in the DAPI (here dark grey) stained nuclei. The scale bar represents $50\mu m$.

The γH2AX-immunofluorescence staining was performed to further exclude inhomogeneous irradiation. 30 minutes after α-particle irradiation with 3.2 Gy, cells on the total foil area were fixed with PFA in the ring system and examined for γH2AX foci. Only less than 0.1 % of cells did not exhibit any foci after 3.2 Gy α-particle irradiation, see exemplary Fig. 19. To examine the γH2AX foci more close to the protocol of the CFA assay, the γH2AX assay was also performed with cells irradiated in the ring system but trypsinized directly after irradiation and seeded on chamber slides were they were fixed and stained 4 hours after irradiation. As already shown in the γH2AX total ring analysis, there were less than 0.1 % of cells that did not show any foci after 3.2 Gy α-particle irradiation.

7.1.4   Glioblastoma stem cells as radioresistant subpopulation

As inhomogeneous cell irradiation could be excluded it was assumed, that a more radioresistant cell population might be responsible for the high cell survival. Glioblastoma stem cells (GSC) are known to be more radioresistant. One common marker of GSCs is CD133. The flowcytometry analysis of CD133 stained cells (Figure 20) revealed that neither LN229 nor LN18 were CD133$^+$. Caco2, a colon carcinoma cell line served as positive control.
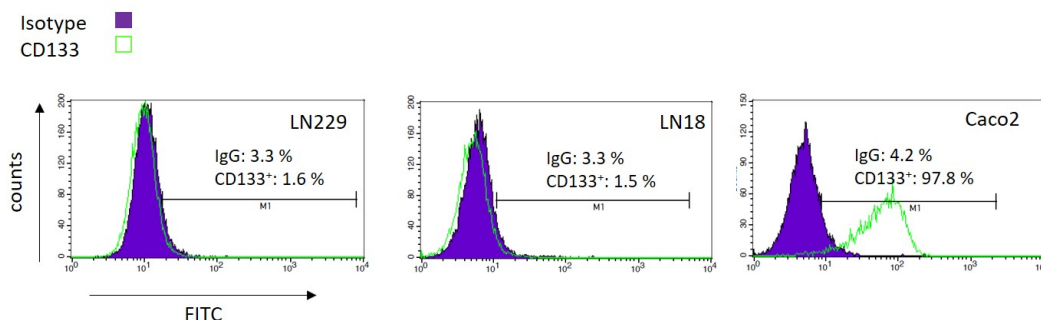
Figure 20: **Exemplary CD133 FACS of established cell lines**
Shown is the FACS analysis of LN229 and LN18 as well as of the positive control, Caco2. The experiment was performed three times.

7.1.5   CFA with a non-cancerogeneous hamster cell line CHO

As both, inhomogeneous irradiation, as well as a radioresistant $CD133^+$ subpopulation could be excluded another CFA with a non-human, non-cancerogeneous cell line, CHO, was performed to exclude that the observed phenomenon is specific for cancer cells. The PE of CHO cells was determined as $58\% \pm 2\%$. As Fig. 21 shows a dose of $0.1\,\text{Gy}\,\alpha$-particle irradiation caused a cell survival of $81\% \pm 1.6\%$, $0.2\,\text{Gy}$ caused a survival fraction of $83\% \pm 1.7\%$, $0.4\,\text{Gy}$ caused $51\% \pm 0.7\%$, $0.8\,\text{Gy}$ leaded to $31\% \pm 0.4\%$ survival, $1.6\,\text{Gy}$ $14\% \pm 0.2\%$ and a dose of $3.2\,\text{Gy}$ showed a survival fraction of $8\% \pm 1\%$ of CHO cells. Hence, the survival curve of CHO cells showed a similar behaviour as observed for LN229 and LN18.
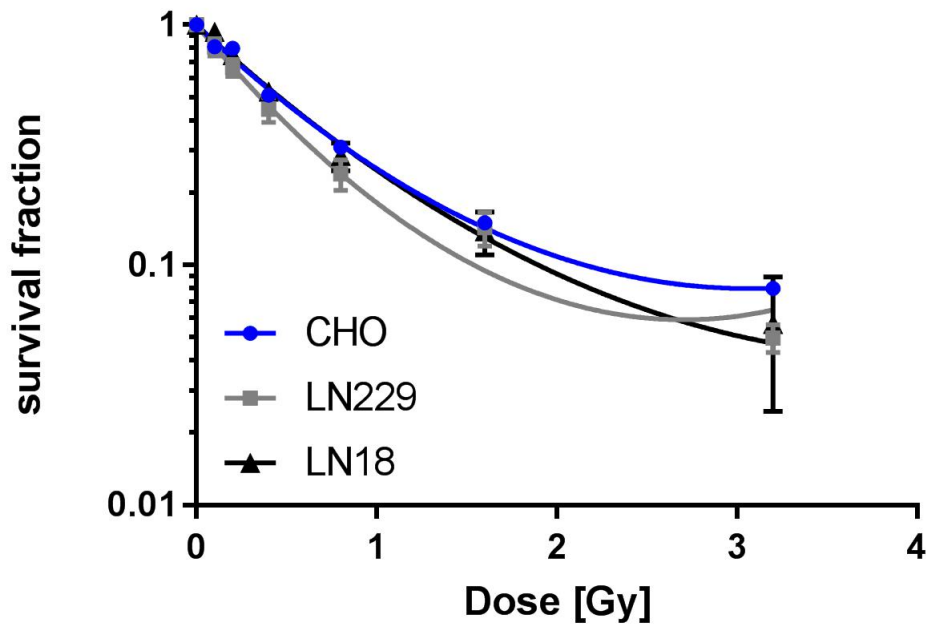
Figure 21: **CFA of CHO cells**
Shown is the CFA after α-particle irradiation of LN229 and LN18 compared to non-cancerogeneous CHO cells. The CHO CFA was only performed once but each survival fraction was calculated from 144 values. The error bars represent the SEM of the technical replicates from the CHO CFA.

7.1.6   LEM Modell

In a cooperation with the GSI Darmstadt (Dr. Thomas Friedrich) the LEM Modell was applied to generate α-particle survival curves of LN229 and LN18. First, cell nuclei were stained with DAPI and cells were imaged with a microscope and finally the cell size was determined. Nuclei of both cell lines showed a size of $150\,\mu\text{m}^2 \pm 70\,\mu\text{m}^2$. Furthermore, it

was noticed that both cell lines showed a certain amount of very small fragments of about $15\,\mu m^2$, which were excluded for cell size measurement. Based on the nuclei size and the X-ray cell survival data from LN229 and LN18, which were experimentally determined (see Fig. 22), Dr. Friedrich simulated the α-particle irradiation survival graphs. As shown in red, the cell survival after α-particle irradiation was expected to follow a linear equation. Dr. Friedrich also plotted the experimentally determined survival data of LN229 and LN18 after X-ray irradiation in black. Dotted lines symbolize the SEM.
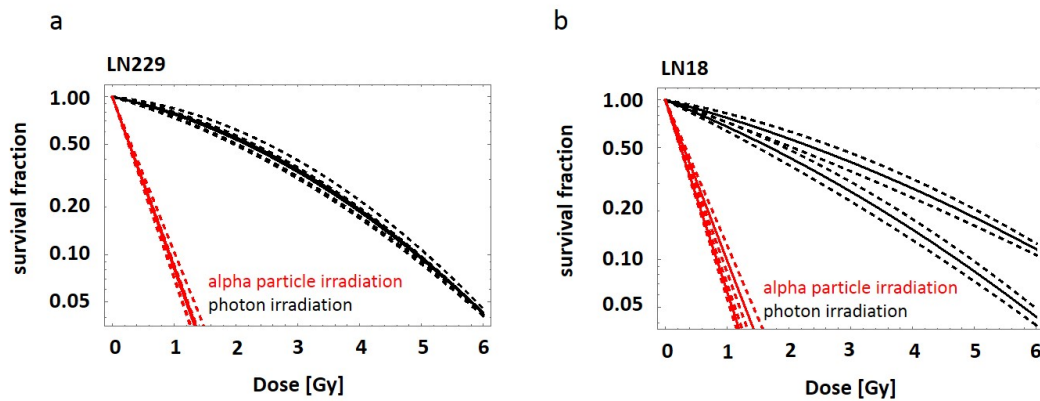
Figure 22: **LEM Modell**
The survival fraction of LN229 (a) and LN18 (b) is shown (in red) after α-particle irradiation as estimated according to the LEM Model. Additionally, the two experimentally determined survival fractions of both cell lines are plotted in black. Dashed lines represent the standard deviation. Credits to Dr. Th. Friedrich from the GSI in Darmstadt.

7.1.7   Elucidation of the reason for high-survival fractions

CFA with changed irradiation conditions
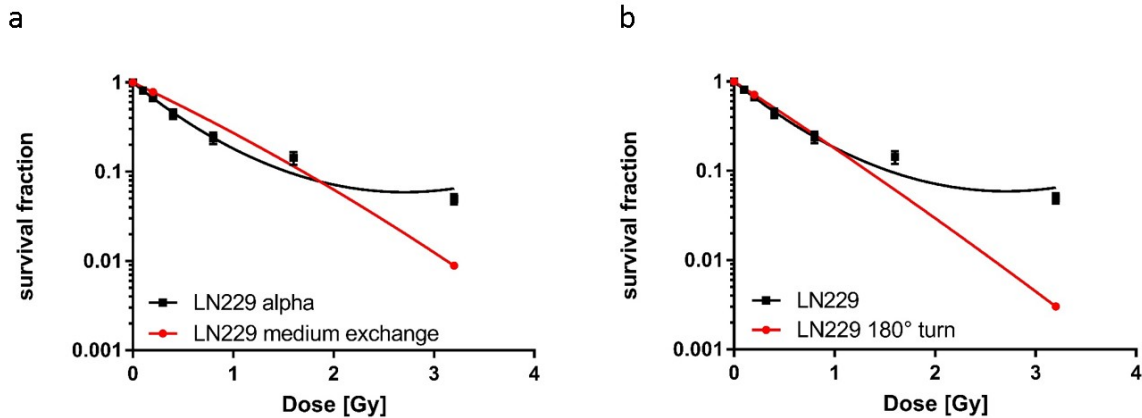
Figure 23: **CFAs with changed irradiation conditions**
The image shows the results of the two CFAs with changed irradiation settings. In a) the medium was exchanged after half the irradiation time. In b) the ring system was turned by 180° after half the irradiation time. Both analyses were only performed once but with each 144 technical replicates per dose. The SEM is shown and the survival curves were fitted with the LQM.

To test for possible dose inhomogeneities in the irradiation field of the α-particle irradiation device, additional CFAs were performed, with sham, 0.2 and 3.2 Gy alpha particles. For one examination the medium was exchanged after half the irradiation time. In the other examination, the ring system was turned by 180° after half the irradiation time. Both analyses revealed that the survival fraction after 3.2 Gy α-particle irradiation was diminished to less than 1 %, see figure 23.

7.2   Comparison of the ring system and usual plastic flasks

As the ring system was newly established it was necessary to show that the results are comparable to the conventionally used plastic culture flasks. Therefore, CFAs with both systems (plastic flasks / ring system) were performed after X-ray irradiation and their survival curves were compared. The PE of LN229 cells cultivated in both systems was similar as the plastic system showed a PE of 55 % ± 4 % and the ring system a PE of 56 % ± 2 %. As shown in Fig. 24, the cell survival fraction from both systems is comparable over all doses for LN229.
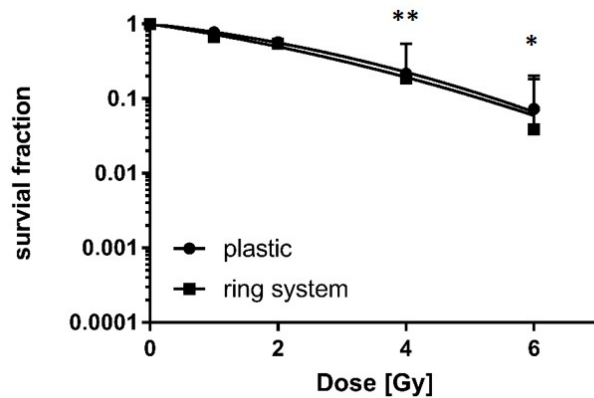
Figure 24: **CFA to compare survival fractions after plastic and ring system seeding**
Shown is the CFA of LN229 after different seeding system procedures. Experiments were performed in triplicates and error bars represent the SEM.

In both curves, the cell survival is significantly ($p \leq 0.001$) reduced after $4\,\text{Gy}$ (plastic: $22\,\% \pm 2.3\,\%$, ring system: $19\,\% \pm 0.4\,\%$) X-ray irradiation, followed by a cell survival of $7\,\% \pm 0.1\,\%$ (plastic), respectively $4\,\% \pm 0.1\,\%$ (ring system) after $6\,\text{Gy}$ ($p \leq 0.01$).

7.3 Basic characterization of the two established GBM cell lines LN229 and LN18

7.3.1 Comparison of the radiosensitivity of LN229 and LN18 using CFAs

A CFA was also applied to analyse the radiosensitivity of LN229 and LN18 cells. Both survival curves indicated a dose-dependent survival and the typical low-LET shoulder formation at $1\,\text{Gy}$ X-ray irradiation. There was no significant difference between the two cell survival curves at any dose. LN18 already showed a significant reduction at $1\,\text{Gy}$ ($p \leq 0.05$) to $76\,\%$ cell survival as well as after $2\,\text{Gy}$ to $50\,\%$ survival ($p \leq 0.05$). At $4\,\text{Gy}$ both cell lines showed a significant reduction (LN18: $27\,\%$ survival with $p \leq 0.05$; LN229: $19\,\%$ survival with $p \leq 0.001$). Likewise, at 6 and $8\,\text{Gy}$, both cell lines showed significant reduction to $18\,\%$ (LN18) and $19\,\%$ (LN229) with a p-value ≤ 0.01, respectively $3\,\%$ (LN18) and less than $1\,\%$ (LN229) ($p \leq 0.001$). As already demonstrated in Fig. 16, both cell lines exhibited a similar PE, a comparable D50 and similar cell survival fractions and were therefore considered to be comparable radiosensitive.

7.3.2   DNA damage repair of LN229 and LN18 after X-ray irradiation

γH2AX FACS

First, a γH2AX FACS was performed, measuring the mean fluorescence intensity (MFI) of the γH2AX signal in the sample. The γH2AX signal was monitored 6 and 24 hours after irradiation with 4 Gy X-rays. As Fig. 25a reveals, 6 hours after 4 Gy X-ray irradiation the
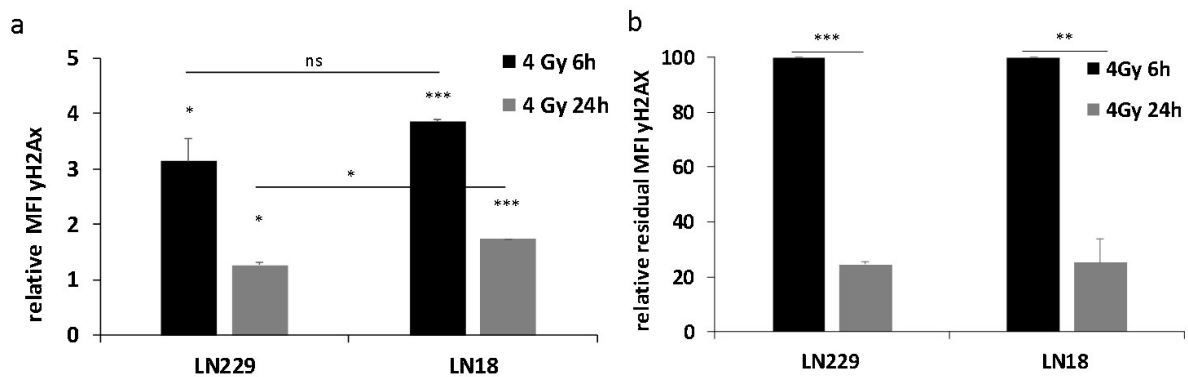
Figure 25: **γH2AX FACS of LN229 and LN18 after 4 Gy X-ray irradiation**
a) shows the relative MFI of X-ray irradiation induced γH2AX. Values were normalized to 0 Gy, which was set as one. Significances were calculated towards sham irradiated cells as well as between the cell lines. b) shows the residual MFI of the γH2AX signal, 24 hours after irradiation, normalized to the γH2AX signal 6 hours after irradiation. Therefore, the 6 hour value was set to 100 %. All experiments were performed three times and the error bar represents the SEM. Student's T-test was applied to calculate significance.

γH2AX MFI significantly increased in both cell lines (LN229: 3.1-fold $p \leq 0.05$; LN18: 3.8-fold $p \leq 0.001$). 24 hours after 4 Gy irradiation the MFI of γH2AX was still significantly increased towards the sham irradiated cells (LN229: 1.3-fold $p \leq 0.01$; LN18: 1.7-fold $p \leq 0.001$). Comparing the residual γH2AX MFI after 24 hours, showed that both cell lines exhibit only 25 % of the γH2AX MFI as they had shown 6 hours after 4 Gy X-ray irradiation (LN229: 24.5 % $p \leq 0.001$; LN18: 25 % $p \leq 0.01$), see figure 25b. LN229 and LN18 were therefore considered to show a comparable DNA damage repair capacity.

53BP1 Foci

Fig. 26a shows the 53BP1 Foci, counted 0.5 hours, as well as 24 hours after 0 and 4 Gy X-ray irradiation. The initial damage (0.5 hours after irradiation) was significantly increased in both cell lines towards the sham irradiated cells (LN229: 14-fold ± 0.7 $p \leq 0.001$; LN18: 27-fold ± 2.7 $p \leq 0.01$). 24 hours after irradiation the number of unrepaired foci was still significantly higher than in sham irradiated cells (LN229: 2.3-fold $\pm$ 0.3 $p \leq 0.01$; LN18: 2-fold $\pm$ 0.2 $p \leq 0.01$). Fig. 26b demonstrates the comparison between the residual foci of

the two cell lines, 24 hours after irradiation, normalized to the 53BP1 foci 0.5 hours after irradiation. LN229 showed 7 % ± 0.6 % foci remaining ($p \leq 0.001$) and LN18 6.7 % ± 0.8 % ($p \leq 0.001$). It was concluded that LN229 and LN18 show similar DNA damage repair.
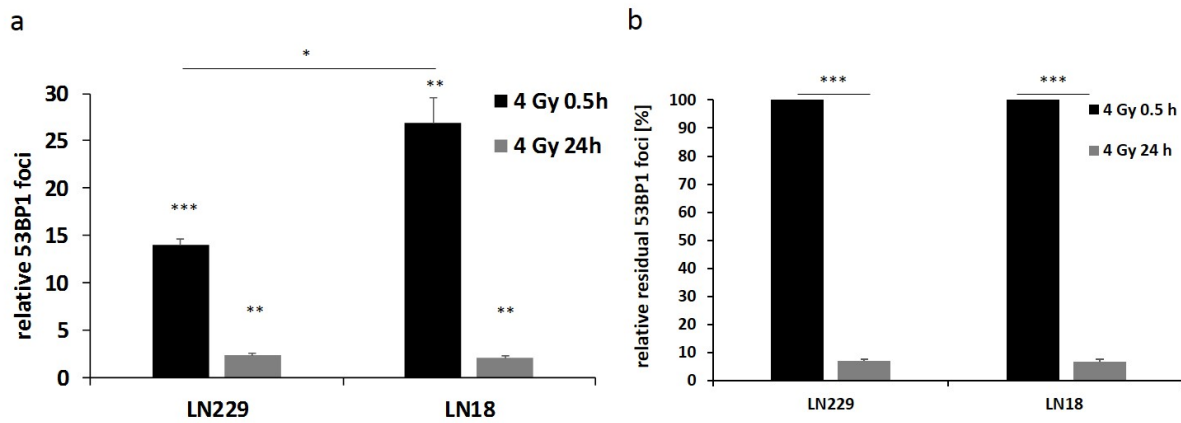
Figure 26: **53BP1 Foci of LN229 and LN18 after 4 Gy X-ray irradiation**
a) shows the relative amount of 53BP1 foci 30 minutes after 4 Gy X-ray irradiation normalized to sham irradiation. 0 Gy values were set to one. Significances were calculated towards sham irradiated cells, as well as in between the cell lines. b) shows the relative residual 53BP1 foci, 24 hours after irradiation, normalized to the 53BP1 foci 0.5 hours after 4 Gy irradiation, which were set to 100 %. All experiments were performed three times and the error bar represents the SEM. Student's T-test was applied to calculate significances.

In summary, both DNA damage repair assays showed that 4 Gy X-ray irradiation caused comparable DNA damage in LN229 and LN18. Additionally, both cell lines showed similar DNA repair capacity.

7.3.3   Cell cycle distribution of LN229 and LN18 after X-ray irradiation

24 hours after X-ray irradiation with 0, 2, 4, 6 and 8 Gy the cell cycle distribution was measured by FACS analysis. As Fig. 27 presents LN229 (a) as well as LN18 (b) showed a dose dependent G2M arrest. LN229 exhibited a significantly higher population in G2M arrest after irradiation with 4 Gy ($p \leq 0.05$), 6 Gy and 8 Gy ($p \leq 0.01$); LN18 showed a significant G2M increase after 6 Gy ($p \leq 0.01$) and 8 Gy ($p \leq 0.05$). LN18 naturally presented a large population in S-phase (47 %) that is not significantly affected by irradiation. In contrast, for LN229 the proportion of cells in S-phase was significantly diminished after 4, 6 and 8 Gy ($p \leq 0.001$) X-ray irradiation.

a
b
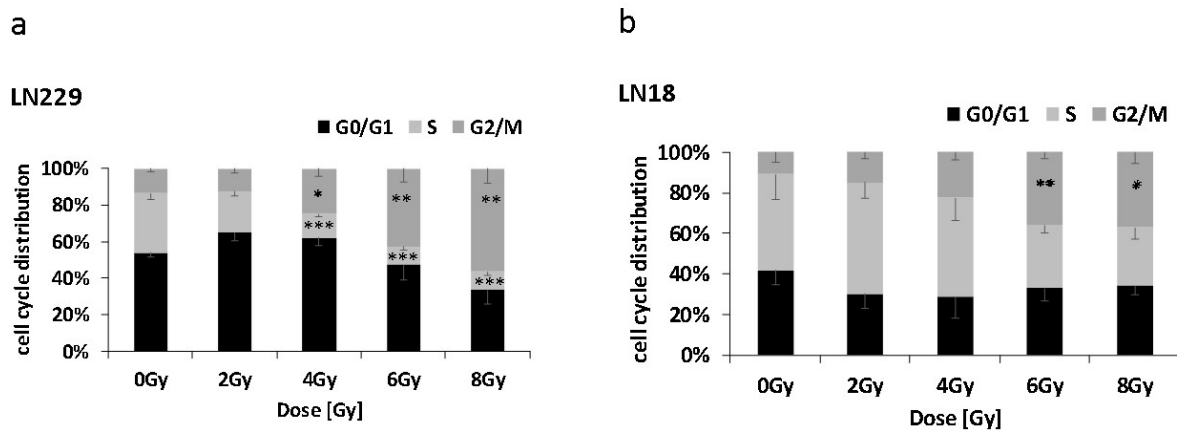
Figure 27: **Cell cycle distribution after X-ray irradiation**
Shown is the cell cylce distribution of LN229 a) and LN18 b) 24 hours after X-ray irradiation. All experiments were performed three times and the error bar represents the SEM. Student's T-test was applied to calculate significance.

7.3.4   Doubling time of LN229 and LN18 with and without X-ray irradiation

The doubling time of the two established cell lines was measured with and without irradiation. Cells were irradiated with 0 and 4 Gy and cell numbers were determined every 24 hours for up to one week. The doubling time of unirradiated LN229 cells (16 ± 1 hours) was not significantly affected by irradiation with 4 Gy (21 ± 2.5 hours). In contrast, the doubling time of unirradiated LN18 cells (13 ± 1.3 hours) was significantly increased by 4 Gy X-ray irradiation (19.4 ± 1.5 hours; $p \leq 0.05$). Summing up, only the doubling time of LN18 significantly increased 1.5-fold after 4 Gy X-ray irradiation compared to sham irradiation.

7.4   The basal invasive capacity of LN229, LN18 and U87

For the main assay of the thesis, the invasion assay, a third established human GBM cell line, U87 was added. Prior to determining the influence of irradiation on the invasion of the established glioblastoma cells their basal invasion capacity without irradiation was measured with a matrigel coated transwell assay. To provide a reference value, brain fibroblasts CRL2270, were investigated. All experiments were nomalized against CRL2270 cells and the value of CRL2270 was plotted with a value of one in Fig. 28. All three tested established cell lines were significantly more invasive than CRL2270. LN229 was 5.7-fold $\pm$ 0.6 ($p \leq 0.001$) as invasive, LN18 7.3-fold $\pm$ 0.8 ($p \leq 0.001$) and U87 7.5-fold $\pm$ 1.7 ($p \leq 0.001$). The invasion between the three GBM cell lines was not significantly different.
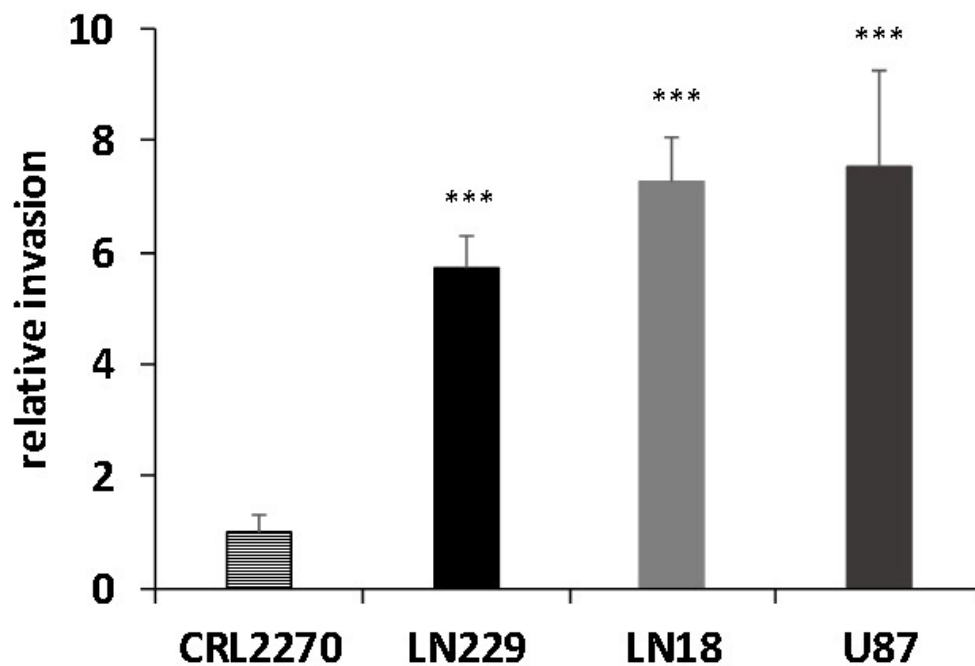
Figure 28: **Basal invasion of LN229, LN18 and U87**
The basal invasion of the three established GBM cell lines normalized to control brain fibroblasts (CRL2270), measured with a matrigel coated transwell assay. All experiments were performed three times and the error bar represents the SEM. Student's T-test was applied to calculate significance compared to CRL2270.

7.5 The influence of irradiation on the invasive behaviour of LN229, LN18 and U87
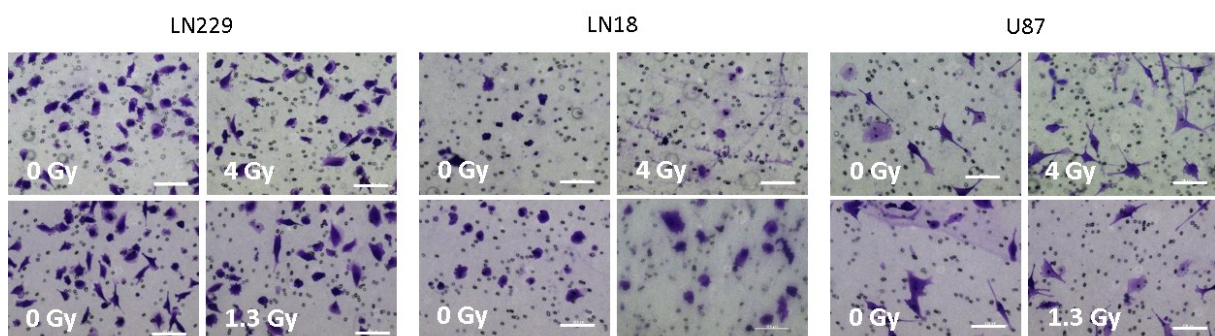
Figure 29: **Exemplary figures of the invasion assay**
Exemplary pictures of the invasion assay of LN229, LN18 and U87 after 4 Gy X-ray or the equivalent dose of 1.3 Gy α-particle irradiation are shown. The scale bar represents 100 μm.

24 hours after X-ray irradiation with 0 (sham), 2 and 4 Gy the invasion through matrigel coated transwell inserts was measured, see exemplary figures 29. As shown in Fig. 30a,

2 Gy X-ray irradiation did not change the invasive capacity of any of the three tested cell lines. A dose of 4 Gy X-ray irradiation changed the invasion in a cell line dependent manner. 2 out of 3 cell lines, LN229 1.5-fold $\pm$ 0.16 ($p \leq 0.001$) and U87 1.5-fold $\pm$ 0.06 ($p \leq 0.01$), showed a radiation-enhanced invasion, whereas one cell line, LN18, exhibited a significantly decreased invasion of 0.57-fold $\pm$ 0.05 ($p \leq 0.05$). Neither 0.43 Gy (equivalent
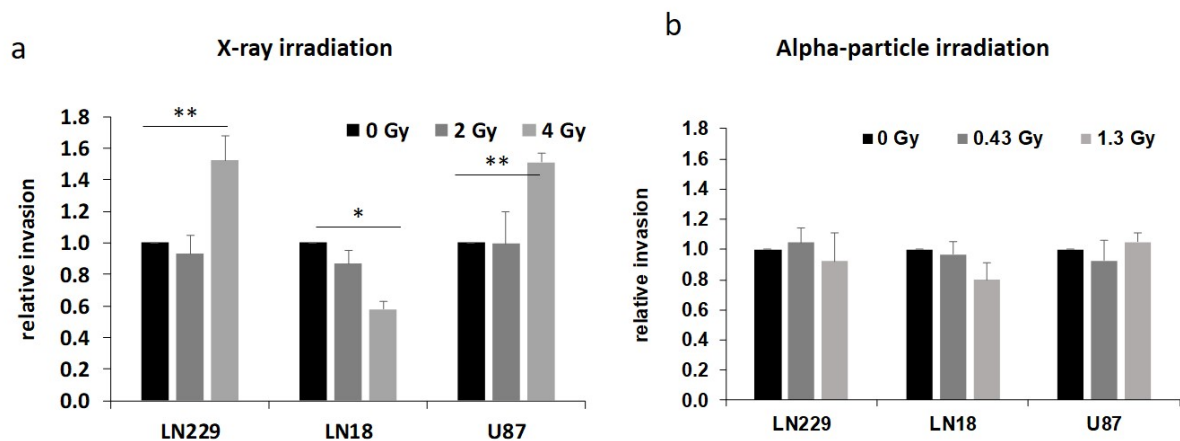
Figure 30: **Invasion of LN229, LN18 and U87 after irradiation**
Shown is the invasion of the three established GBM cell lines after X-ray (a) and α-particle (b) irradiation, normalized to sham irradiation. All experiments were performed at least three times and the error bar represents the SEM. Student's T-test was applied to calculate significance towards sham irradiated cells.

dose to 2 Gy X-ray irradiation) nor 1.3 Gy (equivalent dose to 4 Gy X-ray irradiation) α-particle irradiation showed any changes in the invasive potential of any of the three tested cell lines, see Fig. 30 b.

7.6   Investigating the phenomenon of X-ray irradiation-enhanced invasion

In order to find possible reasons for the X-ray enhanced invasion which is not observed after α-particle irradiation the biological and physical properties of both radiation qualities were analysed.

7.6.1   DNA damage

DNA damage caused by the different radiation sources was measured by γH2AX FACS and compared. Initial damage, measured 0.5 hours after 4 Gy X-ray respectively 1.3 Gy α-particle irradiation was used for normalization. As shown in Fig. 31, LN229 exhibited

24.5 % ± 9 % ($p \leq 0.001$) residual γH2AX signal 24 hours after X-ray irradiation but twice as much after α-particle irradiation, 51.3 % ± 24.6 % ($p \leq 0.01$). LN18 revealed 25.1 % ± 8.7 % residual γH2AX signal 24 hours after 4 Gy X-ray irradiation and 45.5 % ± 15.5 % ($p \leq 0.001$) after an equivalent dose of α-particle irradiation. U87 showed 60.7 % ± 9.9 % ($p \leq 0.05$) residual damage after X-ray irradiation and 54.2 % ± 11 % ($p \leq 0.001$) after α-particle irradiation. Differences between the cell lines were not significant.
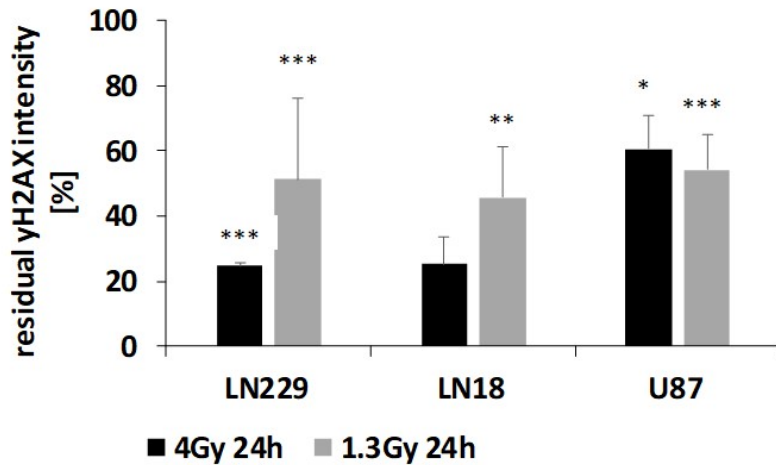
Figure 31: **Residual γH2AX Foci**
Shown is the residual γH2AX signal 24 hours after 4 Gy X-ray and the equivalent dose of 1.3 Gy α-particle irradiation, normalized to the γH2AX damage after 6 hours. All experiments were performed three times and the error bar represents the SEM. Student's T-test was applied to calculate significance towards sham irradiated cells.

7.6.2 Proteom profiler

To identify proteases involved in the radiation-enhanced invasion of LN229 and U87 cells, a proteome profiler was applied to screen 35 human proteases as well as 32 protease inhibitors. As only one membrane per sample was used, each quantified value was generated from two technical replicates of one biological sample. Statistics are therefore not possible and all changes are considered to be tendencies. Only changes of at least 20 % were considered. As table 9 shows, the profiler revealed most protease changes (19: 14 up-regulated and 5 down) in the LN229 cell line after 4 Gy X-ray irradiation, followed by LN18 with 9 (all up-regulated) and U87 with four (3 up- and 1 down-regulated) changes above 20 % in protease expression. Comparing these proteases (with a change larger than 20 %) in the three established cell lines, 2 shared proteases were identified. MMP-1 and MMP-7 were up-regulated in all three cell lines. But there was only one protease identified that was increased in LN229 and U87 but remained unchanged in LN18 after 4 Gy X-ray irradiation; CathepsinD (LN229 1.5-fold, LN18 0.9-fold, U87 2.2-fold).

When applying the same filter (at least 20 % change) to the protease inhibitor quantifica-

tion, LN229 exhibited most changes 24 hours after irradiation with 4 Gy X-rayagain, again (see 10). LN229 showed 19 (4 up- and 15 down-regulated) protease inhibitors that were affected by a fold change of at least ± 0.2, followed by LN18 with 4 changed protease inhibitors (3 up- and 1 down-regulated) and U87 with 7 changed protease inhibitors (1 up- and 6 down-regulated). Most important TIMP-2, Serpine B5, Lipocalin-1 and APP were down-regulated by 4 Gy X-ray irradiation in LN229 and U87 whereas they remained unaffected in LN18. Additionally, it was noticed, that Cystatin A was down-regulated in LN229 (0.1-fold) and U87 (0.5-fold), whereas LN18 was 6.6-fold up-regulated.

Table 9: List of affected proteases revealed by the proteom profiler. Data are shown as fold-change between 4 Gy X-ray irradiated an unirradiated values. Empty columns symbolize non-significant fold-changes.

	LN229	LN18	U87
MMP-7	1.6	1.4	1.6
Kallikrein 6	1.3		
Kallikrein 7	0.7	1.6	
Kallikrein 11	0.6	2.7	
Kallikrein 13	1.2	4.8	
MMP-1	1.4	2.5	1.4
MMP-2	1.2	0.9	0.9
MMP-3	1.3	1.0	0.3
Cathepsin L	0.5		
DRPIV	2.2		
Kallikrein 3	2.1		
Kallikrein 5	1.2		
ADAM 8	0.1		
ADAM 9	0.4		
ADAMTS 13	1.4	5.9	
Cathepsin A	1.3	6.5	
Cathepsin B	1.4	1.9	
Cathepsin C	1.4	2.7	
Cathepsin D	1.5	0.9	2.2

Table 10: List of affected protease inhibitors revealed by the proteom profiler. Empty columns symbolize non-significant fold-changes.

	LN229	LN18	U87
TFPI	0.4	0.7	0.5
TIMP-2	0.8	1.0	0.7
TIMP-3	0.2		
Serpin B5	0.7	1.0	0.7
Serpin B6	1.8	0.9	0.8
PAI-1	0.4	1.4	0.9
Serpin F1	0.4		
Testican 1	0.7		0.9
Latexin	0.7	1.2	1.3
Lipocalin-1	0.7	0.9	0.5
Lipocalin-2	0.8		
RECK	1.3		
Serpin A5	0.5		
Serpin A8	0.5		
APP	0.8	1.1	0.8
Cystatin A	0.1	6.7	0.5
Cystatin C	0.7	0.9	1.0
Cystatin E	1.3	2.0	
HAI-1	2.0		

7.6.3   uPA and MMP-2 ELISA

As urokinase-type plasminogen activator (uPA) and Matrix metalloproteinases (MMPs) are considered to be major players of invasion their expression in the cell culture supernatants of the X-ray and α-particle irradiated established GBM cell lines was examined by ELISA. The basal uPA secretion of unirradiated cells is shown in Fig. 32a. LN229 showed no uPA secretion at all, whereas U87 secreted significantly ($p \leq 0.001$) more uPA than LN18. 24 hours after X-ray (4 Gy) and alpha (1.3 Gy) irradiation, the uPA secretion in LN18 did not change, whereas U87 significantly ($p \leq 0.01$) decreased the secreted amount of uPA 0.65-fold $\pm$ 0.09 after X-ray irradiation and did not show a significant change (0.89-fold $\pm$ 0.06) after α-particle irradiation (Fig. 32b).
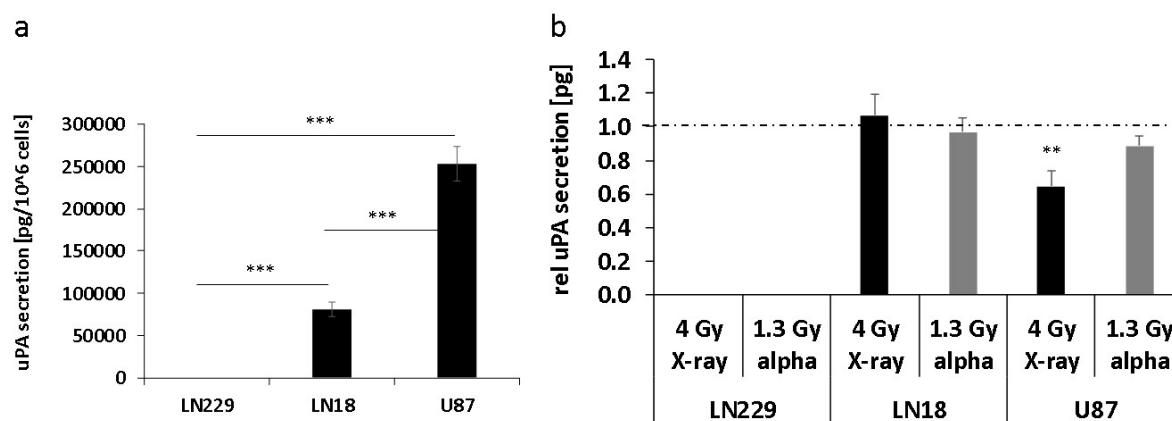
Figure 32: **uPA secretion**
Fig. a shows the basal uPA secretion. Fig. b shows the relative uPA expression of the three established cell lines 24 hours after 4 Gy X-ray or the equivalent dose of 1.3 Gy α-particle irradiation, normalized to sham irradiated cells. Significance was measured compared to sham irradiated cells. All experiments were performed three times and error bars represent the SEM. Student's T-test was applied to calculate significance.

Compared to LN229 and LN18 the basal secretion of MMP-2 was significantly highest ($p \leq 0.01$) in U87 with a secretion of $1457\,\text{ng}/10^6\text{cells} \pm 83\,\text{ng}/10^6\text{cells}$. MMP-2 secretion was not significantly different in LN229 and LN18 (Fig. 33a). 24 hours after X-ray irradiation with 4 Gy the amount of secreted MMP-2 in LN229 significantly decreased (0.86-fold $\pm$ 0.05, $p \leq 0.05$) but not after α-particle irradiation (1.1-fold, $p \geq 0.05$). Likewise, the secreted amount of MMP-2 in LN18 decreased significantly (0.8-fold $\pm$ 0.05, $p \leq 0.01$) 24 hours after 4 Gy X-ray irradiation but not after α-particle irradiation. The amount of secreted MMP-2 in U87 showed a tendency towards a decrease after X-ray irradiation (0.7-fold $\pm$ 0.21, $p = 0.15$) but not after α-particle irradiation, see Fig. 33b.

7.6.4   Generic MMP activity assay

In order to measure active MMPs, a generic MMP activity assay was performed. The assay was performed with cell lysates (Fig. 34a), cell culture supernatants 24 hours after irradiation (Fig. 34b) and cell culture supernatants 48 hours after irradiation (Fig. 34c). The examination of the lysates showed no significant MMP activity change 24 hours after X-ray and α-particle irradiation. Likewise, the supernatants taken 24 hours after irradiation did not reveal any significant changes in the generic MMP activity. After irradiation with 4 Gy X-ray, LN229 and U87 showed a trend towards a decreased generic MMP activity (LN229: 0.8-fold change $\pm$ 0.19, U87 0.7-fold change $\pm$ 0.16), whereas α-particle irradiation did not cause such a tendency. MMP activity in LN18 remained unaffected by any irradiation
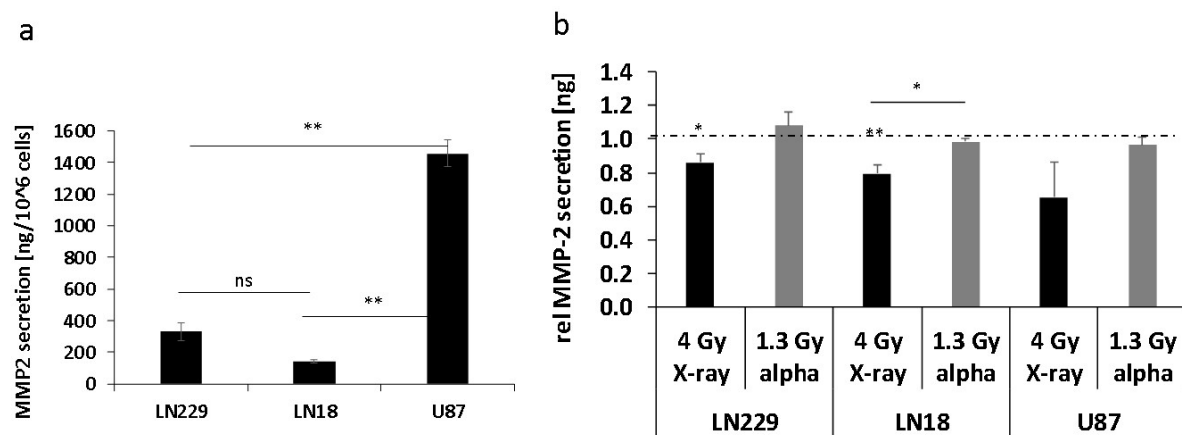
Figure 33: **MMP-2 secretion**
Fig a shows the basal MMP-2 secretion of the three established cell lines. Figure b shows the relative MMP-2 secretion 24 hours after 4 Gy X-ray or the equivalent dose of 1.3 Gy α-particle irradiation, normalized to sham irradiated cells. The significance was calculated compared to sham irradiated cells as well as between low- and high-LET irradiations. All experiments were performed three times and the error bar represents the SEM. Student's T-test was applied to calculate significance.

source. MMP activity measured in the supernatants 48 hours after irradiation with 4 Gy X-ray or 1.3 Gy α-particle likewise showed no significant change in any of the three tested cell lines.

7.6.5   qRT-PCR analysis on 11 potentially relevant genes for invasion

After analysing changes on the protein level, the mRNA-level was examined. Therefore, 11 potentially important genes for invasion were selected and their mRNA expression was analysed 24h after 4 Gy X-ray irradiation and 1.3 Gy α-particle irradiation by qRT-PCR (Fig. 35). Fold-changes ≤ 0.5 and ≥ 1.5 were considered significant. CDH1 was not detectable in LN229 and U87 cells, as well as uPA was not expressed in LN229 cells. 24 hours after 4 Gy X-ray irradiation mRNA expression of MMP-10 (2-fold), MMP-3 (1.5-fold) and Serpine1 (1.6-fold) was significantly up-regulated in LN229. After α-particle irradiation MMP-3 (1.6-fold) and Serpine-1 (4-fold) were likewise significantly up-regulated whereas MMP-10 was not up-regulated (1.0-fold). 24 hours after 4 Gy X-ray irradiation LN18 only had significantly up-regulated uPA (1.5-fold) which was not up-regulated after the equivalent dose of alpha- particle irradiation (1.0-fold). But after 1.3 Gy α-particle irradiation LN18 showed significantly up-regulated CSTA (4-fold), MMP-10 (2.3-fold) and MMP-3 (2.2-fold). U87 significantly up-regulated CSTA (2.4-fold) and MMP-3 (1.6-fold) after 4 Gy X-ray irradiation and after the equivalent dose of α-particle irradiation CSTA (3-fold) as well as MMP-3 (2.9-fold) were likewise significantly up-regulated. Additionally, CTSA (2.1-fold), MMP-2

a

b

c
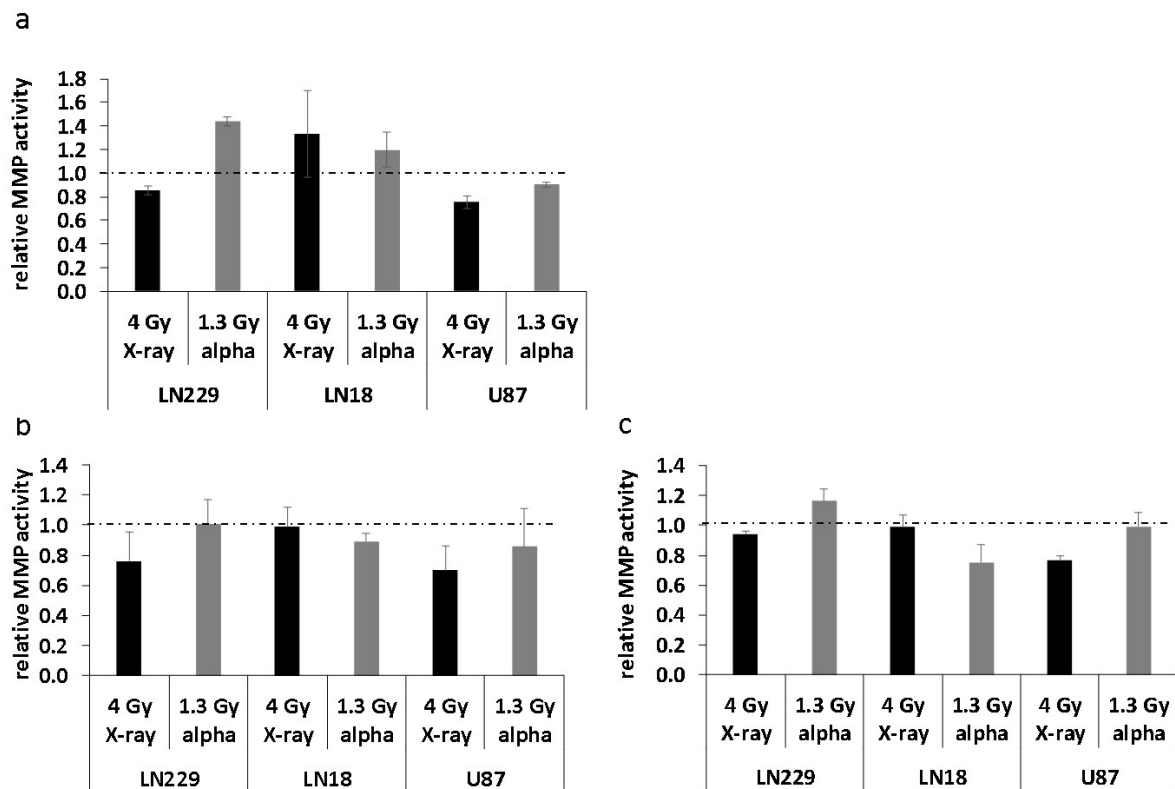
Figure 34: **Generic MMP activity**
Shown is the activity of several MMPs, measured after X-ray and alpha particle irradiation in the cell lysate (a), in the cell supernatant 24 hours after irradiation (b) or in the cell supernatant harvested 48 hours after irradiation. All experiments were performed three times and the error bar represents the SEM. Student's T-test was applied to calculate significance.

(1.9-fold), Serpine 1 (1.7-fold) and TIMP-2 (1.9-fold) were significantly up-regulated by α-particle irradiation in U87.

7.6.6 Epithelial-to-mesenchymal (EMT) Profiler

EMT plays an important role in the invasion of many cancer types. In order to expand the 11 invasion-relevant genes an EMT profiler on mRNA level was performed, see Fig. 36. As LN229 and U87 showed a low-LET irradiation-enhanced invasion, which was not observed in LN18, genes that were affected in the same way in LN229 and U87 but not in LN18 were searched for. CDH-1, GSC, DSP and MST1R were only expressed in LN18 but not in LN229 and U87. Likewise, 2 genes - CAV2 and FOCX2 - were only expressed in LN229 and U87 but not in LN18. Beside those genes, there were two more gene groups of interest. In the first group, consisting of CTNNB1, VCAN, NUDT13, PDGFRB and ZEB2, the mRNA expression after 4 Gy X-ray irradiation only decreased (ratio ≤ 0.6) in LN18 but remained unaffected in LN229 and U87. In the second group, consisting of TCF4,
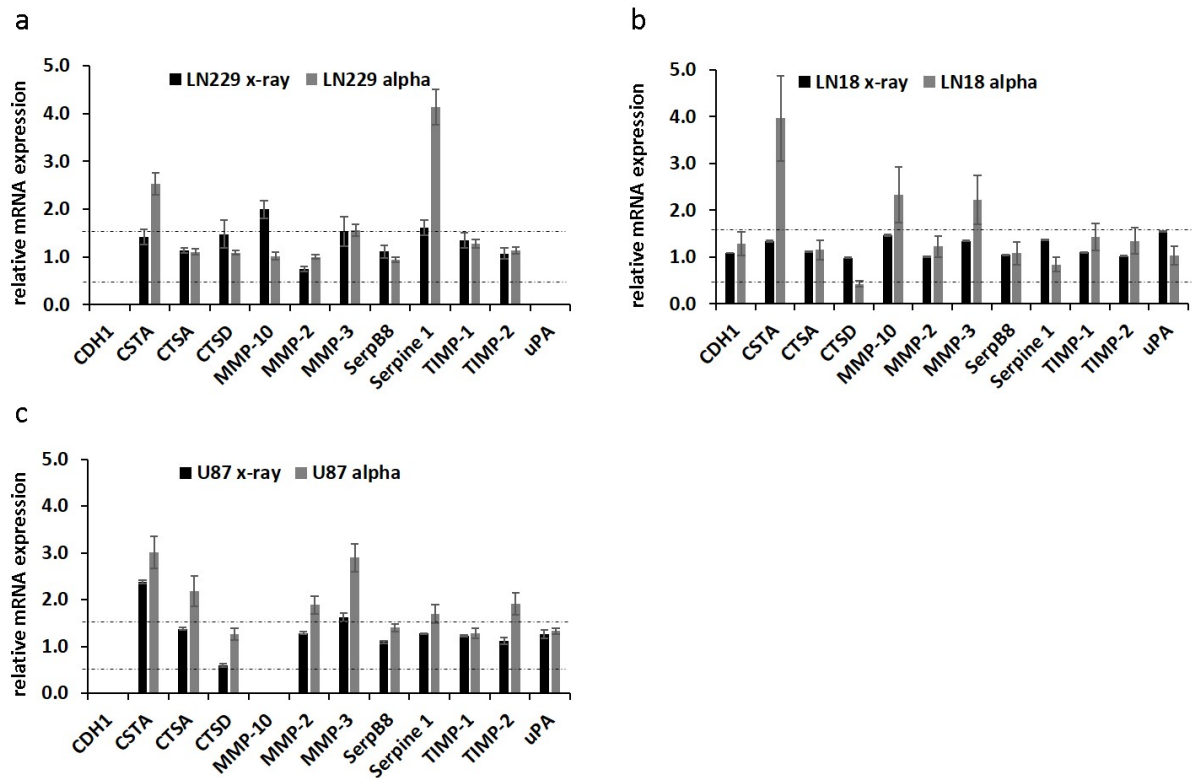
Figure 35: **qPCR analysis of potentially relevant genes for invasion**
Shown is the qPCR analysis of 11 potentially relevant genes for invasion of LN229 (a), LN18 (b) and U87 (c). All experiments were performed three times and the error bar represents the SEM. A fold-change larger than 50% was considered significant.

NOTCH1, TCF3, TMEFF1, FGFBP1 and SPP1, the mRNA ratio only increased (ratio ≥ 1.2) in LN18 but remained unaffected in LN229 and U87. After α-particle irradiation there were overall more genes up-regulated than after X-ray irradiation but there was only one gene, NOTCH1, whose expression changed the same way after X-ray irradiation and α-particle irradiation in LN229 and U87, whereas it changed the other way in LN18.

Table 11: List of fold-changes of the LN229 EMT-qPCR results

gene name	LN229 X-ray ratio	LN229 alpha ratio
AHNAK	0.63	1.96
COL5A2	0.71	1.39
F11R	0.45	1.92
FOXC2	1.31	1.69
ITGA5	1.69	1.95
NoDAL	1.21	1.82
NOTCH1	0.69	1.27
SERPINE1	3.57	4.47

Table 11: Continuation list of fold-changes of the LN229 EMT-qPCR results

gene name	LN229 X-ray ratio	LN229 alpha ratio
SNAI3	0.55	1.57
TCF4	0.71	1.57
VP13A	0.71	1.75
WNT5A	1.24	1.99

Table 12: List of fold-changes of the LN18 EMT-qPCR results

gene name	LN18 X-ray ratio	LN18 alpha ratio
CDH-1	0.63	1.17
CTNNB1	0.27	1.01
FGFBP1	1.40	4.20
GSC	0.74	1.89
MAP1B	1.40	1.79
MST1R	2.71	1.24
NOTCH1	1.21	1.80
NUDT13	0.51	1.79
SPP1	1.53	0.88
WNT5A	0.72	0.97
ZeB1	0.77	1.09
ZEB2	0.60	1.13

Table 13: List of fold-changes of the U87 EMT-qPCR results

gene name	U87 X-ray ratio	U87 alpha ratio
ERBB3	0.76	2.83
FGFBP1	0.53	1.88
NOTCH1	0.73	1.23
SERPINE1	0.73	0.86
SNAI3	1.28	0.94
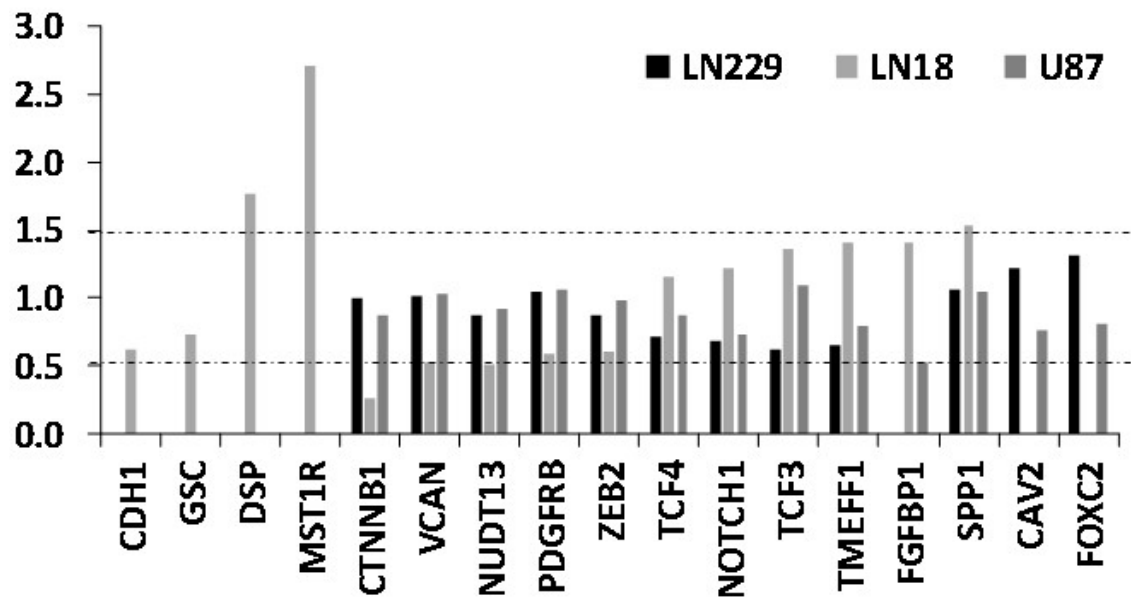
Figure 36: **qPCR on genes relevant for epithelial to mesenchymal transition**
LN229, LN18 and U87 were irradiated with 4 Gy X-ray and mRNA was isolated 24 hours afterwards. qPCR was only perfomed once as a RT^2-Profiler (Qiagen) was applied.

7.6.7 EMT Immunofluorescence staining

Relative Vimentin intensity

In order to validate findings from the gene level on protein level an EMT immunofluorescence staining was performed on the three established cell lines, see figure 37. An immunofluorescence staining for Vimentin was performed as an increasing Vimentin intensity provides evidence for mesenchymal transition. As shown in Fig. 38a, 24 hours after 4 Gy X-ray irradiation the intensity of Vimentin in LN229 was not changed at all, whereas LN18 was significantly (1.6-fold ± 0.2; $p \leq 0.05$) increased. U87 showed a relative Vimentin intensity of 1.4-fold $\pm$ 0.3 ($p = 0.53$) 24 hours after 4 Gy X-ray irradiation. After α-particle irradiation there was no detectable intensity change of the Vimentin signal.

Correlating Vimentin to DAPI

Correlating the DAPI signal with the Vimentin signal gives evidence for cytoplasmic changes. If the ratio of the two signals is small, that means that the cytoplasm is wrapping the nuclei, expressing only little attachment area but if the ratio is large that means that the cell is strongly attached to the coverslip, expressing a lot of filopodia. Fig. 38b demonstrated that there was no significant difference but rather a tendency that 4 Gy X-ray irradiation diminished the cytoplasmic attachment area 24 hours after irradiation, indicated as the ratio of DAPI to Vimentin is 0.7 $\pm$ 0.3 for LN229 and 0.88 $\pm$ 0.2 for LN18, as well as
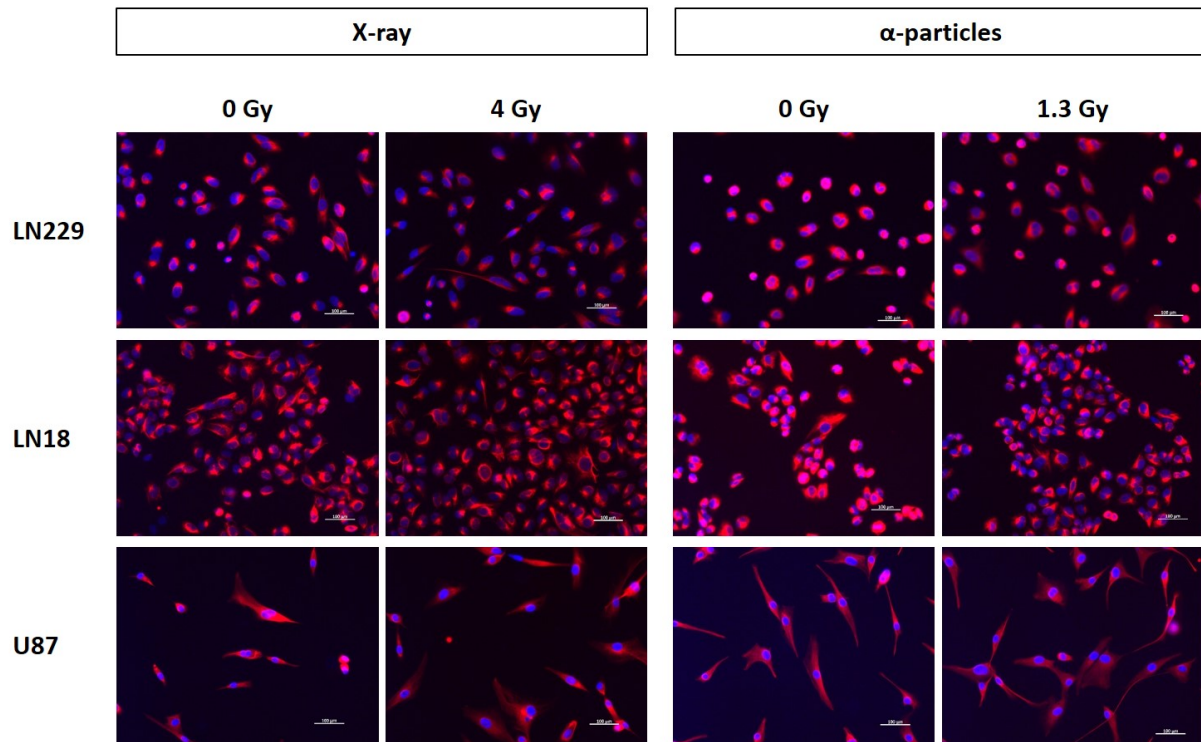
Figure 37: **Exemplary figures of the Vimentin immunofluorecence staining**
Exemplary images of the Vimentin staining of LN229, LN18 and U87 after 4 Gy X-ray and the equivalent dose of 1.3 Gy α-particle irradiation are shown. Red cytoplasmic staining is the Vimentin signal and blue staining is the counterstaining of the nucleus (DAPI).

0.9 $\pm$ 0.2 for U87. Likewise, the correlation of the DAPI to Vimentin signal revealed no significant changes 24 hours after α-particle irradiation (LN229: 1.0 $\pm$ 0.1, LN18: 1.1 $\pm$ 0.1, U87: 1.0 $\pm$ 0.02).

7.7   Pathway analysis

7.7.1   Igenuity pathway analysis (IPA)

To identify the mechanism underlying the low-LET irradiation-enhanced invasion several potentially important signaling pathways for GBM invasion were determined via the IPA. One GBM cell line that showed radiation-enhanced (LN229) and one that did not result in radiation-enhanced invasion (LN18) were chosen for the IPA. First, several canonical pathways were analyzed for differences after 4 Gy X-ray irradiation, see figure 39a. This analysis revealed major differences in the activation score after 4 Gy X-ray irradiation in both cell lines. Amongst others the GBM signaling was affected (Fig. 39b). Based on all up- and down-regulated proteins the impact on the cell line invasion was analysed. As depicted in Fig. 39 c/d, the IPA suggested an increased invasion of both cell lines after 4
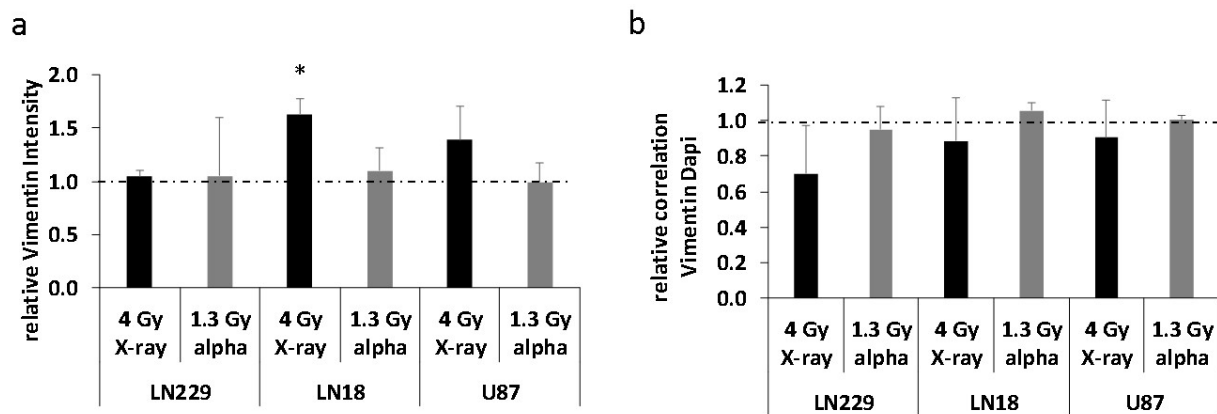
Figure 38: **Analysis of the immuno-fluorecence staining of Vimentin**
Shown is the relative intensity of Vimentin a) after 4 Gy X-ray irradiation or the equivalent dose of 1.3 Gy α-particle irradiation, normalized to sham irradiated cells. Figure b) shows the relative correlation of the Vimentin signal towards the nucleus (stained with DAPI). Experiments were performed three times and the SEM is depicted.

Gy X-ray irradiation.

In a second IPA the influence of 4 Gy X-ray and 1.3 Gy α-particle irradiation on each cell line were compared, see figure 40 a/b. As illustrated, both irradiation sources caused different canonical pathway activation scores. After implementing those scores to the invasion prediction, the IPA again suggested up-regulated invasion of both cell lines after α-particle irradiation (see figure 40 c/d).

Based on those assumptions a third IPA was performed. Analyzing the most relevant canonical pathways, being altered in both cell lines as measured with the IPA 1 and IPA 2. Hence, the third IPA questioned for canonical pathways being altered in LN229 and LN18 after 4 Gy X-ray or 1.3 Gy α-particle irradiation, see figure 41. Through this IPA query the Wnt-signaling, the AKT signaling and the TGF-β signaling pathway were determined to seem to play major roles in GBM invasion.
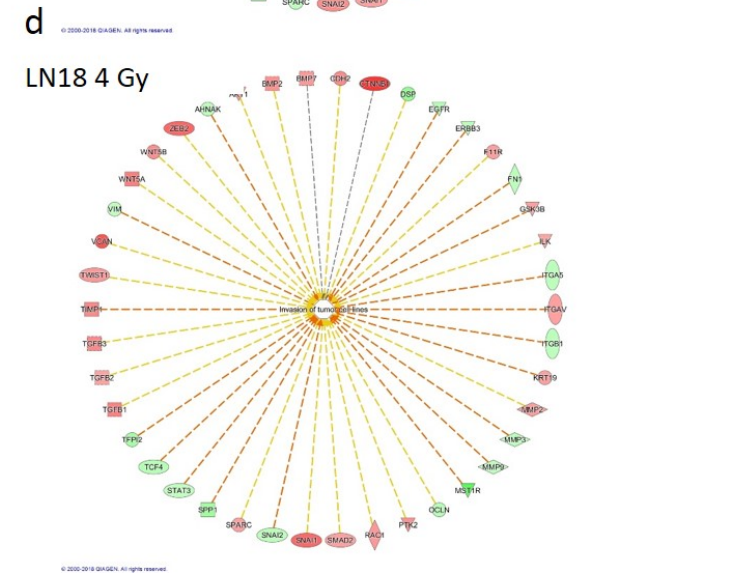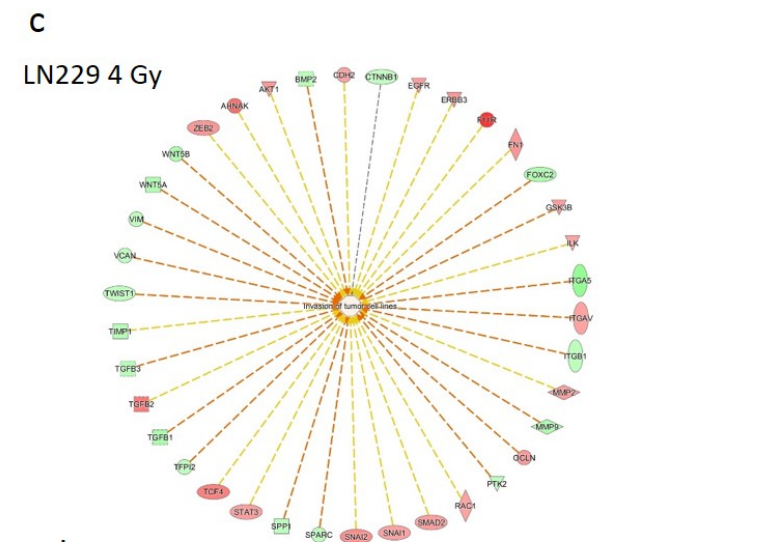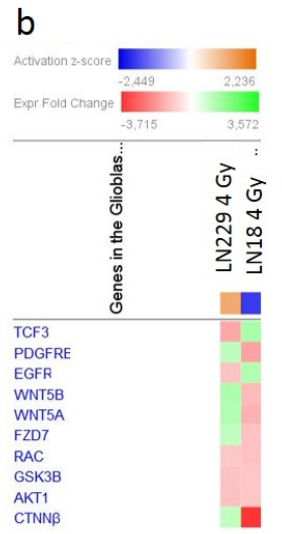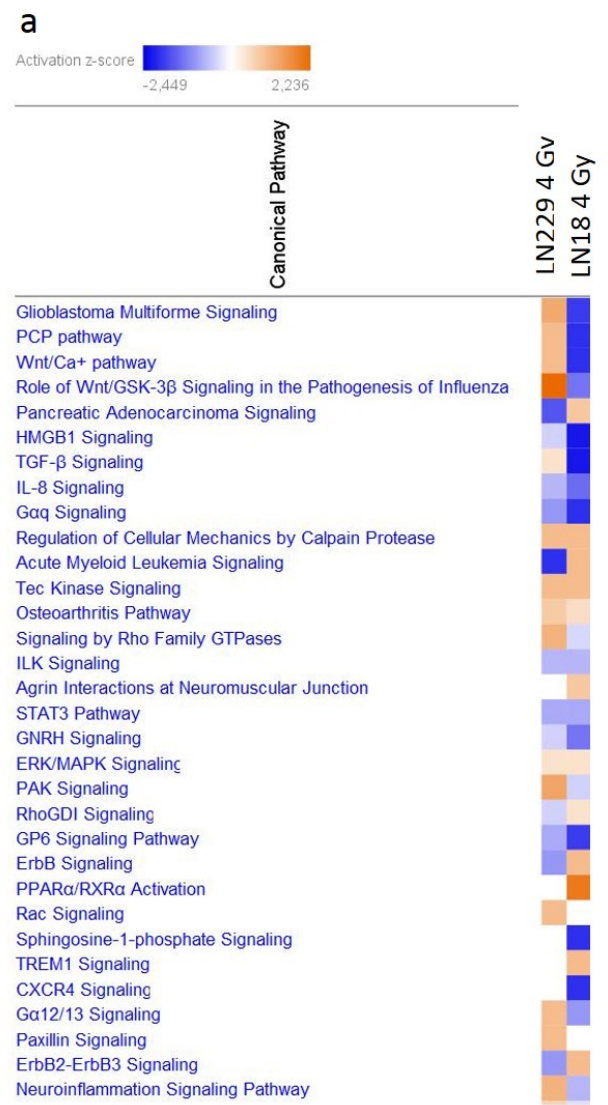
Figure 39: **Ingenuity pathway analysis of LN229 and LN18 after X-ray irradiation**
The image represents the IPA of LN229 and LN18 after 4 Gy X-ray irradiation. a) shows the activation scores of the canonical pathways. Blue labels represent down-regulated and orange labels represent up-regulated pathways. b) depicts fold-changes (red down- and green up-regulated) of proteins of the GBM signaling pathway after 4 Gy X-ray irradiation. c) and d) represent the prediction of the tumor cell invasion. Proteins being up-regulated after X-ray irradiation are marked in green while proteins causing a down-regulated invasion are marked in red. The orange circle centre represents predicted up-regulated tumor cell invasion.
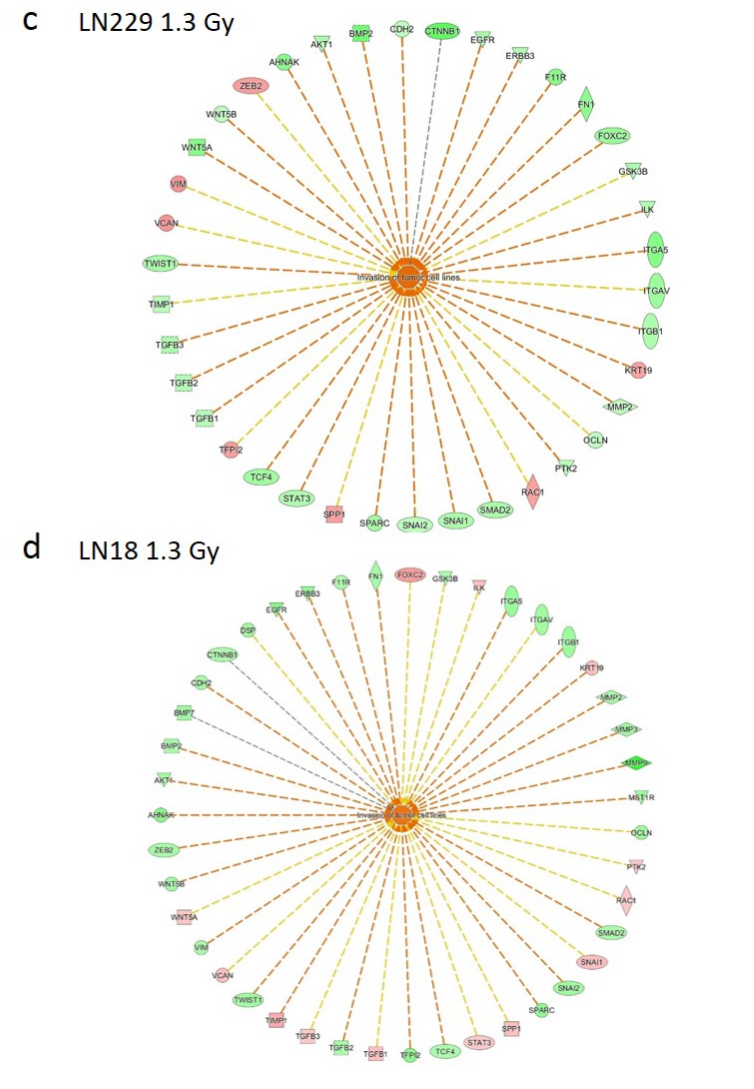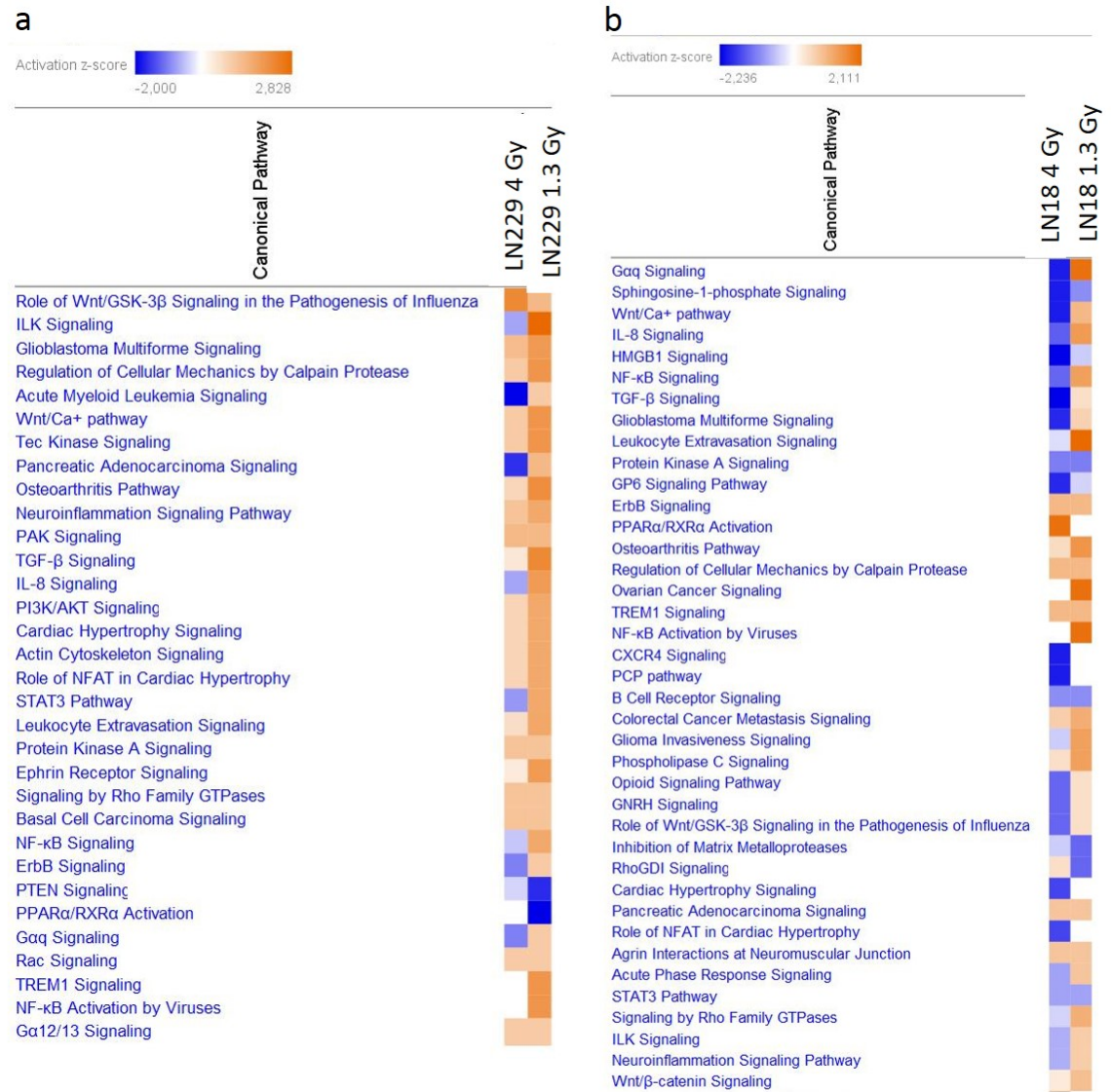
Figure 40: Ingenuity pathway analysis of LN229 and LN18 after X-ray irradiation compared to α-particle irradiation

The image represents the IPA of LN229 and LN18 after 4 Gy X-ray and 1.3 Gy α-particle irradiation. Activation scores of the canonical pathways in LN229 (a) respectively in LN18 (b) are depicted. Blue labels represent down-regulated and orange labels represent up-regulated pathways. c) and d) represent the prediction of the tumor cell invasion after 1.3 Gy α-particle irradiation. Proteins being up-regulated after X-ray irradiation are marked in green while proteins causing a down-regulated invasion are marked in red. The orange circle centre represents predicted up-regulated tumor cell invasion.
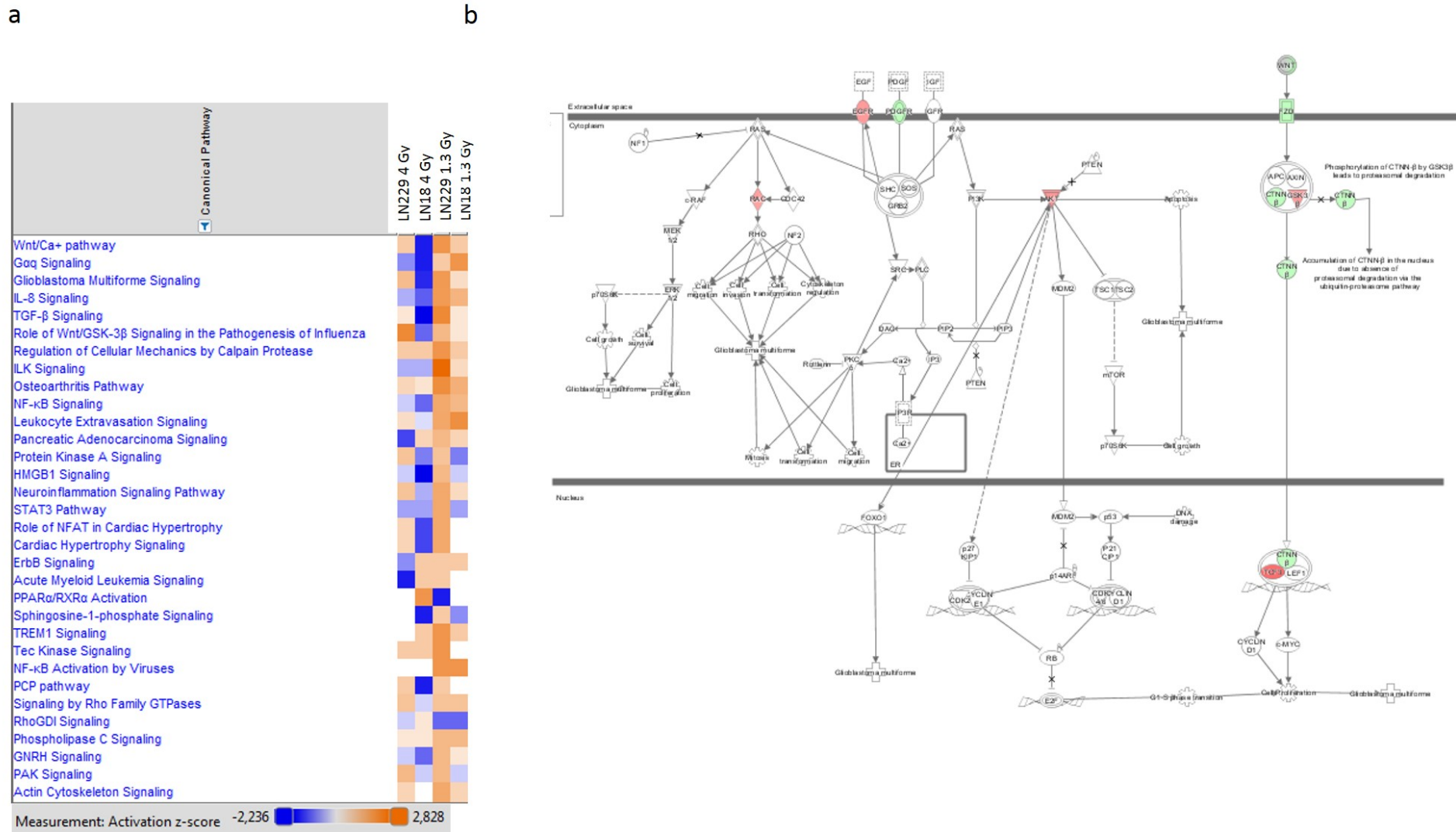
Figure 41: [**Altered canonical pathways of LN229 and LN18 after X-ray irradiation compared to α-particle irradiation**
The image represents altered canonical pathways of LN229 and LN18 after 4 Gy X-ray and 1.3 Gy α-particle irradiation. a) shows the activation scores of the canonical pathways in LN229, respectively in LN18, after irradiation. Blue labels represent down-regulated and orange labels represent up-regulated pathways. b) represents the predicted pathways. Proteins being up-regulated are marked in green while proteins that are down-regulated are marked in red.

7.7.2   Determination of pathway activity

Proteins playing major roles in those pathways were therefore examined by Western Blotting on their un- and phosphorylated expression, see exemplary figures 42. β-Catenin and phosphorylated β-Catenin as well as GSK3B and phosphorylated GSK3B as playors of the Wnt signaling, AKT and phosphorylated AKT as major components of the AKT signaling and SMAD2/3 and phosphorylated SMAD2/3 as important actors of the TGF-β signaling pathways were analysed for activation levels after 4 Gy X-ray or 1.3 Gy α-particle irradiation.
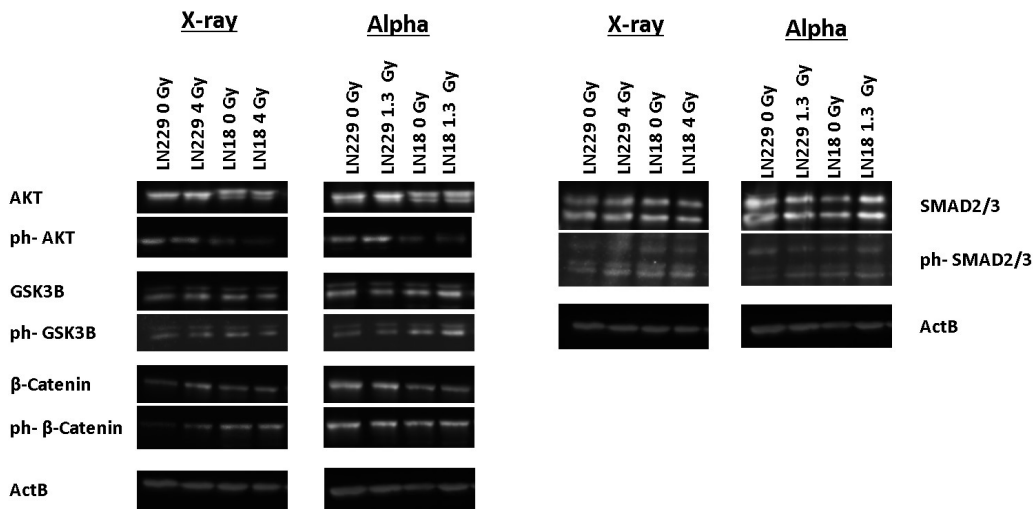
Figure 42: **Exemplary Western Blot images**
The picture shows exemplary WB images of LN229 and LN18 after 4 Gy X-ray irradiation or the equivalent dose of 1.3 Gy α-particle irradiation. Shown are the proteins AKT, GSK3, β-Catenin and SMAD2/3 in their un- and phosphorylated form. Bands were normalized to the loading control ActinB (ActB).

As shown in figure 43b) and c) all levels of GSK3 respectively phosphorylated GSK3 and β-Catenin, respectively phosphorylated β-Catenin remained unaffected by X-ray and α-particle irradiation.

But the AKT pathway analysis revealed a significant down-regulation of activated (phosphorylated) AKT in LN18 after 1.3 Gy α-particle irradiation. Likewise 1.3 Gy α-particle irradiation showed no influence on LN229. The equivalent dose of 4 Gy X-ray irradiation on the other hand revealed, even though not significant, a tendency towards an up-regulated AKT activation, see figure 43a). In figure 43d) it can be seen, that 4 Gy X-ray irradiation significantly increased the activation of SMAD2/3 whereas the phosphorylated levels of SMAD2/3 remained unaffected in LN18 or after α-particle treatment of LN229 and LN18.
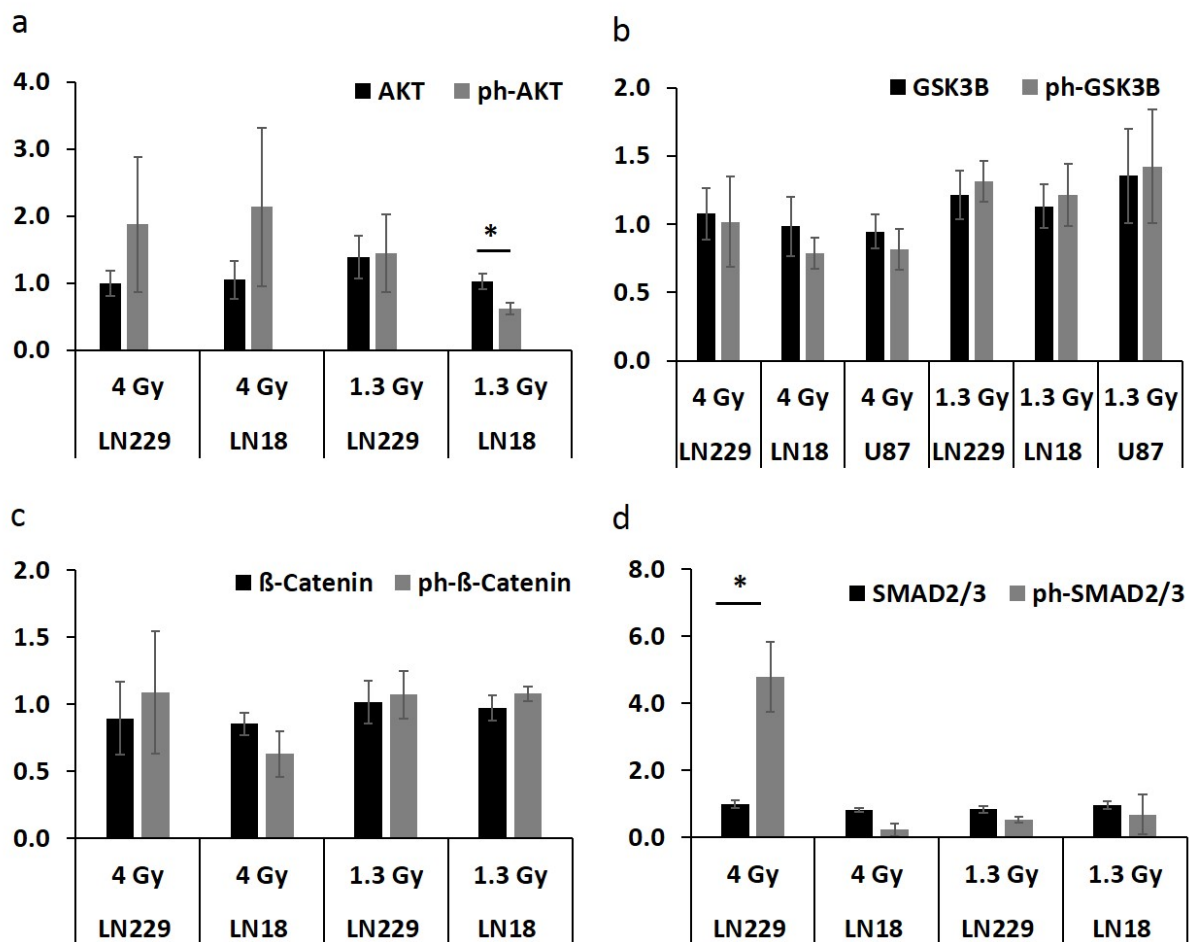
Figure 43: **Western Blot analysis of pathway activity**
Shown are the un- and phosphorylated amounts of AKT (a), GSK3B (b), β-Catenin (c) and SMAD2/3 (d) of LN229 and LN18 after 4 Gy X-ray irradiation or the equivalent dose of 1.3 Gy α-particles. Each value was determined of two biological and two technical replicates. SEM are depicted. Significance was determined applying the Student's T-Test with $p \leq 0.05$ being $*$

7.8   Primary cell culture

In order to transfer results from established cell lines into clinical settings, the RadGlio study was initiated in cooperation with the Neurosurgery of the Klinikum rechts der Isar. This study provided the possibility to isolate and analyse patient-derived primary GBM cells for their basic characteristics as well as their invasive capacity after irradiation with low- and high-LET irradiation.

7.8.1   Patient-derived primary glioma cell isolation

In order to ensure that the freshly isolated tumor cells are of glial origin, a glial fibrillary acidic protein (GFAP) staining was performed. As can be seen in table 14 all freshly isolated primary cells are positive for GFAP.

Table 14: GFAP staining of patient-derived primary cells
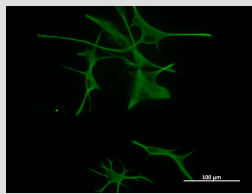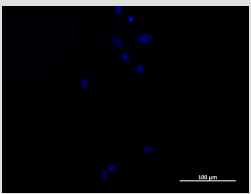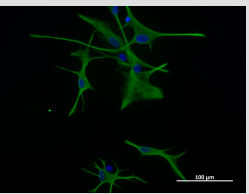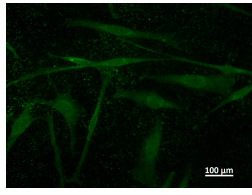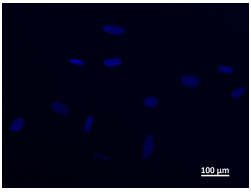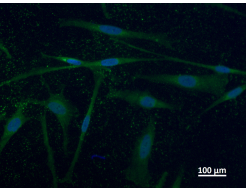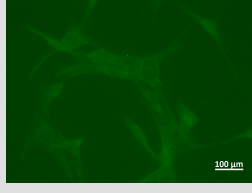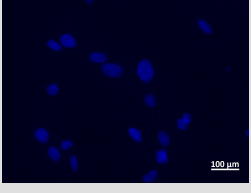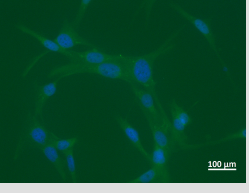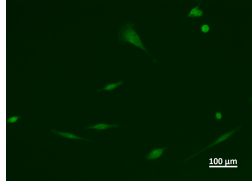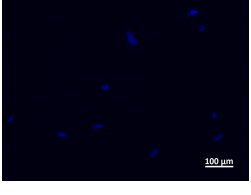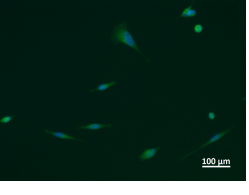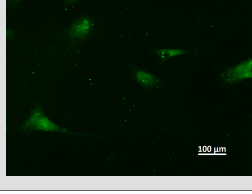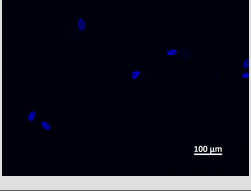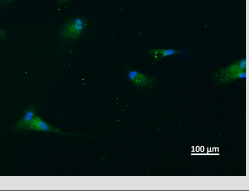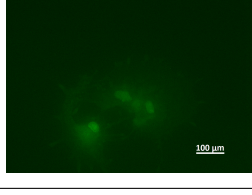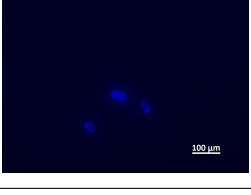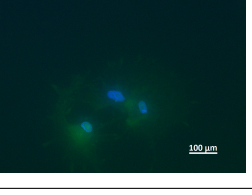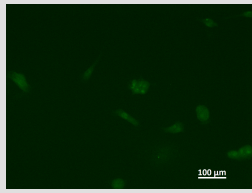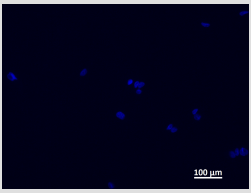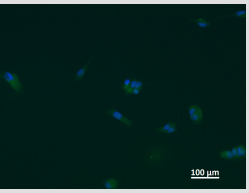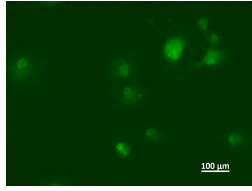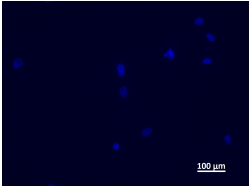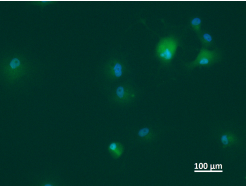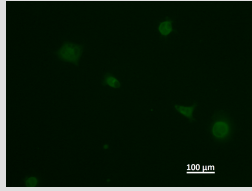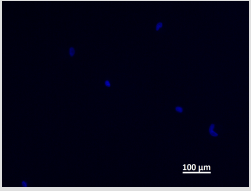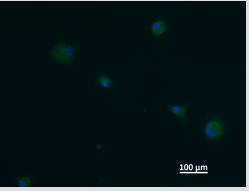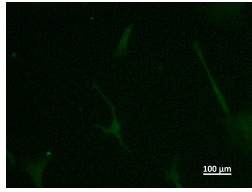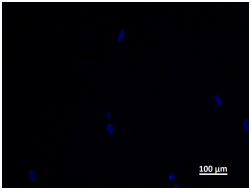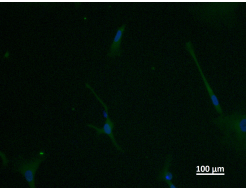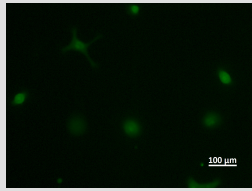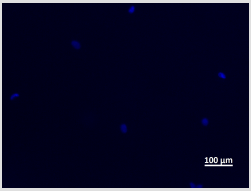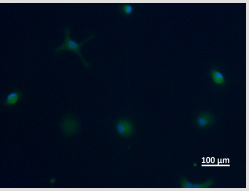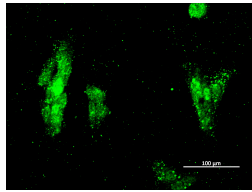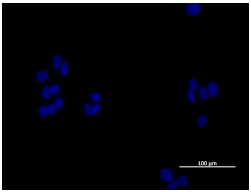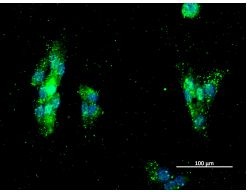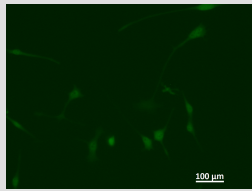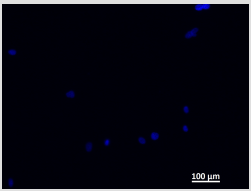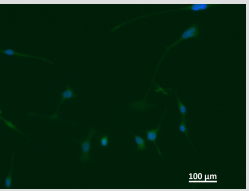
cell line	GFAP	DAPI	merge
H2			
H5			
H9			
H19			
H23			
H27			

Table 14: Continuation of the GFAP staining

cell line	GFAP	DAPI	merge
H34			
H37			
H41			
H45			
H46			
T76			
T84			

7.8.2   CFA with primary glioma cells

For five primary glioma cell lines (T76, T84, H5, H9, H19) CFAs after X-ray irradiation were performed. The PE depended on the cell line, T76 showed a PE of $31\% \pm 6\%$, T84 $26\% \pm 3\%$, H5 $23\% \pm 4\%$, H9 $19\% \pm 6\%$ and H19 showed a PE of $6\% \pm 2\%$. As Fig. 44 and table 15 show the survival fraction was dose dependent, even though the survival drastically depended on the cell line, again an indication for the heterogeneity known of glioma cells. All cell lines demonstrated the typical shoulder formation of low-LET irradiation and followed the linear quadratic model.
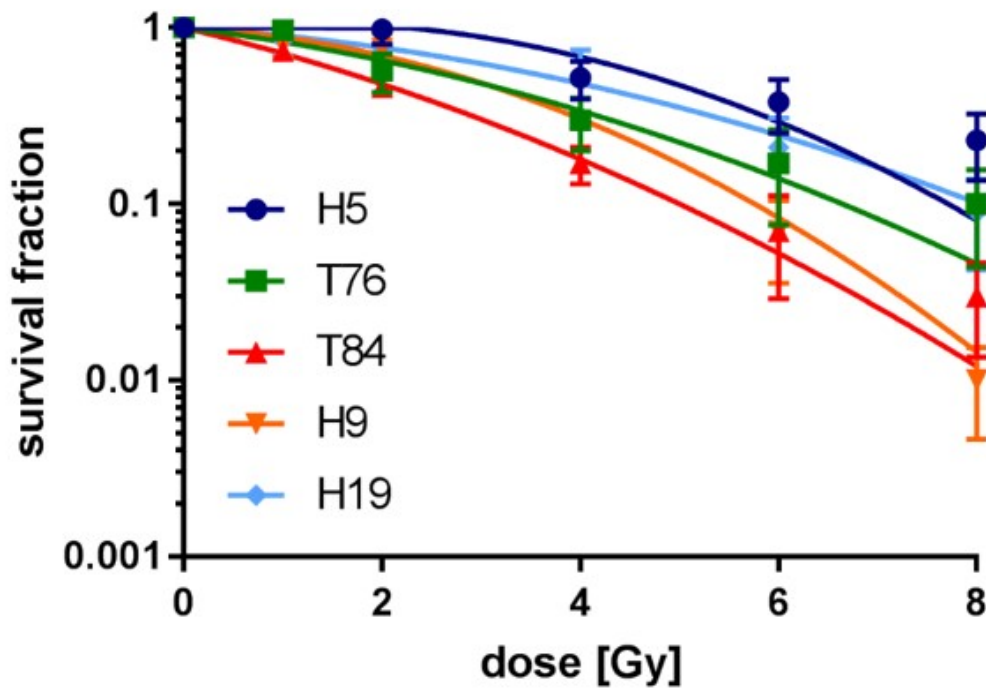
Figure 44: **CFA assay of the primary glioma cells**
The survival fraction of five primary glioma cell lines is shown, 12 days after X-ray irradiation. Experiments were performed in triplicates and the SEM is depicted.

Table 15: Calculations of the primary cell CFA

cell line	$\alpha\,[\mathrm{Gy^{-1}}]$	$\beta\,[\mathrm{Gy^{-2}}]$	D50 [Gy]	D10 [Gy]
T76	0.021	0.01	3.0	8.2
T84	0.48	-0.01	1.5	5.1
H5	0.031	0.032	4.2	8.0
H9	-0.03	0.08	3.1	5.4
H19	0.08	0.03	3.7	7.5

7.8.3   Doubling time calculation in dependency of X-ray irradiation

Doubling time after IR with 0 Gy and 4 Gy
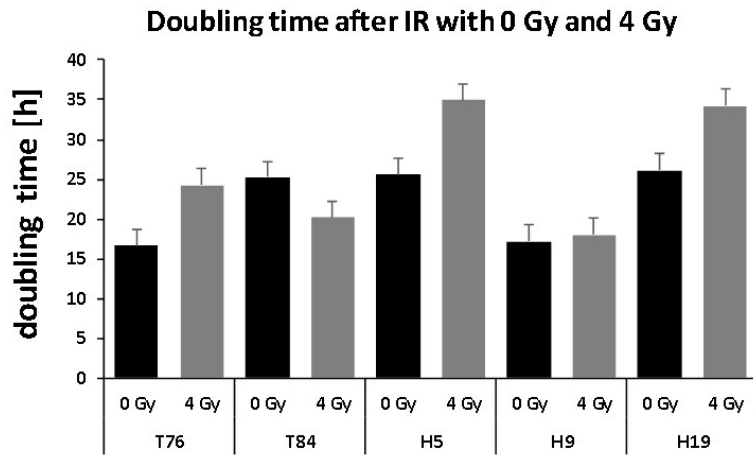
Figure 45: **Doubling time of primary glioma cells**
The doubling time of five primary GBM cell lines after 4 Gy X-ray irradiation is shown. Experiments were performed at least three times and the SEM is depicted.

To examine the influence of X-ray irradiation on the proliferation of the primary cells a growth curve was performed over 96 hours. As shown in figure 45, for most primary cell lines the doubling time showed an increasing tendency, whereas the doubling time of T84 was 25 hours without and 20 hours after 4 Gy X-ray irradiation. In case of H9 doubling time remained unaffected from irradiation as their doubling time was 17 hours with or without irradiation. All changes in doubling time were not significant.

7.8.4   Cell cycle distribution of primary glioma cells after X-ray irradiation
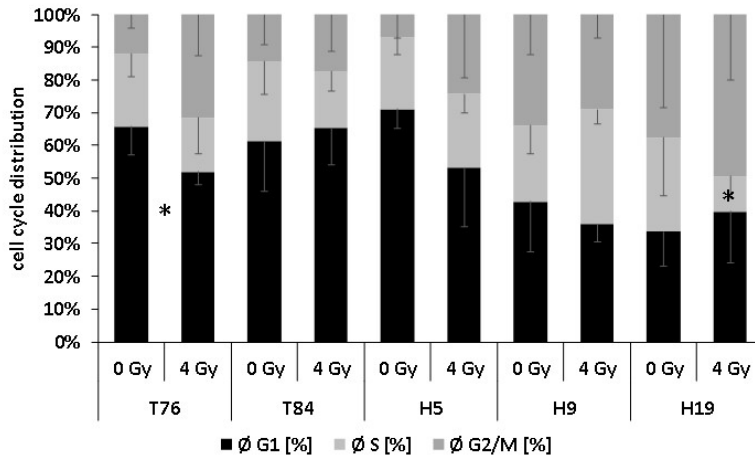
Figure 46: **Cell cycle distribution of primary glioma cells**
The cell cycle distribution of five primary cell lines after 4 Gy X-ray irradiation is shown. Experiments were performed in triplicates and the SEM is depicted.

The same 5 primary cell lines (T76, T84, H5, H9 and H19) were used to measure cell cycle distribution 24 hours after 4 Gy X-ray irradiation. Except for H9 all other primary cells show a radiation-induced G2M arrest, even though this finding is not significant for any cell line, see Fig. 46.

7.8.5   Basal invasion of primary glioma cells

Glioma cells are considered to be naturally highly invasive. Therefore, freshly-isolated primary glioma cell invasion was analysed and compared to human-brain-fibroblasts (CRL-2270). All sixteen isolated and analysed primary glioma cells demonstrated enhanced invasive potential compared to brain fibroblasts (CRL), see Fig. 47. T76 was 3.4-fold $\pm$ 0.6 as invasive ($p \leq 0.05$), H19 3.1-fold $\pm$ 0.3 ($p \leq 0.01$), H46 1.3-fold $\pm$ 0.1 ($p \leq 0.05$), H23 4-fold $\pm$ 0.9 ($p \leq 0.05$), H27 5.3-fold $\pm$ 0.9 ($p \leq 0.01$), H37 8-fold $\pm$ 1.7 ($p \leq 0.05$), H45 4.4-fold $\pm$ 1.1 ($p \leq 0.05$) and H9 9.9-fold $\pm$ 1.7 ($p \leq 0.01$). All other cell lines (T75, T84, H5, H33, H34, H41; H1, H24) showed a tendency towards increased invasiveness but were not significantly more invasive than the control fibroblasts. Depending on the their invasive capacity there is no clear diffentiation between the glioma subgroups possible.

Figure 47: **Basal invasion of the primary glioma cell lines**
The basal invasion of the patient-derived primary glioma cell lines, normalized to control brain fibroblasts (CRL) is shown. Astrocytomas are abbreviated by Astro., Oligodendroglioma are abbreviated by Oligo. and relapsed gliomas are abbreviated by R. Experiments were performed in triplicates and the SEM is depicted. Students T-test was applied and p≤ 0.05 was considered significant ∗,p ≤ 0.01 ∗ ∗.

7.8.6   Invasive capacity of primary glioma cells after irradiation

The invasive capacity of the primary glioma cells after low-LET irradiation

16 primary glioma cell lines were tested for their invasive capacity 24 hours after 4 Gy X-ray irradiation. As shown in figure 48 a the invasion of 12 primary glioma cell lines was affected. The invasion of T76 was significantly increased 1.4-fold $\pm$ 0.09 ($p \leq 0.05$), T84 1.4-fold $\pm$ 0.1 ($p \leq 0.05$), H2 1.9-fold $\pm$ 0.1 ($p \leq 0.01$), H23 2-fold $\pm$ 0.4 ($p \leq 0.05$), H27 1.6-fold $\pm$ 0.2 ($p \leq 0.05$), H33 1.5-fold $\pm$ 0.1 ($p \leq 0.01$), H34 1.7-fold $\pm$ 0.3 ($p \leq 0.05$), H45 1.6-fold $\pm$ 0.2 ($p \leq 0.05$). But also H5, H10, H24 and H46 showed a tendency of changed invasion after 4 Gy X-ray irradiation but were not significantly increased. H9, H19, H37 and H41 showed no changes in their invasive capacity 24 hours after 4 Gy X-ray irradiation.

The invasive capacity of primary glioma cells after high-LET irradiation

After high-LET α-particle irradiation (Fig. 48 b) none of the tested primary glioma cell lines demonstrated irradiation-enhanced invasion. In contrast to low-LET irradiation the invasion of all 9 tested primary glioma cell lines remained unaffected.

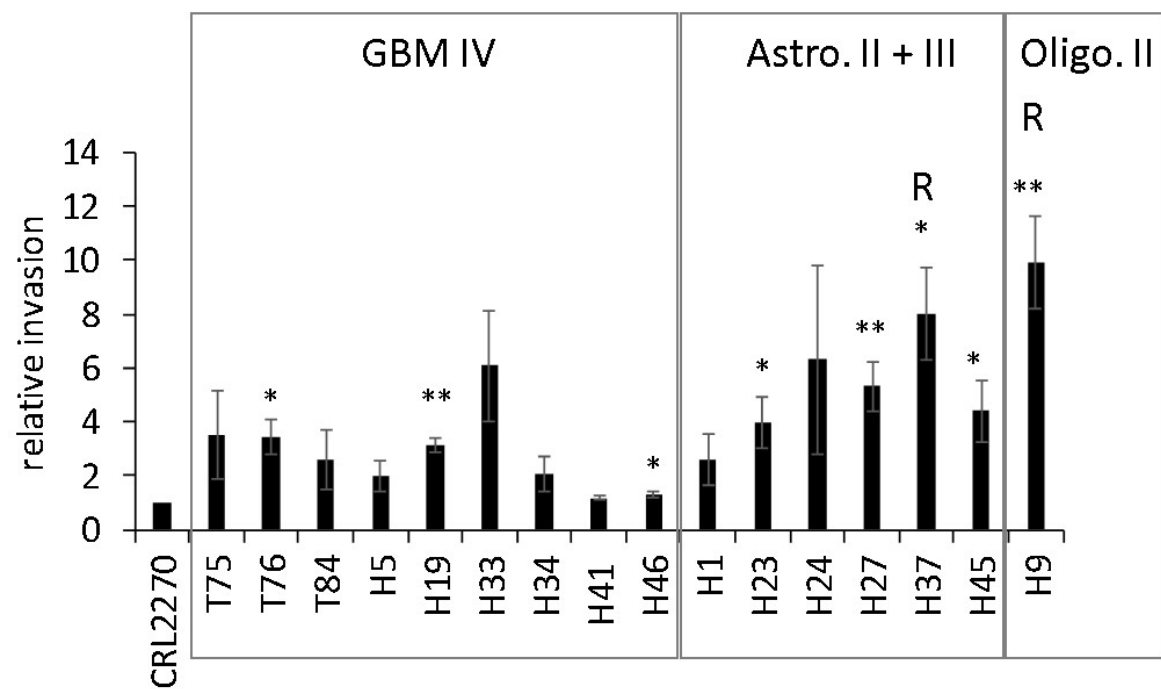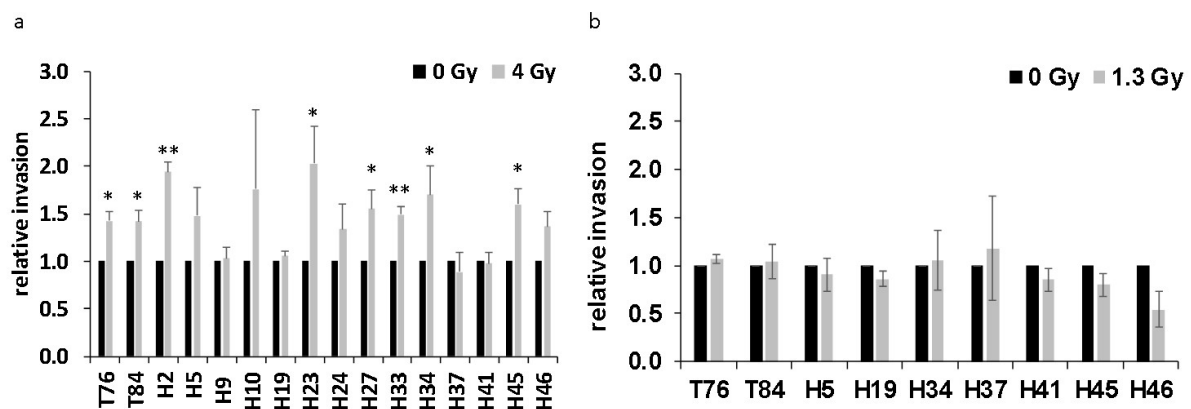Figure 48: **Invasion of the primary glioma cell lines**
The relative invasion of the patient-derived primary glioma cell lines, normalized to sham irradiated cells 24 hours after 4 Gy X-ray (a) or 1.3 Gy α-particle (b) irradiation is shown. Experiments were performed in triplicates and the SEM is depicted. Students T-test was applied and $p \leq 0.05$ was considered significant $*$, $p \leq 0.01 * *$.

7.9   Immunohistochemistry on patient-derived tumor tissue

From each patient tissue sample that took part in the RADGlio trial, a tissue-tumor sample was also stored in the pathology and tissue sections were produced. In cooperation with the pathology of the Helmholtz Zentrum Munich, 10 patient-derived tumor tissues were stained for E-Cadherin and Vimentin. From the staining analysis several features were extracted. Finally, average marker expression, average marker expression of high-expressed areas, mean border index and mean compactness were calculated and compared to the basal invasion of the same patient-derived material, but isolated and cultured as cells. As figure 51 shows, the expression patterns of Vimentin and E-Cadherin were completely different between the patient samples. Shown are three exemplary types of staining intensities. Figure 49 a) depicts the calculated features of the E-Cadherin staining while b) shows the same features of the Vimentin staining. While all sections of all patients were positive for Vimentin, the E-Cadherin staining allowed the recognition of more diverse expression patterns. Comparing the relative invasion of the patient-derived cell culture after 4 Gy X-ray irradiation, measured with the invasion assay, to the E-Cadherin staining results showed that the mean border index, as well as the compactness of the E-Cadherin positive cells showed similar patterns. High invasion seems to correlate with high mean boarder index and mean compactness, see figure 50. The Vimentin staining appeared not to follow such trends.
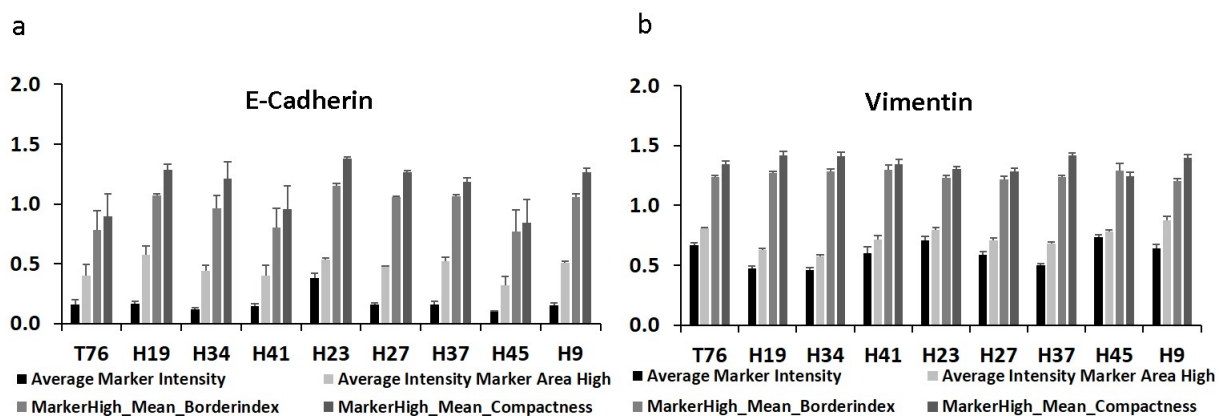
Figure 49: **Analysis of the E-Cadherin and Vimentin staining on patient-derived glioma tissue**
Average marker intensity, average marker intensity of high marker expression, mean border index and mean compactness in high marker regions of E-Cadherin (a) and Vimentin (b) stainings are shown. The value was calculated of ten visual fields and the SEM is depicted.
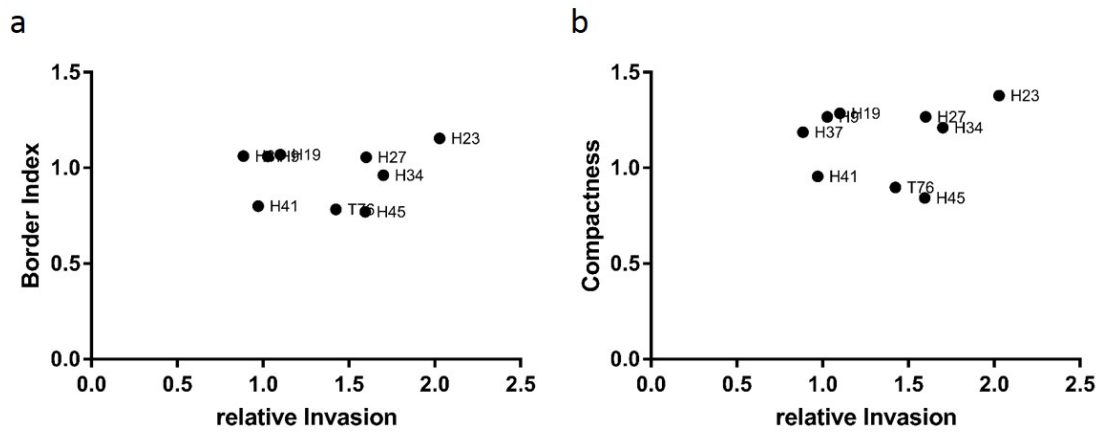
Figure 50: **Correlation of the E-Cadherin staining on patient-derived glioma tissue with the relative invasion after 4 Gy X-ray irradiation**
Correlations of the mean border index a) and mean compactness b)in high marker regions of the E-Cadherin stained cells and the relative invasion after 4 Gy X-ray irradiation are shown.
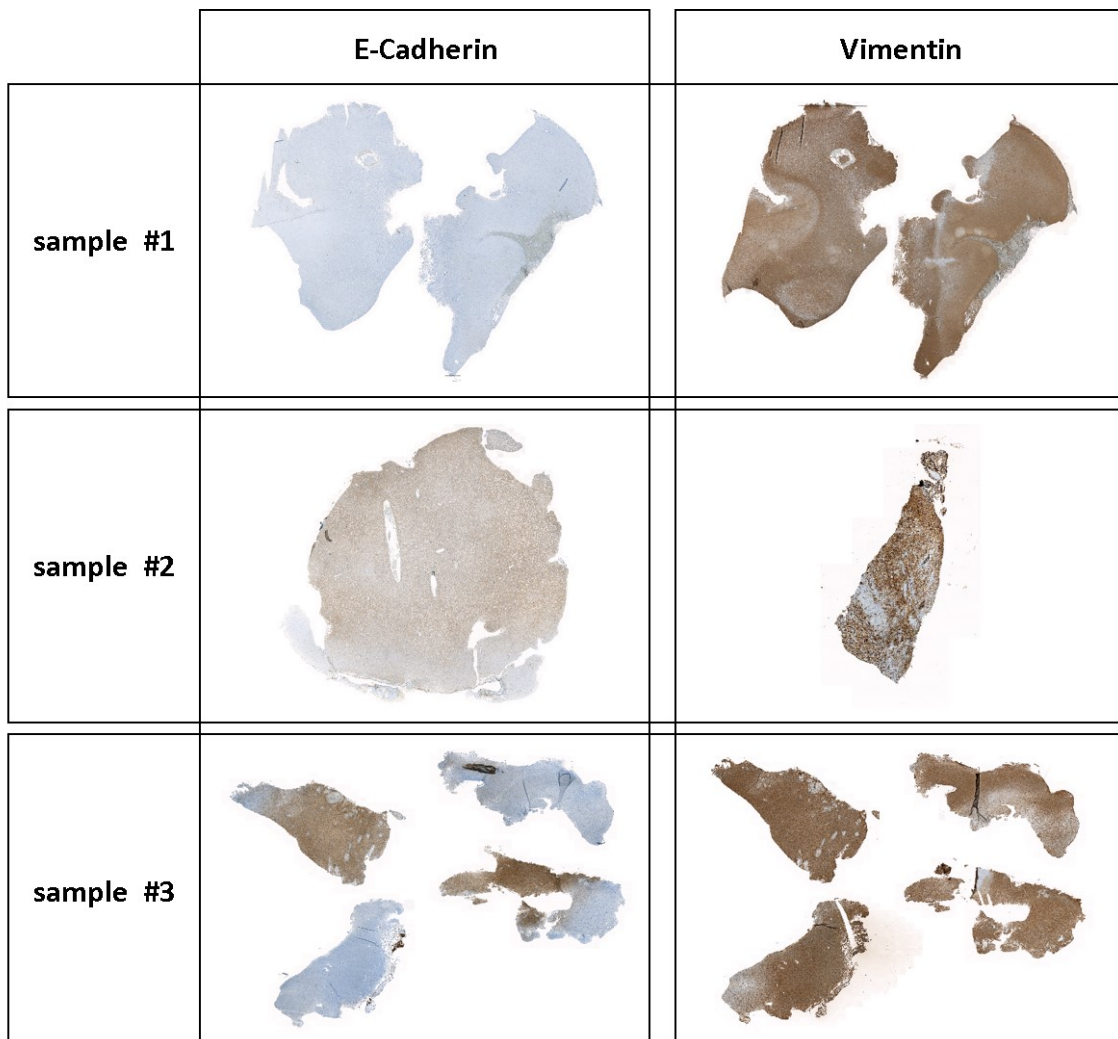
Figure 51: **Exemplary figures of the E-Cadherin and Vimentin immunohistochemical staining**
Shown are three exemplary figures of the E-Cadherin and Vimentin staining on patient-derived glioma tissue. a) shows low E-Cadherin expression but overall high Vimentin expression. b) shows medium E-Cadherin expression and unhomogeneous Vimentin expression. c) shows inhomogeneous E-Cadherin expression and high Vimentin expression.

7.10   Correlation of the invasive potential with clinical outcome

As shown in figure 48 a) the invasive capacity of 16 primary glioma cell lines that were isolated in the RadGlio trial was determined. Of these, seven were low-grade and nine high-grade gliomas. It was noted, that independent of the grading all gliomas could result in radiation-enhanced invasion. However, there were two recurrent gliomas (H9 and H37) that were isolated in the RadGlio trial and both showed that low-LET irradiation has no effect on their invasive behaviour.

To correlate the invasive capacity with the clinical outcome the sixteen patient samples were analysed for their treatment regime, progression-free and overall survival. As not all patients were treated at the Klinikum rechts der Isar the follow-up could only be performed on eight high-grade and three low-grade glioma patients. Two out of eight high-grade patients died within a year, however, the reason can not clearly be attributed to the GBM. As shown in table 16, 83.3 % high-grade glioma patients suffered from a relapse within several months (2-4 months), whereas only 33.3 % of the low-grade glioma patients revealed tumor recurrence at all.

Table 16: Correlation of the relative invasion with clinical parameters. The table lists nine primary glioma cell lines, their grading, therapy concept and progression-free survival. Adjuvant is abbreviated as adjuv., hyopfract. stands for hypofractionated, RT for radiotherapy, TMZ for Temozolomide, R for recurrence, sig. for significantly and m for months.

| #	grading	RT	TMZ	rel invasion	R
T84	IV	adjuv. hypofract	concurrent	sig. enhanced	3 m
H5	IV	adjuv. hypofract	concurrent	trend enhanced	3 m
H19	IV	adjuv. hypofract	concurrent	no effect	3 m
H33	IV	abortion at 28 Gy à 2 Gy	concurrent but aborted	sig. enhanced	2 m
H34	IV	adjuv. hypofract	concurrent	sig. enhanced	4 m
H46	IV	unknown	unknown	trend enhanced	no
H37	II	unknown	unknown	no effect	no
H45	II	59.4 Gy à 1.8 Gy	concurrent	sig. enhanced	1 m
H9	III	denied	yes	no effect	no

Since follow-up data is still missing, it was not possible to correlate basal tumor or relative tumor invasion after 4 Gy X-ray irradiation with the progression-free survival, yet. However,

the RadGlio trial is still ongoing and further data are generated.

8   Discussion

8.1   Clonogenic cell survival after α-particle irradiation

The survival of cancer cells after ionizing radiation is measured with the colony formation assay (CFA), as gold standard. In order to quantitatively describe the survival fraction to the dose of irradiation received, the linear-quadratic model (LQM) is commonly used [120]. The constants alpha and beta are experimentally determined values that describe the linear (alpha) and quadratic term (beta). Alpha symbolizes the intrinsic radiosensitivity of the cells and is describing the initial slope of the dose-response curve. Beta represents the repairable sub-lethal portion of the damage. In theory, the beta value cannot be negative. However, the results from this study showed that after high-LET irradiation the beta-values were negative.

There are two possible reasons for this finding:
a) The survival fraction after 3.2 Gy α-particle irradiation was higher than expected and
b) it has to be discussed, whether the LQM is the correct model to fit high-LET survival data.

8.1.1   Excluding inhomogeneous irradiation as the reason for high survival fractions

To validate the phenomenon of those remarkably high survival fractions another CFA with a dose of 7.2 Gy α-particles was performed. In accordance with the other results, it was shown that the survival fraction of LN229 after 7.2 Gy α-particles did not fall below 13 %. This finding is in line with the 6 % survival fraction of LN229 observed after 3.2 Gy and the negative beta calculated with the LQM. However, this is no reasonable finding for such high α-particle doses, therefore, the α-particle irradiation device was tested for in-homogeneous irradiation: As the results from the ring centre cell seeding showed the same survival than after usual cell seeding, a second test to exclude inhomogeneous irradiation of the α-particle irradiation device was performed. To ascertain that α-particles hit every cell, a γH2AX foci staining of LN229 cells, irradiated with 3.2 Gy α-particles was conducted. The results demonstrated that less than 0.1 % of cells did not exhibit any foci (see figure 19), which means that the α-particles hit all cells.

8.1.2   Excluding a more radioresistant subpopulation as the reason for high survival fractions

Another possibility for this high survival fraction was supposed to be the existence of a more radioresistant subpopulation. The GBM is known to be a very heterogeneous cell collection. Glioblastoma stem cells (GSCs) are furthermore known to be a more radioresistant cell population [13]. To identify those GSCs, a CD133 staining and flowcytometry analysis was performed. However, all three established cell lines were negative for CD133$^+$ stem cells and did not explain the findings. Hence, the idea of a more radioresistant subpopulation of 6 %, being cancer stem cells was rejected. This is well in line with current literature as reported by Wang et al. and Hong et al. , who also showed that U87 and LN229 are negative for CD133 [116, 134]. As a next step, a CFA with a non-cancerogeneous, non-human cell lines, CHO-K1, was performed. But again a survival of 8 % was observed and cell line or even organism-specific survival could therefore be excluded (see figure 21).

8.1.3   Validation of cell survival by comparison with the prediction RBE model, LEM

As an inhomogeneous-irradiation of the irradiation device, floating cells caused by the transport to the α-particle device, a CD133$^+$ subpopulation, as well as cell line specific survival could be excluded, a cooperation with Thomas Friedrich from the GSI Darmstadt, was initiated. Dr. Friedrich performed calculations with the local effect model (LEM), a predicting model currently implemented in the treatment plan system for radiotherapy with heavy ions, to predict the cell survival after α-particle irradiation, based on the experimentally determined X-ray survival data that were provided. As the LEM revealed, the survival fractions of LN229 and LN18 after α-particle irradiation are expected to follow a linear decrease with increasing dose. The predicted results (see figure 22) from the LEM are quite different to our measurements but in line with the expectations that were assumed for LN229 and LN18 based on other studies with different high-LET irradiation qualities. With the help of the model the search for the reason, explaining this phenomenon continued.

8.1.4   Changing irradiation conditions

Another test to analyse inhomogeneous irradiation of the α-particle irradiation device, a CFA with changed irradiation conditions was performed. In this setting, the survival after 3.2 Gy was measured but each time after half the irradiation time, the ring system was turned by 180° in the irradiation device to exclude that one spot does not receive any dose, causing a 6 % survival fraction. After turning the ring system after half the irradiation time and a irradiation with 3.2 Gy, the survival fraction was only 0.3 %, being significantly reduced compared to the survival fractions of the usual irradiation procedure.

Since α-particles are not able to transfer over a large distance another idea that might explain the 6 % survival fraction after a dose of 3.2 Gy α-particles, was that cells might detach from the foil in the ring system during the transportation. Those cells might settle down and attach during irradiation, therefore getting only some of the irradiation dose, showing higher survival. For this, the medium (with probably floating cells inside) was replaced after half the irradiation time. It could be shown that the survival fraction after 3.2 Gy was reduced to 0.9 %.

Both analyses (turn by 180° after half the irradiation time, as well as the medium exchange after half the irradiation time) revealed a survival of less than 1 %, which is in line with the predicted data from the LEM. The only similarity between the two assays was that the α-particle source was stopped after half the irradiation time and started again some seconds later, after the ring system was turned, respectively after the medium in the ring system was exchanged. Those results may indicate that there could be an issue with the α-particle device, e.g. the wobbler is not equally turning the collimator over the irradiation period, respectively the speed of the wobbler may slow down. By stopping and restarting the system, this may be circumvented. To rule out any technical problems of the α-particle device a possible next step could be not only to prove – like it was done in this study – that each cell is hit by irradiation but also that the cells are continuously irradiated and receive the full dose. For example, a dosimeter could be applied to detect whether the device is continuously irradiating. However, the same experiments should be validated and additionally a control with the same irradiation as performed before (7 Gy in full 30 minutes) should be performed.

Solving this problem is crucial for further high-LET studies with the α-particle device at high doses but does not affect the other experiments of the study as those analyses were

performed with only $1.3\,\mathrm{Gy}$ irradiation.

8.1.5   The LQM as the mathematical model for high-LET irradiations

Another criterion that has to be considered is the LQM, as a model for the survival data after high-LET irradiation. As the LQM does not consider negative beta values, it has to be discussed whether the LQM is the correct model to describe dose-response curves after high-LET irradiation [120]. This study is not the first that has dealt with survival curves with a negative beta or at least a very low beta value, as such dose-responses have been observed after 12-C irradiation [51,125]. While Joiner et al. discuss that the damage repair is not efficiently enough considered in the LQM [67], Holloway et al. suggest comparing only survival fractions of the same LET with the LQM [60]. The group of Brahme et al. even proposes another, more suitable fitting model "Repairable-Conditionally-Repairable (RCR)-Fit" to exhibit more efficiently the damage interaction between high- and low-LET irradiation [16]. In addition to this proposal, the group of Carter et al. just applied a linear fit to their high-LET survival data sets [20]. There is much controversial discussion whether the LQM model is the correct model to fit high-LET irradiation survival fractions. Furthermore, as determined in the CFAs where the dose of $3.2\,\mathrm{Gy}$ was split into two sections the survival fraction, showed to follow a linear trend as proposed by the LEM model. Even though there is evidence that another mathematical model is needed to meet the challenges of survival fractions after high-LET irradiation and studies using high-LET irradiation are evolving, it will take more time to figure out whether the routinely applied, conventional LQM is suitable for high-LET irradiation or whether there is a need for a new model that takes complex DNA damage into account.

8.2   Basic characterization of the applied cell lines

8.2.1   Establishment of the ring system

First of all, this study showed the successful establishment of a new cell culture system, the ring system, that was developed in this work to allow cell irradiation with the α-particle device. As already written in detail in the results chapter, cultivation of cells in conventional plastic flasks - as well as in the ring system caused a plating efficiency of $56\,\%$, measured

with the CFA as an endpoint. The survival fractions after irradiating the cells with X-rays in both systems were comparable.

8.2.2   Establishment of the primary cell isolation system

This study is the first that analysed more than 16 freshly isolated primary cell lines derived from patient tumor-tissue. As all cells expressed the GFAP marker, the system is considered to be a successful system to isolate primary glioma cells from patient-derived tumor tissue, which enables further analysis of adherent primary glioma cell lines.

8.2.3   Basal invasion

This study demonstrated that all three established GBM cell lines are very invasive, which is in line with the current standard of knowledge and is even described as a hallmark of GBM [59]. It was observed, that although not significantly, U87 showed to be 7.5-fold as invasive as the control fibroblasts, whereas LN229 was only 5.7-fold as invasive. That U87 is more invasive than LN229 was also observed by Wick et al. [131]. In addition, all isolated patient-derived primary cells were naturally very invasive, as tested with the matrigel transwell assay, compared to the CRL2270 fibroblasts.

8.2.4   Irradiation increases doubling time of established and primary cell lines by causing G2M arrest

In this study, the doubling time was determined by counting cells, seeded in a 12-well plate, over several days. The doubling time of LN229 was determined as $16\,\mathrm{h} \pm 1\,\mathrm{h}$ and $13\,\mathrm{h} \pm 1.3\,\mathrm{h}$ for LN18. This finding differs from the current literature. Pyrko et al. identified a doubling time of 22 hours for LN229 while Cowley et al. [30, 100] calculated 31 hours. Diserens [37] determined the doubling time of LN18 as 72 hours after 115 passages. A possible reason could be that in the current study cells were only passaged until passage 25. Another difference to the studies cited above might be that this study cultured the established GBM cells in RPMI instead of DMEM. As both media contain different supplements, this fact might have a major impact on the proliferation and therefore on the doubling time of the cells. The method used to determine the doubling time has to be considered, too. We used manual cell counting while others used the Bromdesoxyuridine- or AlamarBlue assay.

As also shown in the study of Adeberg [1] both GBM cell lines exhibit a dose-dependent G2M arrest, 2 hours after X-ray irradiation.

The doubling time of the isolated primary glioma cells was increasing with increasing dose as well, even though not significantly, after 4 Gy X-ray irradiation. This is in line with the previous finding and therefore validating findings of established cells. Furthermore, this study revealed a tendency towards G2M arrest after 4 Gy X-ray irradiation of the primary cells, again validating the results of the established cell lines.

Correlating the radiation-induced G2M arrest to the increased doubling time after 4 Gy X-ray irradiation, it is likely that the G2M arrest is causing an increased doubling time. The arrest in the G2M-phase enables the cells to repair their DNA damage before continuing to mitosis [95]. Therefore, an increasing doubling time after irradiation is well in line with the current standard of knowledge [78, 106].

8.2.5   Comparable radiosensitivity of established cell lines but not of primary cell lines

Even though LN229 and LN18 were generated from different GBM IV tumor patients and even originated from different parts of the brain they show the same oncogene expression pattern [63]. Furthermore, this thesis revealed that they are comparable radiosensitive. This finding is in accordance with Adeberg et al. [1], who showed similar survival fractions of LN229 and LN18 after 2 and 6 Gy photon irradiation. Likewise, Combs et al. [28] could show that both cell lines are comparable radiosensitive.

The γH2AX flowcytometry revealed that both cell lines exhibited increased γH2AX mean fluorescence. The same assay showed that the repair capacity of both cell lines is comparable, as both cell lines displayed 25 % remaining γH2AX signaling 24 hours after 4 Gy X-ray irradiation. The 53BP1 foci assay also showed similar DNA damage repair of the two cell lines 24 hours after X-ray irradiation. As both tests indicated the same finding, this study could prove the finding of comparable DNA damage repair of both cell lines with several assays.

For five primary cell lines (T76, T84, H5, H9 and H19) colony formation assays have been established. As shown in the results section the D50 strongly varies in between the glioma cell lines, which confirms that tumors are heterogeneous in their radiation response [58]. This finding is well in line with current literature as it is known that primary glioma cells

exhibit a broad spectrum of radiation sensitivities [65, 119]. At least in the first passages, primary cells contain more CSCs which are likewise known to enhance radioresistance [19, 21].

8.3   Low-LET irradiation-enhanced invasion

Radiotherapy is one of the gold standards in cancer treatment. The currently applied low-LET photon irradiation has proven its benefits in several clinical studies. But still some tumors show recurrence and metastasis after initial treatment and even worse, it is controversially discussed whether low-LET irradiation might even promote the tumors natural invasion.

In accordance with several other studies, this study showed that X-ray irradiation exhibited radiation-enhanced invasion of LN229 and U87 GBM cells [94, 101, 132]. As in this study, Park et al. [94] showed low-LET irradiation promoted invasion of U87 but not of LN18 after X-ray irradiation. However, the group of Wild-Bode et al. also found radiation-enhanced invasion of LN18 but they applied different doses than in this study (Wild-Bode et al.: 1/3/6 Gy, here: 4 Gy). On the other hand, and in line with findings from this study, Cordes et al. found that low-LET irradiation did not change the invasion of LN18 [29]. But again, in contrast to the results in this study, Cordes et al. also showed that the invasion of LN229 is not affected by X-ray irradiation. Rieken et al. demonstrated a low-LET radiation-induced migration of U87 and LN229, supporting our results that irradiation increased aggressiveness [101]. In summary, several studies showed X-ray irradiation-enhanced invasion of several GBM cell lines, whereas others showed divergent results. Even though the same cell lines were examined, they revealed different results, dependent of the research institute. These different findings might be due several reasons, like the applied irradiation doses, the time cells were exposed to serum starvation, the different applied chemo-attractants and the various methods (Boyden chamber, transwell-assay, scratch assay) that were applied to measure the invasion.

In this study, a system to isolate patient-derived primary glioma cells was established. With those primary glioma cells, findings of the established GBM cell lines were validated. Altogether 16 patient-derived primary glioma cell lines were tested for their invasion 24 hours after X-ray irradiation. Half the primary cell lines showed significantly radiation-enhanced invasion, further 4 cell lines showed a tendency of radiation-enhanced invasion and in 4

primary cell lines, X-ray radiation did not affect invasion. It is therefore concluded, that the observed radiation-enhanced invasion differed inter-individually between the cell lines. This finding clearly demonstrates that there is an extensive biological heterogeneity within the primary glioma cell population that differentially responds to low-LET irradiation. In accordance with the results from this study Baulch et al. found a radiation-enhanced invasion of primary GBM cells [11].

As low-LET RT is still the standard of GBM therapy [6], avoidance of RT-related invasion might be a potential approach to improve GBM patient survival in the future. The importance of a new and innovative radiotherapy treatment concept for GBM patients is known and the application of carbon ions is due to the physical advantages like a more precise dose deposition, currently the most chosen high-LET source. In accordance with the data from this study Goetze et al. [49] as well as Rieken et al. [102] could already show the beneficial impact of high-LET irradiation (Carbon ions) on GBM. Both authors showed that carbon ions do not cause radiation-enhanced invasion or migration of U87 GBM cells. Furthermore, our findings of established cell lines were validated with primary patient-derived cell lines. As all 16 tested primary cell lines showed no radiation-enhanced invasion after high-LET irradiation reults of this study let assume that high-LET irradiation might be an alternative for GBM patient treatment. However, up to now, there are only *in vitro* studies that concluded that high-LET irradiation might be a beneficial tumor treatment option in order to avoid radiation-induced invasion [9, 15, 57]. At the moment there are some ongoing clinical trials analysing the effects of high-LET irradiation on GBM patients. However, results from these clinical trials confirming these *in vitro* findings are still missing [26, 27, 87]. It has to be mentioned that some centers which offer heavy ion radiotherapy treat other tumor entities but not GBM. This fact reflects the complexity of high-LET RT of GBM and underlines the urgency for further preclinical radiobiological research.

As not all tested GBM cell lines showed X-ray radiation-enhanced invasion, another conclusion that can be drawn from this study is that there is an urgent prerequisite to distinguish those patients that suffer from a radiation-enhanced invasion from those that benefit from. This finding goes along with a theme that was addressed several years ago: "individualized or personalized medicine". As low-LET irradiation is the method of choice for basically all GBM patients today, it is even more important to develop new and innovative biomarkers to separate GBMs with enhanced invasion after low-LET irradiation from the others that

do not and therefore might benefit from low-LET irradiation. By separating those patients, potential treatment failures might be reduced. Besides high-LET irradiation other concepts could be followed. As shown by several publications before, gliomas follow a clear dose-response relationship as the survival is higher the higher the given dose is [126, 127]. Therefore, target volume increase or higher doses per fraction could help those patients to avoid low-LET irradiation-enhanced invasion. However, the resulting toxicity of dose-escalation should not be neglected [130].

8.4   Analysing the mechanisms that may explain low-LET irradiation-enhanced invasion

Previous studies have already shown that changes in the extra-cellular-matrix (ECM) are of utmost importance for cancer cell invasion. In order to invade into the surrounding tissue, the tumor needs to exploit several mechanisms. Adhesion of the tumor cell to the extra-cellular-matrix (ECM), degradation of the ECM and cell motility through the ECM are the main players of this complex phenomenon. Starting with the discussions around low-LET enhanced invasion, publications investigating this phenomenon in more detail, e.g. protease expression, cell-cell junctions and the epithelial-to-mesenchymal transition (EMT), appeared [83, 89]. Analysing the mRNA and protein expression pattern of the GBM cell lines is therefore a prerequisite for revealing the mechanisms responsible for the radiation-enhanced invasion.

8.4.1   DNA damage as the reason for low-LET enhanced invasion

To understand the observed phenomenon of low-LET irradiation-enhanced invasion which is not observable after high-LET irradiation several potentially relevant mechanisms of invasion have been analysed. This study showed that the residual DNA damage (determined by γH2AX flowcytometry) of LN229 and LN18 is twice as much after $1.3\,\text{Gy}$ α-particle irradiation compared to the equivalent dose of X-ray ($4\,\text{Gy}$) irradiation. This finding is well in line with current literature which shows that high-LET irradiation causes more complex DSBs, which take longer to be repaired [5, 57, 72]. Whether this fact is sufficient to explain why high-LET irradiation does not lead to radiation-enhanced invasion has to be proven on gene and protein level.

8.4.2 Analysing the mechanisms of irradiation on protein level

Analysing ECM degrading enzymes via ELISA

Nalla et al. [90] as well as Rofstad et al. [104] showed increased uPA expression after ionizing irradiation. However, Qian et al. could show a decrease of uPA in pancreatic cancer cells after X-ray irradiation. This finding is well in line with the data of this study, as it was shown that U87 exhibited significantly decreased amounts of secreted uPA 24 hours after X-ray irradiation but not after α-particle irradiation. LN18 on the other hand, did not show any changes in the uPA secretion after X-ray nor α-particle irradiation. The role of uPA in the radiation-enhanced invasion remains unclear. Likewise, the MMP secretion in correlation with the radiation-enhanced invasion was investigated. It was shown that the amount of secreted MMP-2 is significantly decreased in LN229 and LN18, 24 hours after X-ray irradiation but not affected by α-particle irradiation. In U87 MMP-2 secretion remained unaffected after X-ray and α-particle irradiation. In addition to the analysis of MMP-2 and uPA, a generic MMP activity ELISA was performed, which validated earlier findings of this study, as it revealed no significant change in generic MMP activity measured after 24 hours after irradiation with 4 Gy X-ray and the equivalent dose of 1.3 Gy α-particles.

However, these findings are contrary to current knowledge, as uPA as well as MMP-2 are two important proteases that seem to play a major role in the invasion [48, 64]. Several other studies showed up-regulated MMP-2 secretion in all tested glioma cell lines after irradiation [94, 132]. Even though, Steinle et al. [114] correspond to the findings of this study, as they showed that only one of their tested glioma cell lines exhibited increased MMP-2 secretion after irradiation, whereas two others did not. Comparing the findings of this study to the current literature, it has to be mentioned, that different cell lines, time points and measuring systems have been applied. Furthermore, in this study the levels of secreted uPA and MMP-2, as well as generic MMP activity, were only determined 24 hours after irradiation. Hence, the measurement of both proteases and the determination of their activation should be repeated earlier after irradiation e.g. 6 hours or 12 hours in order not to miss important changes that might have happened within the first 24 hours after irradiation.

Extending the analysis of ECM degrading enzymes via Proteome profiler

In line with the knowledge that MMP activation is mandatory for the invasive process the proteome profiler in this study revealed that MMP-1 and MMP-7 were significantly up-

regulated 24 hours after X-ray irradiation in all three established cell lines (LN229, LN18 and U87). Furthermore, the proteome profiler revealed, that Cathepsin-D, a protease, was up-regulated in the two cell lines that showed radiation-enhanced invasion. This finding is in line with the result of Dubey et al.. They could show that Cathepsin-D is an important player in cancer invasion [41]. Furthermore, CathepsinD was already shown to be a marker of poor prognosis in breast cancer [118, 133]. In addition, the proteome profiler demonstrated low-LET radiation-induced reduction of four protease inhibitors (TIMP-2, Serpine B5, Lipocalin-1 and APP) in LN229 and U87. Only in LN18, the cell line that did not show radiation-enhanced invasion those protease inhibitors remained unaffected. This finding is in line with the current literature, showing that TIMP-2 up-regulation decreased glioma invasion [116]. In addition, this finding corresponds well to the current knowledge, that Serpine B5 is a tumor suppressor that blocks cancer invasion. Another finding of the proteome profiler of this study was that Cystatin A was decreased in LN229 and U87, the two cell lines that showed radiation-enhanced invasion, but increased in LN18, the cell line that did not show radiation-enhanced invasion. This finding is validated by current literature, showing that Cystatin A inhibits EMT, a process that is involved in invasion [81]. In summary, the proteome profiler revealed several proteases and protease inhibitors being affected by X-ray irradiation. Since matrix reorganisation is an important factor in tumor invasion, this study confirmed the radiation-enhanced GBM invasion. All determined proteases as well as protease inhibitor changes fit the current literature. This provides the first evidence that the reason for a radiation-enhanced invasion might be an interplay of several factors.

8.4.3   Analysis of underlying signaling causing low-LET irradiation-enhanced invasion

Analysis of the radiation-induced EMT

An EMT staining on Vimentin, a marker for mesenchymal cells was performed. This EMT staining validated the findings from the EMT gene profiler as it showed increased Vimentin after X-ray irradiation in LN18. Additionally, the EMT staining revealed a tendency towards more Vimentin expression after 4 Gy X-ray irradiation in U87, indicating ongoing EMT after 4 Gy X-ray irradiation. In contrast, LN229 showed no increasing Vimentin intensity after X-ray irradiation. These findings might not explain why low-LET irradiation enhances invasion of LN229 and U87 but it demonstrates that EMT is taking part in GBM

invasion as they have all exhibited high basal invasion. The qPCR analysis of eleven potentially relevant genes for invasion showed up-regulated mRNA expression of several genes important for EMT, after α-particle irradiation however, the EMT staining indicated no EMT after high LET irradiation. It has to be considered that between gene regulation and phenotypical appearance many processes may interfere by silencing gene transcription. For example, miRNAs are considered to be major regulators of gene expression [74]. But also different signaling pathways are crucial in cancer invasion. Several downstream pathway proteins can get activated, mutated, deleted or even epigenetically silenced, thereby changing the invasive process [21, 112]. This might explain why the Vimentin staining was not increased after α-particle irradiation, even though the expression of several mRNAs for EMT were up-regulated.

Most important NOTCH1 mRNA expression that was down-regulated by 4 Gy X-ray irradiation in LN229 and U87 but not in LN18 was up-regulated in all three cell lines after α-particle irradiation in the EMT profiler. Consequently, it might be concluded that an up-regulated NOTCH1 expression is an indicator of low invasion. As already mentioned in the introduction another protein tightly connected to the EMT is the protein kinase B (AKT). The importance of AKT in the invasive process has been studied extensively [21, 82]. In accordance with this, the IPA of this study revealed that the AKT pathway is affected by irradiation in LN229 and LN18. Likewise Datta et al., as well as Hung et al. already proved that irradiation leads to AKT pathway activation [34, 61]. Furthermore, the IPA suggested radiation-induced changes in the Wnt- and TGF-β pathways. The canonical Wnt pathway has already been shown to play an important role in cancer metastasis [25, 76]. In accordance with the data of this study the role of the Wnt-signaling in GBM invasion was already shown by Paw et al. [96]. In summary, several important pathways are associated with the invasive capacity and might, depending on their activation level, influence the degree of invasion.

Analysis of potentially responsible pathways

In this study, Western Blots aimed to determine the activation score of LN229 and LN18 after irradiation with 4 Gy X-ray or 1.3 Gy α-particle irradiation. As shown in the results section, the amount of β-Catenin and phosphorylated β-Catenin as well as the amount of GSK3, respectively phosphorylated GSK3 remained unaffected in both cell lines after X-ray or α-particle irradiation. This suggests that there is no radiation-induced canonical Wnt

signal activation. As already shown before, the Wnt-signalling pathway is important for invasion. But as both cell lines already showed a high basal invasion this might explain why there is no further radiation-induced increase in the Wnt-signalling observable. Furthermore, this study revealed a significant down-regulation of the AKT signaling after 1.3 Gy α-particle irradiation in LN18 but not in LN229. Even though not statistically significant, 4 Gy X-ray irradiation showed a trend to an activated AKT signaling in LN229 and LN18. This finding is in line with the prediction of the IPA and validates the current standard of knowledge, that ionizing irradiation is an activator of the AKT signaling [34, 61]. In addition, the Western Blot analysis revealed a significant increase of the phosphorylated-SMAD2/3 after 4 Gy X-ray irradiation in LN229. This increase was not observed in LN18 after X-ray irradiation nor in LN229 or LN18 after the equivalent dose of α-particle irradiation. This experimental finding validates the prediction from the IPA and is in line with the current literature, stating that the TGF-β pathway is an important regulator in GBM invasion, correlating with poor prognosis [17, 53]. As SMAD2 is the substrate of TGF-β receptor I kinase the phosphorylated SMAD2 correlates with the intensity of the TGF-β signaling. As X-ray irradiation only activated SMAD2/3 in LN229, the cell line in which radiation-enhanced invasion was observed, but not in LN18 or after alpha particle irradiation, it can be concluded that the up-regulation of SMAD2/3, hence the TGF-β pathway after X-ray irradiation might be an important factor to predict the radiation-enhanced invasion.

8.5   Immunohistochemical staining on patient-derived tumor tissue

As the isolation and cultivation of primary cells are time-consuming the development of a faster system, predicting the invasive capacity of the tumor, is necessary. With the immunohistochemical staining that was performed on patient-derived tumor tissue such a system was generated. Out of the ten analysed features, only two (mean border index and mean compactness) showed to correlate with the cell invasion. One reason for this finding might be, as shown in figure 51, that the patient tissue does not express the E-Cadherin homogeneously. Again inter- as well as intratumor heterogeneity of the glioma tissue was proven and could imply differences in the analysis. Here, the location of the biopsy is of importance - where in the tumor was the biopsy section taken from? Would the analysis

reveal another result if the biopsy was taken off another spot in the tumor? One more factor challenging this technique is the biopsy removal from the brain, as it might destroy the structural quality of the sample. In addition, the fixation and staining procedure might cause loss of tumor material. Another important factor is the time between generation of the tumor biopsy and fixation in PFA, as protein degradation might occur.

First results showed, that the mean border index as well as the mean compactness in high marker areas correlated with the invasive capacity demonstrated with primary glioma cells in an *in vitro* invasion assay (see figure 50). This is the first study, resulting in such a correlation. However, as only 10 patient samples were analysed up to now, there is a strong need to enlarge this study, validating these preliminary results.

8.6   Correlation with clinical outcome

Sixteen patient-derived primary cells were investigated for their invasive potential. With the goal to find a correlation between the invasive capacity of the isolated primary tumor cells and the patient outcome, data sets were compared as demonstrated in table 16. In accordance to current literature it was shown that five out of six (83.3 %) high-grade gliomas caused a relapse within months while only one out of three (33.3 %) low-grade gliomas recurred [70, 71]. Furthermore, the correlation with the overall survival showed that only high-grade glioma patients died within one year of follow-up [71]. This finding is also in accordance to current knowledge [70]. Due to missing follow-up data from almost half of the participants of the examined primary cells, a correlation was only possible for those nine patients. Thus, a correlation between the invasive potential and the progression- free survival was not possible with the current data set, however, the RadGlio trial is still ongoing and correlation analysis can be performed in future. In accordance to recent literature, our data set revealed, that the high-grade glioma patients showed fast recurrence even though they were treated with the multimodal treatment concept. Despite this aggressive treatment, recurrence was inevitable within month, again demonstrating the high radio- and chemoresistance of gliomas [79].

9 Conclusion

This thesis analysed the impact of high- and low-LET irradiation on the invasion of established GBM cells, as well as patient-derived primary glioma cells and correlated these findings with clinical data. To achieve this, a system to isolate patient-derived primary glioma cell cultures, was successfully established, primary and established cells were characterized and several analyses were performed to study the irradiation-related invasion.

It is important to note, that this is the first study investigating the invasive behaviour of sixteen primary patient-derived glioma cells after irradiation. It was noted that the invasive potential differed significantly, reflecting a high heterogeneity between the cell lines.

This thesis demonstrated, that in contrast to low-LET irradiation, high-LET irradiation did not cause any changes in the invasive potential of established, as well as primary glioma cell lines. Several mechanisms being potentially responsible for the low-LET enhanced invasion were investigated. Higher proportions of remaining DNA damage after high-LET irradiation than after low-LET irradiation were demonstrated. Furthermore, this study could prove that EMT plays an important role in GBM invasion. The up- and down-regulation of several genes was dependent on the irradiation quality. Besides numerous affected proteases and protease inhibitors, the NOTCH1 mRNA expression was proposed to play a major role in GBM invasion. In addition, the AKT as well as the TGF-β signaling pathways were influenced by low-LET irradiation. As several mechanisms showed to be involved in the GBM invasion it can be concluded, that it is not a single gene change that regulates the GBM invasion, more likely it is due to an interplay of several genes and the interference with other players, e.g. miRNAs.

Today, basically all GBM patients are treated with low-LET radiotherapy (RT) [6]. Thus, the avoidance of RT-enhanced invasion might be an essential approach to reduce treatment failures. Since not all evaluated glioma cell lines demonstrated radiation-related invasion, inter-tumor-heterogeneity is an important topic, considering personalized medicine [98]. It is concluded, that glioma heterogeneity is of highest relevance for future glioma therapy. Thus, the translation of these experimental findings into clinic is crucial. Therefore, for future personalized GBM tumor treatment, it may be beneficial to differentiate between those patients that benefit from low-LET irradiation and those that might suffer from low-LET-enhanced invasion. To achieve an improved glioma treatment, a personalized and patient-specific radiation-treatment concept should be followed. However, other

radiation qualities like high-LET irradiation could also be beneficial to improve overall patient outcome. Additionally, other treatment concepts like increasing the treatment field, hypofractionation and dose-escalation could be potential alternatives for GBM treatment.

And finally, the results from primary cell correlation with clinical outcome revealed, that high chemo- and radiation resistance still plays a major role in glioma treatment response.

10   Summary and outlook

In summary, an isolation system for primary glioma cells from patient-derived tumor tissue was established and by exposing those primary cells to different radiation qualities, an evaluation of the patient-specific tumor invasion was possible, validating the results obtained from established GBM cell lines. The isolation of patient-derived primary glioma cells allowed the correlation with clinical data.

Even though the clinical validation is still missing, our *in vitro* findings indicate that low-LET irradiation-enhanced invasion may contribute to recurrences after conventional low-LET RT. Since none of the evaluated glioma cell lines showed high-LET radiation-induced invasion, results from this thesis propose that high-LET irradiation might have the potential for personalized treatment concepts for those patients that might suffer from low-LET increased invasion. Respectively, it should be discussed that this effect of high-LET RT might also be achieved by hypofractionation (higher doses per fraction) prescribed to adequate target volumes [32]. As not all cell lines showed radiation-enhanced invasion, tumor heterogeneity seems to play an important role in GBM treatment. Differentiating between patients that might benefit from low-LET irradiation and patients that might suffer from adverse effects may help to improve patient survival. In summary, a more personalized treatment concept for glioma patients is suggested, considering radio- and chemoresistance, as well as tumor heterogeneity.

Since the highly invasive potential of GBM cells enables the tumor to escape the treatment and thereby causes tumor progression, examining the invasive genotype and pathway signaling may help to identify molecular markers for GBM treatment. In conclusion, the results of this thesis demonstrated the urgent need for further molecular studies identifying novel biomarkers that can predict the invasive response to irradiation and subsequently enable individualized treatment concepts in future.

List of Figures

List of Tables

11 References

[1] S. Adeberg, D. Bernhardt, S. B. Harrabi, N. H. Nicolay, J. Horner-Rieber, L. Konig, M. Repka, A. Mohr, A. Abdollahi, K. J. Weber, J. Debus, and S. Rieken. Metformin enhanced in vitro radiosensitivity associates with g2/m cell cycle arrest and elevated adenosine-5'-monophosphate-activated protein kinase levels in glioblastoma. *Radiol Oncol*, 51(4):431–437, 2017.

[2] I. A. E. AGENCY. *Radiation Biology: A Handbook for Teachers and Students*. Training Course Series. INTERNATIONAL ATOMIC ENERGY AGENCY, Vienna, 2010.

[3] K. Aldape, G. Zadeh, S. Mansouri, G. Reifenberger, and A. von Deimling. Glioblastoma: pathology, molecular mechanisms and markers. *Acta Neuropathol*, 129(6):829–48, 2015.

[4] M. Ammirati, J. H. Galicich, E. Arbit, and Y. Liao. Reoperation in the treatment of recurrent intracranial malignant gliomas. *Neurosurgery*, 21(5):607–14, 1987.

[5] A. Asaithamby and D. J. Chen. Mechanism of cluster dna damage repair in response to high-atomic number and energy particles radiation. *Mutation Research*, 711(1-2):87–99, 2011.

[6] R. Babu, J. M. Komisarow, V. J. Agarwal, S. Rahimpour, A. Iyer, D. Britt, I. O. Karikari, P. M. Grossi, S. Thomas, A. H. Friedman, and C. Adamson. Glioblastoma in the elderly: the effect of aggressive and modern therapies on survival. *J Neurosurg*, 124(4):998–1007, 2016.

[7] A. V. Badiga, C. Chetty, D. Kesanakurti, D. Are, M. Gujrati, J. D. Klopfenstein, D. H. Dinh, and J. S. Rao. Mmp-2 sirna inhibits radiation-enhanced invasiveness in glioma cells. *Plos One*, 6(6), 2011.

[8] S. Bao, Q. Wu, R. E. McLendon, Y. Hao, Q. Shi, and A. B. Hjelmeland. Glioma stem cells promote radioresistance by preferential activation of the dna damage response. *Nature*, 444, 2006.

[9] L. Barazzuol, R. Jena, N. G. Burnet, J. C. Jeynes, M. J. Merchant, K. J. Kirkby, and N. F. Kirkby. In vitro evaluation of combined temozolomide and radiotherapy using x rays and high-linear energy transfer radiation for glioblastoma. *Radiat Res*, 177(5):651–62, 2012.

[10] R. Baskar, K. A. Lee, R. Yeo, and K.-W. Yeoh. Cancer and radiation therapy: Current advances and future directions. *International Journal of Medical Sciences*, 9(3):193–199, 2012.

[11] J. E. Baulch, E. Geidzinski, K. K. Tran, L. Yu, Y. H. Zhou, and C. L. Limoli. Irradiation of primary human gliomas triggers dynamic and aggressive survival responses involving microvesicle signaling. *Environ Mol Mutagen*, 57(5):405–15, 2016.

[12] M. Baumann, M. Krause, and R. Hill. Exploring the role of cancer stem cells in radioresistance. *Nat Rev Cancer*, 8(7):545–54, 2008.

[13] M. Baumann, M. Krause, H. Thames, K. Trott, and D. Zips. Cancer stem cells and radiotherapy. *Int J Radiat Biol*, 85(5):391–402, 2009.

[14] A. C. Begg, F. A. Stewart, and C. Vens. Strategies to improve radiotherapy with targeted drugs. *Nature Reviews Cancer*, 11:239, 2011.

[15] S. Benzina, A. Altmeyer, F. Malek, P. Dufour, J.-M. Denis, J. Gueulette, and P. Bischoff. High-let radiation combined with oxaliplatin induce autophagy in u-87 glioblastoma cells. *Cancer Letters*, 264(1):63–70, 2008.

[16] A. Brahme. Accurate description of the cell survival and biological effect at low and high doses and let's. *Journal of Radiation Research*, 52(4):389–407, 2011.

[17] A. Bruna, R. S. Darken, F. Rojo, A. Ocaña, S. Peñuelas, A. Arias, R. Paris, A. Tortosa, J. Mora, J. Baselga, and J. Seoane. High tgfbeta-smad activity confers poor prognosis in glioma patients and promotes cell proliferation depending on the methylation of the pdgf-b gene. *Cancer Cell*, 11(2):147–160, 2007.

[18] S. Burma, B. P. C. Chen, and D. J. Chen. Role of non-homologous end joining (nhej) in maintaining genomic integrity. *DNA Repair*, 5(9):1042–1048, 2006.

[19] R. Carruthers, S. U. Ahmed, K. Strathdee, N. Gomez-Roman, E. Amoah-Buahin, C. Watts, and A. J. Chalmers. Abrogation of radioresistance in glioblastoma stem-like cells by inhibition of atm kinase. *Molecular Oncology*, 9(1):192–203, 2015.

[20] R. J. Carter, C. M. Nickson, J. M. Thompson, A. Kacperek, M. A. Hill, and J. L. Parsons. Complex dna damage induced by high linear energy transfer alpha-particles and protons triggers a specific cellular dna damage response. *Int J Radiat Oncol Biol Phys*, 100(3):776–784, 2018.

[21] L. Chang, P. Graham, J. Hao, J. Ni, J. Deng, J. Bucci, D. Malouf, D. Gillatt, and Y. Li. Cancer stem cells and signaling pathways in radioresistance. *Oncotarget*, 7(10):11002–11017, 2016.

[22] L. Chang, P. H. Graham, J. Hao, J. Ni, J. Bucci, P. J. Cozzi, J. H. Kearsley, and Y. Li. Acquisition of epithelial-mesenchymal transition and cancer stem cell phenotypes is associated with activation of the pi3k/akt/mtor pathway in prostate cancer radioresistance. *Cell Death Dis*, 4:e875, 2013.

[23] A. K. Choucair, V. A. Levin, P. H. Gutin, R. L. Davis, P. Silver, M. S. Edwards, and C. B. Wilson. Development of multiple lesions during radiation therapy and chemotherapy in patients with gliomas. *J Neurosurg*, 65(5):654–8, 1986.

[24] M. F. Clarke, J. E. Dick, P. B. Dirks, C. J. Eaves, C. H. Jamieson, D. L. Jones, J. Visvader, I. L. Weissman, and G. M. Wahl. Cancer stem cells–perspectives on current status and future directions: Aacr workshop on cancer stem cells. *Cancer Res*, 66(19):9339–44, 2006.

[25] H. Clevers and R. Nusse. Wnt/beta-catenin signaling and disease. *Cell*, 149(6):1192–205, 2012.

[26] S. E. Combs, T. Bruckner, J. E. Mizoe, T. Kamada, H. Tsujii, M. Kieser, and J. Debus. Comparison of carbon ion radiotherapy to photon radiation alone or in combination with temozolomide in patients with high-grade gliomas: explorative hypothesis-generating retrospective analysis. *Radiother Oncol*, 108(1):132–5, 2013.

[27] S. E. Combs, M. Kieser, S. Rieken, D. Habermehl, O. Jakel, T. Haberer, A. Nikoghosyan, R. Haselmann, A. Unterberg, W. Wick, and J. Debus. Randomized phase ii study evaluating a carbon ion boost applied after combined radiochemotherapy with temozolomide versus a proton boost after radiochemotherapy with temozolomide in patients with primary glioblastoma: the cleopatra trial. *BMC Cancer*, 10:478, 2010.

[28] S. E. Combs, D. Schulz-Ertner, W. Roth, C. Herold-Mende, J. Debus, and K. J. Weber. In vitro responsiveness of glioma cell lines to multimodality treatment with radiotherapy, temozolomide, and epidermal growth factor receptor inhibition with cetuximab. *Int J Radiat Oncol Biol Phys*, 68(3):873–82, 2007.

[29] N. Cordes, B. Hansmeier, C. Beinke, V. Meineke, and D. van Beuningen. Irradiation differentially affects substratum-dependent survival, adhesion, and invasion of glioblastoma cell lines. *Br J Cancer*, 89(11):2122–32, 2003.

[30] G. S. Cowley, B. A. Weir, F. Vazquez, and W. C. Hahn. Parallel genome-scale loss of function screens in 216 cancer cell lines for the identification of context-specific genetic dependencies. *Sci Data*, 1:140035, 2014.

[31] V. A. Cuddapah, S. Robel, S. Watkins, and H. Sontheimer. A neurocentric perspective on glioma invasion. *Nature reviews. Neuroscience*, 15(7):455–465, 2014.

[32] J. Curran, W. J., C. B. Scott, J. Horton, J. S. Nelson, A. S. Weinstein, A. J. Fischbach, C. H. Chang, M. Rotman, S. O. Asbell, R. E. Krisch, and et al. Recursive partitioning analysis of prognostic factors in three radiation therapy oncology group malignant glioma trials. *J Natl Cancer Inst*, 85(9):704–10, 1993.

[33] R. P. Danam, S. R. Howell, T. P. Brent, and L. C. Harris. Epigenetic regulation of ¡em¿o¡/em¿¡sup¿6¡/sup¿-methylguanine-dna methyltransferase gene expression by histone acetylation and methyl-cpg binding proteins. *Molecular Cancer Therapeutics*, 4(1):61–69, 2005.

[34] K. Datta, S. Suman, and J. Fornace, A. J. Radiation persistently promoted oxidative stress, activated mtor via pi3k/akt, and downregulated autophagy pathway in mouse intestine. *Int J Biochem Cell Biol*, 57:167–76, 2014.

[35] A. J. Davis and D. J. Chen. Dna double strand break repair via non-homologous end-joining. *Translational cancer research*, 2(3):130–143, 2013.

[36] F. De Bacco, P. Luraghi, E. Medico, G. Reato, F. Girolami, T. Perera, P. Gabriele, P. M. Comoglio, and C. Boccaccio. Induction of met by ionizing radiation and its role in radioresistance and invasive growth of cancer. *J Natl Cancer Inst*, 103(8):645–61, 2011.

[37] A. C. Diserens, N. de Tribolet, A. Martin-Achard, A. C. Gaide, J. F. Schnegg, and S. Carrel. Characterization of an established human malignant glioma cell line: Ln-18. *Acta Neuropathol*, 53(1):21–8, 1981.

[38] C. Dong, R. Mi, G. Jin, Y. Zhou, J. Zhang, and F. Liu. Identification of the proliferative effect of smad2 and 3 in the tgf beta2/smad signaling pathway using rna interference in a glioma cell line. *Mol Med Rep*, 12(2):1824–8, 2015.

[39] G. Driessens, B. Beck, A. Caauwe, B. D. Simons, and C. Blanpain. Defining the mode of tumour growth by clonal analysis. *Nature*, 488:527, 2012.

[40] H. J. Dubbink, W. Taal, R. van Marion, J. M. Kros, I. van Heuvel, J. E. Bromberg, B. A. Zonnenberg, C. B. Zonnenberg, T. J. Postma, J. M. Gijtenbeek, W. Boogerd, F. H. Groenendijk, P. A. Smitt, W. N. Dinjens, and M. J. van den Bent. Idh1 mutations in low-grade astrocytomas predict survival but not response to temozolomide. *Neurology*, 73(21):1792–5, 2009.

[41] V. Dubey and S. Luqman. Cathepsin d as a promising target for the discovery of novel anticancer agents. *Curr Cancer Drug Targets*, 17(5):404–422, 2017.

[42] M. Durante and J. S. Loeffler. Charged particles in radiation oncology. *Nat Rev Clin Oncol*, 7(1):37–43, 2010.

[43] L. Edalat, B. Stegen, L. Klumpp, E. Haehl, K. Schilbach, R. Lukowski, M. Kuhnle, G. Bernhardt, A. Buschauer, D. Zips, P. Ruth, and S. M. Huber. Bk k+ channel blockade inhibits radiation-induced migration/brain infiltration of glioblastoma cells. *Oncotarget*, 7(12):14259–78, 2016.

[44] G. I. Evan and K. H. Vousden. Proliferation, cell cycle and apoptosis in cancer. *Nature*, 411(6835):342–8, 2001.

[45] F. Fehlauer, M. Muench, E. Richter, and D. Rades. The inhibition of proliferation and migration of glioma spheroids exposed to temozolomide is less than additive if combined with irradiation. *Oncol Rep*, 17(4):941–5, 2007.

[46] S. Ferluga and W. Debinski. Ephs and ephrins in malignant gliomas. *Growth factors (Chur, Switzerland)*, 32(6):190–201, 2014.

[47] S. Ferrandon, N. Magne, P. Battiston-Montagne, N. H. Hau-Desbat, O. Diaz, M. Beuve, J. Constanzo, C. Chargari, D. Poncet, E. Chautard, D. Ardail, G. Alphonse, and C. Rodriguez-Lafrasse. Cellular and molecular portrait of eleven human glioblastoma cell lines under photon and carbon ion irradiation. *Cancer Lett*, 360(1):10–6, 2015.

[48] C. Gialeli, A. D. Theocharis, and N. K. Karamanos. Roles of matrix metalloproteinases in cancer progression and their pharmacological targeting. *Febs j*, 278(1):16–27, 2011.

[49] K. Goetze, M. Scholz, G. Taucher-Scholz, and W. Mueller-Klieser. The impact of conventional and heavy ion irradiation on tumor cell migration in vitro. *International Journal of Radiation Biology*, 83(11-12):889–896, 2007.

[50] E. H. Grubbé. Priority in the therapeutic use of x-rays. *Radiology*, 21(2):156–162, 1933.

[51] D. Habermehl, K. Ilicic, S. Dehne, S. Rieken, L. Orschiedt, S. Brons, T. Haberer, K. J. Weber, J. Debus, and S. E. Combs. The relative biological effectiveness for carbon and oxygen ion beams using the raster-scanning technique in hepatocellular carcinoma cell lines. *PLoS One*, 9(12):e113591, 2014.

[52] E. J. Hall and A. J. Giaccia. *Radiobiology for the radiologist.* Wolters Kluwer Health/Lippincott Williams and Wilkins, Philadelphia, 2012.

[53] J. Han, C. A. Alvarez-Breckenridge, Q. E. Wang, and J. Yu. Tgf-beta signaling and its targeting for glioma treatment. *Am J Cancer Res*, 5(3):945–55, 2015.

[54] D. Hanahan and R. Weinberg. Hallmarks of cancer: The next generation. *Cell*, 144(5):646–674, 2011.

[55] M. E. Hegi, A. C. Diserens, T. Gorlia, M. F. Hamou, N. de Tribolet, M. Weller, J. M. Kros, J. A. Hainfellner, W. Mason, L. Mariani, J. E. Bromberg, P. Hau, R. O. Mirimanoff, J. G. Cairncross, R. C. Janzer, and R. Stupp. Mgmt gene silencing and benefit from temozolomide in glioblastoma. *N Engl J Med*, 352(10):997–1003, 2005.

[56] C. F. Hess, J. C. Schaaf, R. D. Kortmann, M. Schabet, and M. Bamberg. Malignant glioma: patterns of failure following individually tailored limited volume irradiation. *Radiother Oncol*, 30(2):146–9, 1994.

[57] Y. Hirota, S. Masunaga, N. Kondo, S. Kawabata, H. Hirakawa, H. Yajima, A. Fujimori, K. Ono, T. Kuroiwa, and S. Miyatake. High linear-energy-transfer radiation can overcome radioresistance of glioma stem-like cells to low linear-energy-transfer radiation. *J Radiat Res*, 55(1):75–83, 2014.

[58] W. N. Hittelman, Y. Liao, L. Wang, and L. Milas. Are cancer stem cells radioresistant? *Future Oncol*, 6(10):1563–76, 2010.

[59] D. B. Hoelzinger, L. Mariani, J. Weis, T. Woyke, T. J. Berens, W. McDonough, A. Sloan, S. W. Coons, and M. E. Berens. Gene expression profile of glioblastoma multiforme invasive phenotype points to new therapeutic targets. *Neoplasia*, 7(1):7–16, 2005.

[60] R. P. Holloway and R. G. Dale. Theoretical implications of incorporating relative biological effectiveness into radiobiological equivalence relationships. *The British Journal of Radiology*, 86(1022):20120417, 2013.

[61] S. C. Hung, R. R. Pochampally, S. C. Chen, S. C. Hsu, and D. J. Prockop. Angiogenic effects of human multipotent stromal cell conditioned medium activate the pi3k-akt pathway in hypoxic endothelial cells to inhibit apoptosis, increase survival, and stimulate angiogenesis. *Stem Cells*, 25(9):2363–70, 2007.

[62] K. Ichimura, D. M. Pearson, S. Kocialkowski, L. M. Bäcklund, R. Chan, D. T. W. Jones, and V. P. Collins. Idh1 mutations are present in the majority of common adult gliomas but rare in primary glioblastomas. *Neuro-oncology*, 11(4):341–347, 2009.

[63] N. Ishii, D. Maier, A. Merlo, M. Tada, Y. Sawamura, A.-C. Diserens, and G. Meir Erwin. Frequent co-alterations of tp53, p16/cdkn2a, p14arf, pten tumor suppressor genes in human glioma cell lines. *Brain Pathology*, 9(3):469–479, 2006.

[64] A. Jacob and R. Prekeris. The regulation of mmp targeting to invadopodia during cancer metastasis. *Front Cell Dev Biol*, 3:4, 2015.

[65] M. Jamal, B. H. Rath, P. S. Tsang, K. Camphausen, and P. J. Tofilon. The brain microenvironment preferentially enhances the radioresistance of cd133(+) glioblastoma stem-like cells. *Neoplasia*, 14(2):150–8, 2012.

[66] R. B. Jenkins, H. Blair, K. V. Ballman, C. Giannini, R. M. Arusell, M. Law, H. Flynn, S. Passe, S. Felten, P. D. Brown, E. G. Shaw, and J. C. Buckner. A t(1;19)(q10;p10) mediates the combined deletions of 1p and 19q and predicts a better prognosis of patients with oligodendroglioma. *Cancer Res*, 66(20):9852–61, 2006.

[67] M. C. Joiner, B. Marples, and H. Johns. *The Limitation of the Linear-Quadratic Model at Low Doses per Fraction*, pages 51–66. Springer Berlin Heidelberg, 1993.

[68] R. Kalluri and R. A. Weinberg. The basics of epithelial-mesenchymal transition. *J Clin Invest*, 119(6):1420–8, 2009.

[69] O. Kargiotis, A. Geka, J. S. Rao, and A. P. Kyritsis. Effects of irradiation on tumor cell survival, invasion and angiogenesis. *J Neurooncol*, 100(3):323–38, 2010.

[70] P. Kleihues, P. C. Burger, and B. W. Scheithauer. The new who classification of brain tumours. *Brain Pathol*, 3(3):255–68, 1993.

[71] D. Krex, B. Klink, C. Hartmann, A. von Deimling, T. Pietsch, M. Simon, M. Sabel, J. P. Steinbach, O. Heese, G. Reifenberger, M. Weller, and G. Schackert. Long-term survival with glioblastoma multiforme. *Brain*, 130(Pt 10):2596–606, 2007.

[72] M. Krämer and G. Kraft. Track structure and dna damage. *Advances in Space Research*, 14(10):151–159, 1994.

[73] S. Lehnert. *Biomolecular action of ionizing radiation*. Taylor and Francis, Boca Raton, 2007.

[74] B. P. Lewis, C. B. Burge, and D. P. Bartel. Conserved seed pairing, often flanked by adenosines, indicates that thousands of human genes are microrna targets. *Cell*, 120(1):15–20, 2005.

[75] S. L. Liauw, P. P. Connell, and R. R. Weichselbaum. New paradigms and future challenges in radiation oncology: An update of biological targets and technology. *Science translational medicine*, 5(173):173sr2–173sr2, 2013.

[76] C. Y. Logan and R. Nusse. The wnt signaling pathway in development and disease. *Annu Rev Cell Dev Biol*, 20:781–810, 2004.

[77] M. E. Lomax, L. K. Folkes, and P. O'Neill. Biological consequences of radiation-induced dna damage: relevance to radiotherapy. *Clin Oncol (R Coll Radiol)*, 25(10):578–85, 2013.

[78] G. Lossaint, E. Besnard, D. Fisher, J. Piette, and V. Dulic. Chk1 is dispensable for g2 arrest in response to sustained dna damage when the atm/p53/p21 pathway is functional. *Oncogene*, 30(41):4261–74, 2011.

[79] D. N. Louis, H. Ohgaki, O. D. Wiestler, W. K. Cavenee, P. C. Burger, A. Jouvet, B. W. Scheithauer, and P. Kleihues. The 2007 who classification of tumours of the central nervous system. *Acta Neuropathologica*, 114(2):97–109, 2007.

[80] D. N. Louis, A. Perry, G. Reifenberger, A. von Deimling, D. Figarella-Branger, W. K. Cavenee, H. Ohgaki, O. D. Wiestler, P. Kleihues, and D. W. Ellison. The 2016 world health organization classification of tumors of the central nervous system: a summary. *Acta Neuropathologica*, 131(6):803–820, 2016.

[81] Y. Ma, Y. Chen, Y. Li, K. Grun, A. Berndt, Z. Zhou, and I. Petersen. Cystatin a suppresses tumor cell growth through inhibiting epithelial to mesenchymal transition in human lung cancer. *Oncotarget*, 9(18):14084–14098, 2018.

[82] Y. S. Ma, Z. J. Wu, R. Z. Bai, H. Dong, B. X. Xie, X. H. Wu, X. S. Hang, A. N. Liu, X. H. Jiang, G. R. Wang, J. J. Jiang, W. H. Xu, X. P. Chen, G. H. Tan, D. Fu, J. B. Liu, and Q. Liu. Drr1 promotes glioblastoma cell invasion and epithelial-mesenchymal transition via regulating akt activation. *Cancer Lett*, 423:86–94, 2018.

[83] L. J. McCawley and L. M. Matrisian. Matrix metalloproteinases: they're not just for matrix anymore! *Current Opinion in Cell Biology*, 13(5):534–540, 2001.

[84] S. McGuire. World cancer report 2014. geneva, switzerland: World health organization, international agency for research on cancer, who press, 2015. *Adv Nutr*, 7(2):418–9, 2016.

[85] K. McNeill, K. Aldape, and H. A. Fine. *Adult High-Grade (Diffuse) Glioma*, pages 77–93. Springer New York, 2015.

[86] M. Metha, J. Buckner, and R. Sawaya. Neoplasms of the central nervous system. *Cancer:principles and practice of oncology*, 8, 2008.

[87] J. E. Mizoe, H. Tsujii, A. Hasegawa, T. Yanagi, R. Takagi, T. Kamada, H. Tsuji, and K. Takakura. Phase i/ii clinical trial of carbon ion radiotherapy for malignant gliomas: combined x-ray radiotherapy, chemotherapy, and carbon ion radiotherapy. *Int J Radiat Oncol Biol Phys*, 69(2):390–6, 2007.

[88] C. Muth, Y. Rubner, S. Semrau, P. F. Ruhle, B. Frey, A. Strnad, R. Buslei, R. Fietkau, and U. S. Gaipl. Primary glioblastoma multiforme tumors and recurrence : Comparative analysis of the danger signals hmgb1, hsp70, and calreticulin. *Strahlenther Onkol*, 192(3):146–155, 2016.

[89] M. Nakada, Y. Okada, and J. Yamashita. The role of matrix metalloproteinases in glioma invasion. *Front Biosci*, 8:e261–9, 2003.

[90] A. K. Nalla, S. Asuthkar, P. Bhoopathi, M. Gujrati, D. H. Dinh, and J. S. Rao. Suppression of upar retards radiation-induced invasion and migration mediated by integrin beta 1/fak signaling in medulloblastoma. *PLOS ONE*, 5(9):e13006, 2010.

[91] J. A. Nickoloff. Photon, light ion, and heavy ion cancer radiotherapy: paths from physics and biology to clinical practice. *Ann Transl Med*, 3(21):336, 2015.

[92] S. Osuka and E. G. Van Meir. Overcoming therapeutic resistance in glioblastoma: the way forward. *J Clin Invest*, 127(2):415–426, 2017.

[93] S. Panier and S. J. Boulton. Double-strand break repair: 53bp1 comes into focus. *Nature Reviews Molecular Cell Biology*, 15:7, 2013.

[94] C. M. Park, M. J. Park, H. J. Kwak, H. C. Lee, M. S. Kim, S. H. Lee, I. C. Park, C. H. Rhee, and S. I. Hong. Ionizing radiation enhances matrix metalloproteinase-2 secretion and invasion of glioma cells through src/epidermal growth factor receptor-mediated p38/akt and phosphatidylinositol 3-kinase/akt signaling pathways. *Cancer Res*, 66(17):8511–9, 2006.

[95] J. Parmar, E. S. Marshall, G. A. Charters, K. M. Holdaway, A. N. Shelling, and B. C. Baguley. Radiation-induced cell cycle delays and p53 status of early passage melanoma cell lines. *Oncol Res*, 12(3):149–55, 2000.

[96] I. Paw, R. C. Carpenter, K. Watabe, W. Debinski, and H. W. Lo. Mechanisms regulating glioma invasion. *Cancer Lett*, 362(1):1–7, 2015.

[97] A. K. Percy, L. R. Elveback, H. Okazaki, and L. T. Kurland. Neoplasms of the central nervous system. *Epidemiologic considerations*, 22(1):40–40, 1972.

[98] J. Polivka, J., J. Polivka, L. Holubec, T. Kubikova, V. Priban, O. Hes, K. Pivovarcikova, and I. Treskova. Advances in experimental targeted therapy and immunotherapy for patients with glioblastoma multiforme. *Anticancer Res*, 37(1):21–33, 2017.

[99] A. Pompos, M. Durante, and H. Choy. Heavy ions in cancer therapy. *JAMA Oncol*, 2(12):1539–1540, 2016.

[100] P. Pyrko, A. H. Schonthal, F. M. Hofman, T. C. Chen, and A. S. Lee. The unfolded protein response regulator grp78/bip as a novel target for increasing chemosensitivity in malignant gliomas. *Cancer Res*, 67(20):9809–16, 2007.

[101] S. Rieken, D. Habermehl, A. Mohr, L. Wuerth, K. Lindel, K. Weber, J. Debus, and S. E. Combs. Targeting alphanubeta3 and alphanubeta5 inhibits photon-induced hypermigration of malignant glioma cells. *Radiat Oncol*, 6:132, 2011.

[102] S. Rieken, D. Habermehl, L. Wuerth, S. Brons, A. Mohr, K. Lindel, K. Weber, T. Haberer, J. Debus, and S. E. Combs. Carbon ion irradiation inhibits glioma cell migration through downregulation of integrin expression. *Int J Radiat Oncol Biol Phys*, 83(1):394–9, 2012.

[103] A. L. Rivera, C. E. Pelloski, M. R. Gilbert, H. Colman, C. De La Cruz, E. P. Sulman, B. N. Bekele, and K. D. Aldape. Mgmt promoter methylation is predictive of response to radiotherapy and prognostic in the absence of adjuvant alkylating chemotherapy for glioblastoma. *Neuro Oncol*, 12(2):116–21, 2010.

[104] E. K. Rofstad, B. Mathiesen, and K. Galappathi. Increased metastatic dissemination in human melanoma xenografts after subcurative radiation treatment: radiation-induced increase in fraction of hypoxic cells and hypoxia-induced up-regulation of urokinase-type plasminogen activator receptor. *Cancer Research*, 64(1):13–18, 2004.

[105] E. P. Rogakou, C. Boon, C. Redon, and W. M. Bonner. Megabase chromatin domains involved in dna double-strand breaks in vivo. *The Journal of Cell Biology*, 146(5):905–916, 1999.

[106] A. Sancar, L. A. Lindsey-Boltz, K. Unsal-Kacmaz, and S. Linn. Molecular mechanisms of mammalian dna repair and the dna damage checkpoints. *Annu Rev Biochem*, 73:39–85, 2004.

[107] L. B. Schultz, N. H. Chehab, A. Malikzay, and T. D. Halazonetis. p53 binding protein 1 (53bp1) is an early participant in the cellular response to dna double-strand breaks. *J Cell Biol*, 151(7):1381–90, 2000.

[108] D. Schulz-Ertner, O. Jakel, and W. Schlegel. Radiation therapy with charged particles. *Semin Radiat Oncol*, 16(4):249–59, 2006.

[109] J. Seoane, H.-V. Le, L. Shen, S. A. Anderson, and J. Massagué. Integration of smad and forkhead pathways in the control of neuroepithelial and glioblastoma cell proliferation. *Cell*, 117(2):211–223, 2004.

[110] N. Sethi and Y. Kang. Unravelling the complexity of metastasis - molecular under-standing and targeted therapies. *Nat Rev Cancer*, 11(10):735–48, 2011.

[111] M. Shirahata, T. Ono, D. Stichel, D. Schrimpf, and A. von Deimling. Novel, improved grading system(s) for idh-mutant astrocytic gliomas. *Acta Neuropathol*, 136(1):153–166, 2018.

[112] V. Singh-Gupta, H. Zhang, S. Banerjee, D. Kong, J. J. Raffoul, F. H. Sarkar, and G. G. Hillman. Radiation-induced hif-1alpha cell survival pathway is inhibited by soy isoflavones in prostate cancer cells. *Int J Cancer*, 124(7):1675–84, 2009.

[113] P. Sminia and B. A. Westerman. Blood–brain barrier crossing and breakthroughs in glioblastoma therapy. *British Journal of Clinical Pharmacology*, 81(6):1018–1020, 2016.

[114] M. Steinle, D. Palme, M. Misovic, J. Rudner, K. Dittmann, R. Lukowski, P. Ruth, and S. M. Huber. Ionizing radiation induces migration of glioblastoma cells by activating bk k+ channels. *Radiotherapy and Oncology*, 101(1):122–126, 2011.

[115] R. Stupp, M. E. Hegi, W. P. Mason, M. J. van den Bent, M. J. B. Taphoorn, R. C. Janzer, S. K. Ludwin, A. Allgeier, B. Fisher, K. Belanger, P. Hau, A. A. Brandes, J. Gijtenbeek, C. Marosi, C. J. Vecht, K. Mokhtari, P. Wesseling, S. Villa, E. Eisenhauer, T. Gorlia, M. Weller, D. Lacombe, J. G. Cairncross, and R.-O. Mirimanoff. Effects of radiotherapy with concomitant and adjuvant temozolomide versus radiotherapy alone on survival in glioblastoma in a randomised phase iii study: 5-year analysis of the eortc-ncic trial. *The Lancet Oncology*, 10(5):459–466, 2009.

[116] Z. Sun, S. Wang, and R. C. Zhao. The roles of mesenchymal stem cells in tumor inflammatory microenvironment. *J Hematol Oncol*, 7:14, 2014.

[117] J. C. Tonn and R. Goldbrunner. Mechanisms of glioma cell invasion. *Acta Neurochir Suppl*, 88:163–7, 2003.

[118] J. P. Traynor, H. A. Oun, P. McKenzie, I. R. Shilliday, I. G. McKay, A. Dunlop, C. C. Geddes, and R. A. Mactier. Assessing the utility of the stop dialysate flow method in patients receiving haemodiafiltration. *Nephrol Dial Transplant*, 20(11):2479–84, 2005.

[119] S. Tribius, A. Pidel, and D. Casper. Atm protein expression correlates with radioresistance in primary glioblastoma cells in culture. *Int J Radiat Oncol Biol Phys*, 50(2):511–23, 2001.

[120] S. Unkel, C. Belka, and K. Lauber. On the analysis of clonogenic survival data: Statistical alternatives to the linear-quadratic model. *Radiat Oncol*, 11:11, 2016.

[121] M. J. van den Bent, B. Baumert, and J. M. Kros. Interim results from the catnon trial (eortc study 26053-22054) of treatment with concurrent and adjuvant temozolomide for 1p/19q non-co-deleted anaplastic glioma: a phase 3, randomised, open-label intergroup study. *Lancet*, 390(10103):1645–1653, 2017.

[122] O. van Tellingen, B. Yetkin-Arik, M. C. de Gooijer, P. Wesseling, T. Wurdinger, and H. E. de Vries. Overcoming the blood-brain tumor barrier for effective glioblastoma treatment. *Drug Resist Updat*, 19:1–12, 2015.

[123] F. van Zijl, G. Krupitza, and W. Mikulits. Initial steps of metastasis: cell invasion and endothelial transmigration. *Mutat Res*, 728(1-2):23–34, 2011.

[124] C. F. von Essen. Radiation enhancement of metastasis: a review. *Clin Exp Metastasis*, 9(2):77–104, 1991.

[125] M. Wada, M. Suzuki, C. Liu, Y. Kaneko, S. Fukuda, K. Ando, and N. Matsufuji. Modeling the biological response of normal human cells, including repair processes, to fractionated carbon beam irradiation. *Journal of Radiation Research*, 54(5):798–807, 2013.

[126] M. D. Walker, S. B. Green, D. P. Byar, J. Alexander, E., U. Batzdorf, W. H. Brooks, W. E. Hunt, C. S. MacCarty, J. Mahaley, M. S., J. Mealey, J., G. Owens, n. Ransohoff, J., J. T. Robertson, W. R. Shapiro, J. Smith, K. R., C. B. Wilson, and T. A. Strike. Randomized comparisons of radiotherapy and nitrosoureas for the treatment of malignant glioma after surgery. *N Engl J Med*, 303(23):1323–9, 1980.

[127] M. D. Walker, T. A. Strike, and G. E. Sheline. An analysis of dose-effect relationship in the radiotherapy of malignant gliomas. *Int J Radiat Oncol Biol Phys*, 5(10):1725–31, 1979.

[128] M. Wank, D. Schilling, J. Reindl, B. Meyer, J. Gempt, S. Motov, F. Alexander, J. J. Wilkens, J. Schlegel, T. E. Schmid, and S. E. Combs. Evaluation of radiation-related

invasion in primary patient-derived glioma cells and validation with established cell lines: impact of different radiation qualities with differing let. *J Neurooncol*, 2018.

[129] J. D. Watson and F. H. Crick. The structure of dna. *Cold Spring Harb Symp Quant Biol*, 18:123–31, 1953.

[130] M. Werner-Wasik, C. B. Scott, D. F. Nelson, L. E. Gaspar, K. J. Murray, J. A. Fischbach, J. S. Nelson, A. S. Weinstein, and J. Curran, W. J. Final report of a phase i/ii trial of hyperfractionated and accelerated hyperfractionated radiation therapy with carmustine for adults with supratentorial malignant gliomas. radiation therapy oncology group study 83-02. *Cancer*, 77(8):1535–43, 1996.

[131] W. Wick, A. Wick, J. Schulz, J. Dichgans, H. Rodemann, and M. Weller. *Prevention of irradiation-induced glioma cell invasion by temozolomide involves caspase 3 activity and cleavage of focal adhesion kinase*, volume 62. Cancer Research, 2002.

[132] C. Wild-Bode, M. Weller, A. Rimner, J. Dichgans, and W. Wick. Sublethal irradiation promotes migration and invasiveness of glioma cells: implications for radiotherapy of human glioblastoma. *Cancer Res*, 61(6):2744–50, 2001.

[133] M. Wolf, I. Clark-Lewis, C. Buri, H. Langen, M. Lis, and L. Mazzucchelli. Cathepsin d specifically cleaves the chemokines macrophage inflammatory protein-1 alpha, macrophage inflammatory protein-1 beta, and slc that are expressed in human breast cancer. *Am J Pathol*, 162(4):1183–90, 2003.

[134] S. N. K. Xin Hong, Khalil Chedid. Glioblastoma cell line-derived spheres in serum-containing medium versus serum-free medium: A comparison of cancer stem cell properties. *International Journal of Oncology*, 41(5):1693–1700, 2012.

[135] L. Zhen, J. Li, M. Zhang, and K. Yang. Mir-10b decreases sensitivity of glioblastoma cells to radiation by targeting akt. *J Biol Res (Thessalon)*, 23:14, 2016.

[136] J. W. Zimmerman, H. Jimenez, M. J. Pennison, I. Brezovich, D. Morgan, A. Mudry, F. P. Costa, A. Barbault, and B. Pasche. Targeted treatment of cancer with radiofrequency electromagnetic fields amplitude-modulated at tumor-specific frequencies. *Chinese Journal of Cancer*, 32(11):573–581, 2013.

12   Publication

M. Wank, D. Schilling, J. Reindl, B. Meyer, J. Gempt, S. Motov, F. Alexander, J. J. Wilkens, J. Schlegel, T. E. Schmid and S. E. Combs. Evaluation of radiation-related invasion in primary patient-derived glioma cells and validation with established cell lines: impact of different radiation qualities with differing LET. Journal of Neurooncology, 2018 [128].

13 Acknowledgement